

# MIXING OF DENSITY-STRATIFIED IMPOUNDMENTS WITH BUOYANT JETS

by  
John D. Ditmars

W. M. Keck Laboratory of Hydraulics and Water Resources  
Division of Engineering and Applied Science  
CALIFORNIA INSTITUTE OF TECHNOLOGY  
Pasadena, California

REFERENCE ROOM COPY

RETURN TO ROOM 136

W. M. Keck Engineering Laboratories  
California Institute of Technology

Report No. KH-R-22

September 1970

MIXING OF DENSITY-STRATIFIED IMPOUNDMENTS  
WITH BUOYANT JETS

by

John David Ditmars

Project Supervisor:  
Norman H. Brooks  
Professor of Environmental Science  
and Civil Engineering

Funded by  
Federal Water Pollution Control Administration  
Grant No. 16070 DGY

W. M. Keck Laboratory of Hydraulics and Water Resources  
Division of Engineering and Applied Science  
California Institute of Technology  
Pasadena, California

REFERENCE ROOM COPY

RETURN TO ROOM 136  
W. M. Keck Engineering Laboratories  
California Institute of Technology



## ACKNOWLEDGMENTS

To Dr. Norman H. Brooks, who was a continuous source of guidance, kind advice, and encouragement throughout this study, the writer expresses his sincere gratitude.

The writer is also indebted to Dr. Vito A. Vanoni and Dr. Fredric Raichlen for their comments and encouragement during this study and to Dr. E. John List for his comments during the writing of the thesis.

For their ready assistance in constructing and modifying the experimental apparatus, the writer extends sincere thanks to Mr. Elton F. Daly, Supervisor of the Shop and Laboratory, and to Mr. Robert L. Greenway. Appreciation is also due Mr. Carl A. Green, Jr., who prepared the drawings; Mrs. Arvilla F. Krugh, who typed this manuscript and earlier drafts, Mr. Carl T. Eastvedt, who did the photographic work; Mrs. Patricia A. Rankin, who provided many secretarial services for this study; and Messrs. Yoshiaki Daimon, Steven S. Watkins and Paul T. Wegener, who assisted in performing the experiments and reducing the data.

This research was supported by the Federal Water Pollution Control Administration through Grants No. 16000 DGY and No. 16070 DGY and was conducted in the W. M. Keck Laboratory of Hydraulics and Water Resources at the California Institute of Technology.

The writer gratefully acknowledges the financial assistance received as a U. S. Public Health Service Trainee (1966-70) and a National Science Foundation Trainee (1965-66).

This report was submitted by the writer in August, 1970, as a thesis with the same title to the California Institute of Technology in partial fulfillment of the requirements for the degree of Doctor of Philosophy in Civil Engineering.

## ABSTRACT

This study is an investigation of the mixing of density-stratified impoundments by means of buoyant jets created by a pumping system. The deterioration of water quality which often occurs in density-stratified lakes and reservoirs may be counteracted by mixing. The physical aspects of the mixing process are the primary concern of this study, although several implications regarding changes in water quality are indicated.

A simulation technique is developed to predict the time-history of changes in the density-depth profiles of an impoundment during mixing. The simulation model considers the impoundment closed to all external influences except those due to the pumping system. The impoundment is treated in a one-dimensional sense, except for the fluid mechanics of the three-dimensional jet and selective withdrawal of pumping system. The numerical solution to the governing equations predicts density profiles at successive time steps during mixing, given the initial density profile, the area-depth relation for the impoundment, the elevations of intake and jet discharge tubes, and the jet discharge and diameter. The changes due to mixing in the profiles of temperature and of a conservative, non-reacting tracer can be predicted also.

The results of laboratory experiments and two field mixing experiments in which density-stratified impoundments were mixed using pumping systems show that the simulation technique predicts the response of the impoundment reasonably well.

The results of a series of simulated mixing experiments for impoundments which have prismatic shapes and initially linear density profiles are given in dimensionless form. For these special conditions, the efficiency of the pumping system increased as the jet densimetric Froude number decreased, and the time required for complete mixing was a fraction of the characteristic time,  $T \leq V/Q$  (where  $V$  is the impoundment volume included between intake and jet elevations and  $Q$  is the pumped discharge).

Recommendations are made for the application of the generalized results and for the use of the simulation technique for lakes and reservoirs which are not closed systems.

## TABLE OF CONTENTS

<u>Chapter</u>		<u>Page</u>
1.	INTRODUCTION	1
1.1	Density-Stratified Impoundments	1
1.1.1	Background	1
1.1.2	Alternative Solutions	3
1.2	Previous Work With Pumping Systems	6
1.2.1	Mixing With Fixed Buoyant Jets	6
1.2.2	Mixing With Pumping Systems	7
1.3	Objectives and Scope of Present Study	9
2.	SIMULATION ANALYSIS AND TECHNIQUE	11
2.1	Fluid Mechanical Features of Pumping Systems	11
2.1.1	Description of the Fluid Mechanical Features	11
2.1.2	Relative Importance of Various Features	14
2.2	Development of One-Dimensional Model and Governing Equations	15
2.2.1	General Assumptions	15
2.2.2	Model and Equations	17
2.2.3	Physical View of the Governing Equations	21
2.2.4	Buoyant Jet Mechanics Involved to Obtain $q_e$	23



## TABLE OF CONTENTS (Continued)

<u>Chapter</u>		<u>Page</u>
	2.2.5 Selective Withdrawal Mechanics Involved to Obtain $q_e$	35
	2.2.6 Summary	45
2.3	Solution of Governing Equations	45
	2.3.1 Method of Solution	45
	2.3.2 Finite Difference Solution	46
	2.3.3 Outline of Computation Technique	55
2.4	Flexibility of Computer Simulation	62
3.	MIXING OF A TRACER SUBSTANCE	64
	3.1 Effect of Mixing on a Tracer	64
	3.2 Simulation of the Mixing of a Conservative, Non-Reacting Tracer	65
	3.3 Temperature as a Tracer and the Nonlinear Temperature-Density Relationship	69
	3.4 Extension of the Technique to Reacting Tracer Substances	73
4.	LABORATORY EXPERIMENTS	75
	4.1 Purpose of Experiments	75
	4.2 Experimental Procedure	75
	4.2.1 Description of the Experimental Apparatus	76
	4.2.2 Density Stratification	79
	4.2.3 Determination of Density Profiles	86

## TABLE OF CONTENTS (Continued)

<u>Chapter</u>		<u>Page</u>
4.3	Experimental Results	95
4.3.1	Presentation of Typical Experimental Results	95
4.3.2	General Description of Results	118
4.4	Discussion of Results	122
5.	FIELD AND LABORATORY EXPERIMENTS BY OTHER INVESTIGATORS	130
5.1	Field Experiments	130
5.1.1	Summary of Mixing Experiments	131
5.1.2	Comparison of Field Data and Simulation Results	133
5.2	Laboratory Experiments	137
6.	IMPLICATIONS OF SIMULATION TECHNIQUE	141
6.1	Purpose	141
6.2	Generalized Solutions	141
6.2.1	Dimensional Analysis for Initially Linear Profiles	142
6.2.2	Potential Energy Increase	150
6.2.3	Effect of the Densimetric Froude Number	153
6.2.4	Results of Generalized Simulations	161
6.3	Implications of Simulation for the Design of Pumping Systems	172

## TABLE OF CONTENTS (Continued)

<u>Chapter</u>		<u>Page</u>
7.	SUMMARY AND CONCLUSIONS	176
7.1	Contributions of the Present Study	176
7.1.1	The Simulation Technique	177
7.1.2	The Generalized Solutions	179
7.2	Application of Simulation Technique to Lakes and Reservoirs	181
7.3	Recommendations for Future Research	183
NOTATION		186
LIST OF REFERENCES		191
APPENDIX		199

## LIST OF FIGURES

<u>Number</u>	<u>Description</u>	<u>Page</u>
2.1	Schematic diagram of a pumping system in a density-stratified impoundment	12
2.2	Sketch of impoundment: (a) horizontal cross-sectional area, $A$ , (b) vertical profile of density-stratifying agent, $c$ , (c) elemental section	18
2.3	Pumping system (a) with typical distributions of $q_e$ (b) and integrated $q_e$ (c)	22
2.4	Definition sketch for a buoyant jet in a linearly stratified environment	26
2.5	Comparison of buoyant jet theory for non-linearly stratified environment with Hart's experiment (20)	31
2.6	Sketch of buoyant jet vertical momentum flux, $m_v$ , and center line density, $\rho_j$ , in ambient density profile, $\rho_a$	34
2.7	Definition sketch for turbulent withdrawal layer and solutions of Brooks and Koh (8)	38
2.8	Normalized velocity profile for half of withdrawal layer, Koh's (26) theory and approximate profile	41
2.9	Normalized integrated entrainment from the withdrawal layer	44
2.10	Finite difference schemes for: (a) $v > 0$ and (b) $v < 0$	48
2.11	Irregular space intervals, $\Delta y$ , at each time interval, $\Delta t$	54

## LIST OF FIGURES (Continued)

<u>Number</u>	<u>Description</u>	<u>Page</u>
2. 12	Outline of computation procedure	56
2. 13	Sketch of vertical distributions of: (a) $q_e$ , (b) integrated $q_e$ , (c) $v$ , and (d) $\Delta y$	59
2. 14	Sketch of displacements, $\Delta y$ , from uniform spacing to form irregular spacing	61
3. 1	Schematic diagram of pumping system and tracer profile, $c_s$	66
3. 2	Example of simulated redistribution of a tracer due to mixing.	70
4. 1	Schematic diagram of experimental setup	77
4. 2	Photograph of experimental setup (2m tank)	78
4. 3	Definition sketch of continuous filling technique	82
4. 4	Photograph of surface spreading device	83
4. 5	Sketch of arrangement of plate towed through a two-layer system	85
4. 6	Conductivity probe (from Koh (26))	88
4. 7	Circuit diagram for a conductivity probe used with a Sanborn recorder	90
4. 8	A typical set of calibration curves for a conductivity probe	91
4. 9	Location sketch for the positions of conductivity probes and jet and intake tubes in laboratory tanks	93
4. 10	Measured and simulated density profiles for Experiment Number 5	97

## LIST OF FIGURES (Continued)

<u>Number</u>	<u>Description</u>	<u>Page</u>
4.11	Measured and simulated density profiles for Experiment Number 6	98
4.12	Measured and simulated density profiles for Experiment Number 7	99
4.13	Measured and simulated density profiles for Experiment Number 8	100
4.14	Measured and simulated density profiles for Experiment Number 9	101
4.15	Measured and simulated density profiles for Experiment Number 10, at Station 0.10m	102
4.16	Measured and simulated density profiles for Experiment Number 10, at Station 2.00m	103
4.17	Measured and simulated density profiles for Experiment Number 12, at Station 1.25m	104
4.18	Measured and simulated density profiles for Experiment Number 12, at Station 4.50m	105
4.19	Measured and simulated density profiles for Experiment Number 13, at Station 1.25m	106
4.20	Measured and simulated density profiles for Experiment Number 13, at Station 4.50m	107
4.21	Measured and simulated density profiles for Experiment Number 14, at Station 0.98m	108
4.22	Measured and simulated density profiles for Experiment Number 14, at Station 8.10m	109
4.23	Measured and simulated density profiles for Experiment Number 15	110
4.24	Measured and simulated density profiles for Experiment Number 16	111

## LIST OF FIGURES (Continued)

<u>Number</u>	<u>Description</u>	<u>Page</u>
4.25	Measured and simulated density profiles for Experiment Number 17, at Station 3.34m	112
4.26	Measured and simulated density profiles for Experiment Number 17, at Station 18.50m	113
4.27	Measured and simulated density profiles for Experiment Number 17, at Station 33.66m	114
4.28	Measured and simulated density profiles for Experiment Number 18, at Station 3.50m	115
4.29	Measured and simulated density profiles for Experiment Number 18, at Station 18.50m	116
4.30	Measured and simulated density profiles for Experiment Number 18, at Station 33.50m	117
5.1	Measured and simulated temperature profiles for FWPCA field experiment at Vesuvius Lake	134
5.2	Measured and simulated temperature profile for FWPCA field experiment at Boltz Lake	136
5.3	Simulated density profiles for "Run No. f" of Brush, et al. (9)	139
6.1	Schematic diagram of a pumping system in an impoundment with an initially linear density profile	143
6.2	Generalized simulation results for $F = 1.0$ and $F = 12.0$	155
6.3	Generalized simulation results for $F = 24.0$	156
6.4	Effect of densimetric Froude number on the increase in potential energy with time	157

## LIST OF FIGURES (Continued)

<u>Number</u>	<u>Description</u>	<u>Page</u>
6.5	Generalized simulation results for $P = 2.50 \times 10^{-6}$ and $P = 2.50 \times 10^{-5}$ : $S = 500$ and $F = 3.0$	164
6.6	Generalized simulation results for $P = 2.50 \times 10^{-4}$ and $P = 2.50 \times 10^{-3}$ : $S = 500$ and $F = 3.0$	165
6.7	Generalized simulation results for $P = 2.50 \times 10^{-2}$ : $S = 500$ and $F = 3.0$	166
6.8	Effect of plume parameter, $P$ , on the increase in potential energy with time ( $S = 500$ and $F = 3.0$ )	167
6.9	Generalized simulation results for $P = 1.16 \times 10^{-4}$ and $P = 1.16 \times 10^{-3}$ : $S = 50,000$ and $F = 3.0$	168
6.10	Generalized simulation results for $P = 1.16 \times 10^{-2}$ and $P = 1.16 \times 10^{-1}$ : $S = 50,000$ and $F = 3.0$	169
6.11	Effect of plume parameter, $P$ , on the increase in potential energy with time ( $S = 50,000$ and $F = 3.0$ )	170
6.12	Summary of generalized simulation results: fraction of required potential energy increase as a function of $P$ and $t^*$	171



## LIST OF TABLES

<u>Number</u>	<u>Description</u>	<u>Page</u>
4. 1	Summary of Laboratory Mixing Experiments	80
4. 2	Summary of Locations of Jet and Intake Tubes and Vertical Density Profile Measurements	94
4. 3	Detailed Temperature Data For Experiments Number 17 and Number 18	124
5. 1	Summary of Data From FWPCA Field Experiments	132

## CHAPTER 1

## INTRODUCTION

## 1.1 DENSITY-STRATIFIED IMPOUNDMENTS

This study is an examination of artificial mixing of density-stratified (temperature-stratified) lakes and reservoirs by means of mechanical pumping systems. This technique is one of several alternatives proposed to counter the deterioration of water quality in impoundments which have become density-stratified. Abatement of the deleterious effects of density stratification on water quality is important not only in terms of immediate water supply requirements, but also in terms of long-range consequences such as eutrophication.

1.1.1 Background

The phenomenon of temperature stratification of lakes and reservoirs has been observed for several years. The cycle of the thermal regimes in impoundments in temperate climates includes a period in the summer during which vertical temperature gradients become large. This stratification persists until fall when the temperature becomes uniform throughout the impoundment and the "fall overturn" occurs. The temperature (and density) stratification of the impoundment alters the fluid motion and material transport processes in the impoundment. The gravitational stability of the density stratification tends to confine convective motions to horizontal planes and to

inhibit vertical turbulent diffusion processes. Often the vertical transport is so arrested that little oxygen reaches the lower regions of the impoundment. The resultant vertical profiles of temperature and dissolved oxygen typically show a warm, well oxygenated region close to the surface (epilimnion) and a colder, oxygen scarce region near the bottom (hypolimnion). In some cases these two regions are nearly isothermal but separated by a thermocline region which may act as a barrier to transport due its large density gradient. The formation and development of temperature stratification for a particular impoundment is a complex process governed externally by meteorological conditions and hydrological processes, and internally by fluid motions and diffusion. Studies by Orlob (35), Dake and Harleman (14, 15), Huber and Harleman (22), and Wunderlich and Elder (57) have produced simulations of this process which permit predictions of the thermal structure of the impoundment to be made.

The lack of oxygen transport to the hypolimnion region of the impoundment while oxygen is being consumed in this region often results in anaerobic conditions in the hypolimnion. Under anaerobic conditions some chemical constituents of the impoundment are reduced and appear in solution. Soluble forms of iron, manganese, and phosphorus are found in the hypolimnion in concentrations which are orders of magnitude higher than exist in epilimnion water. Anaerobic degradation of organic matter can add ammonia and hydrogen sulfide to hypolimnion waters. Increased nutrients in solution frequently lead to algae blooms,

some of which produce taste and odor problems as well as becoming the objects of degradation themselves when they sink to the hypolimnion. Reduced forms of iron and manganese, in particular, cause taste and odor problems. Detailed studies and observations of the chemical and biological changes that occur because of density stratification are reported and/or referenced by Weibe (54), Walesh (52), Churchill (11), and Symons (46).

The deterioration of water quality in impoundments used for water supply may present serious operational problems. Water withdrawn from the hypolimnion of such an impoundment may be unsuitable for use until given extensive treatment. Even if the noxious effects of hypolimnion water can be avoided during the period of stratification by withdrawing water from the epilimnion, the fall overturn may subject the entire impoundment to them until reoxygenation is complete. Impoundments which receive large inputs of nutrients and are subject to thermal stratification suffer doubly as the nutrients are kept in solution in the hypolimnion. This is the case of Lake Erie (28, 29) where concentrations of nutrients in the hypolimnion are often ten-fold those in the epilimnion during the summer. The result of this condition is an accelerated rate of eutrophication of the lake.

#### 1. 1. 2 Alternative Solutions

One obvious solution to the problem of deteriorated water quality is increased water treatment when the impoundment is tapped for water supply. While this expanded treatment may be costly, it can solve the water supply problem. However, the condition of the impoundment

itself is not improved. Thus, improving the quality of the water while it is in the impoundment has been attempted. Recognition of the need to plan for and to design methods for the treatment of water in the impoundment or for the prevention of density stratification has led several public agencies to review the possibility of incorporation of such systems in the original designs of reservoirs (37, 50).

Two strategies have been employed to achieve improved water quality in the impoundment. One strategy is that of reoxygenating the impoundment waters, particularly the hypolimnion region, without necessarily altering or eliminating the density stratification. Several techniques have been used to accomplish this, including mechanical surface aerators (40), compressed-air diffusers (4), and devices for supersaturating the water with air or pure oxygen (43). The second strategy is to mix the impoundment so that the density stratification is eliminated or altered enough for the natural processes of convection and diffusion to provide the required oxygen. Attempts to artificially mix density-stratified impoundments have been of two types: 1) mixing caused by releasing compressed-air bubbles at depth; and 2) mixing caused by the discharge of buoyant jet of water into the impoundment.

The compressed-air mixing techniques have been used to mix several impoundments. In some cases the compressed-air has been used to operate simple air-lift pumps at the bottom of the impoundment which act to induce mixing with an air-water mixture (4, 7, 10). In other cases the compressed-air is forced from perforated pipes or diffuser stones at the bottom of the impoundment to create air-bubble

plumes which induce mixing (21, 25, 30, 47, 48, 49). Many of the mixing attempts using compressed-air systems have been successful in eliminating the density stratification and in providing for reoxygenation of the hypolimnion. Attempts to mix some large reservoirs (30) have met with varied degrees of success. The principal feature of most compressed-air systems is the addition of a source of buoyancy, the air bubbles, which provides the vertical driving force required to initiate mixing. The reoxygenation which occurs in impoundments mixed with compressed-air systems seems to be due primarily to natural processes acting in the absence or reduction of density stratification. Aeration due to gas transfer from the compressed-air system, except in cases of large systems in relatively small impoundments, is a secondary effect, and alteration of the density structure is the primary function of the system. Several of the field applications of the compressed-air techniques have been successful in preventing the formation of density stratification or in preventing its recurrence by intermittent operation after an initial mixing.

Although several compressed-air systems are, or have been, employed to mix stratified impoundments (49), design information and criteria are scarce. Field experiments have permitted little control of the variables and have yielded little empirical data of a general nature. Laboratory experiments with compressed-air systems by Brainard (6) and Brush, et al. (9) isolate aspects of the problem, but they do not provide enough information for design.

The second type of technique used in attempting to mix density-stratified impoundments is that of the mechanical pumping system. It consists of a pumping apparatus which simply takes water from one elevation in the impoundment and jets it out at another. The operation of such a system is the object of this study.

## 1.2 PREVIOUS WORK WITH PUMPING SYSTEMS

The application of mechanical pumping systems for mixing impoundments has been more limited than the use of compressed-air systems. However, pumping systems may provide more efficient mixing than compressed-air systems. And they may be better suited for mixing large impoundments than air systems.

### 1.2.1 Mixing With Fixed Buoyant Jets

In 1954 Cooley and Harris (13) reported on the design of a system using buoyant jets to prevent stratification in water supply reservoirs in London. The jet inflows were located along the bottoms of the reservoirs. Since the river water inflows were warmer than the hypolimnion waters of the reservoirs, buoyant jets were created. The buoyant jet mixing successfully eliminated the density stratification and attendant water quality problems. Subsequently, jet inlet structures were designed for other reservoirs specifically to create mixing which would assure the prevention of density stratification (41).

A similar, though untoward, situation exists in the storage reservoirs of many pumped-storage hydropower projects as pointed out by Reynolds (38). Typically, the lower detention pond to which the

generators discharge is small and shallow. Temperatures of the water in this pond are larger than those in the hypolimnion of the deeper (upper) reservoir. When the water is pumped to the upper reservoir for storage, a buoyant jet is created as the water leaves the penstock. Thus, the possibility of mixing of the storage reservoir due to regular return flows exists.

### 1.2.2 Mixing With Pumping Systems

A series of reservoir mixing experiments with pumping systems has been performed by a group of investigators with the Federal Water Pollution Control Administration (23, 46, 47, 48, 49). Mixing using a similar technique has been accomplished in England (41). The pumping systems used by these groups were mounted on barges and were capable of being moved to various locations in the impoundment. Water was pumped from the lower region of the impoundment and jetted in the upper region. The jet's negative buoyancy with respect to the warm surface water causes it to move downward as well as horizontally. Such a pumping system could be operated in the reverse manner; that is, withdrawal from the surface region and jet discharge into the bottom region.

The mixings of density-stratified impoundments using this type of pumping system showed that stratification could be eliminated after relatively short periods of pumping. Improvement of water quality was observed upon the elimination of density-stratification. Studies showed that intermittent pumping of the impoundment throughout the summer



could prevent the recurrence of density stratification. The important observation was made that the pumping system was mixing much greater volumes of water than that which passed through the pump. The volumes of water pumped were always less than the volume of the impoundment.

While some data concerning the water quality parameters were gathered for these mixings, little data concerning the physical mixing were obtained. The efficiencies of the systems were calculated based on the energies supplied and the energies added to the impoundments. In some cases, unmixed lakes in the vicinity were observed in an attempt to separate natural on-going processes from the imposed mixing. However, consistent design criteria are difficult to extract from the field results and comparisons among mixings of different impoundments cannot be made on a common basis.

Some preliminary laboratory experiments with pumping systems were conducted by Brush, et al. (9). The mixing was characterized by parameters which were related to the total time for mixing of impoundments with discrete two-layer stratification. These parameters are not related to the details of the mixing process, and the experimental results were scattered over a rather small range of the parameters. The study was too limited to develop design criteria, but it represents an attempt to generalize the physical aspects of the mixing process in terms of some dimensionless parameters.

### 1.3 OBJECTIVES AND SCOPE OF PRESENT STUDY

This study deals specifically with mixing by means of mechanical pumping systems. It seeks to provide a simulation model for mixing with a pumping system which predicts the results of such mixing. The simulation model developed is limited to the physical aspects of the pumping and mixing processes and allows comparisons of results among pumping systems and with other mixing techniques. Simulation of the chemical and biological aspects of mixing may follow from an understanding of the physical mixing. Generalized results which reflect the important parameters for the design of efficient pumping systems are sought from the simulation model and laboratory experiments.

Chapter 2 presents the development of the simulation technique. Equations governing the simulation are derived, and the fluid mechanical features of selective withdrawal and buoyant jets coupled with these equations are discussed. The numerical solution of the governing equations is treated as well as a physical explanation of the simulated mixing process.

The redistribution of a conservative, non-reacting tracer by a pumping system can also be predicted by the simulation technique (Chapter 3). The use of temperature as a tracer and the incorporation of the nonlinear temperature-density relationship in the simulation is discussed.

The results of laboratory experiments are given in Chapter 4 and are compared with the results predicted by the simulation technique. A discussion of the agreement between the experimental and simulated results includes an evaluation of the assumptions underlying the simulation model.

The simulation results are compared with field and laboratory experiments by other investigators in Chapter 5.

Generalized results from several simulated mixing computations are given in Chapter 6. Dimensionless parameters for the special case of an impoundment with an initially linear density profile are used in the presentation of the results of the simulations. The calculation of relative efficiencies and a gross measure of the degree of mixing (based on energy considerations) allow an evaluation of the importance of the various dimensionless parameters. This evaluation of the generalized solutions provides some fundamental design criteria.

A summary of the simulation technique and generalized results, an evaluation of the applicability of the simulation technique to lakes and reservoirs, and recommendations for future research are given in Chapter 7.

## CHAPTER 2

### SIMULATION ANALYSIS AND TECHNIQUE

#### 2.1 FLUID MECHANICAL FEATURES OF PUMPING SYSTEMS

A pumping system, for the purposes of this study, is simply the means of removing fluid from one elevation in a density-stratified impoundment and of returning it to another elevation in the form of a jet (Fig. 2.1). In this sense, the pumping system is characterized by its properties of transport to and from the stratified body of fluid, and the details of its supporting structure and other hardware are not of primary concern.

##### 2.1.1 Description of the Fluid Mechanical Features

In its natural state, without pumping, the impoundment may experience fluid motions induced by the wind, the earth's rotation, local atmospheric pressure anomalies, inflows, and outflows. In addition to induced convective motions, radiation, evaporation, and, molecular and turbulent diffusion of heat and mass act to determine the density structure of the impoundment.

Operation of the pumping system creates additional fluid motion. The clearly notable features of this motion are the buoyant jet generated at the discharge end of the system and the withdrawal layer established where the intake withdraws fluid selectively from a stratified environment (Fig. 2.1).

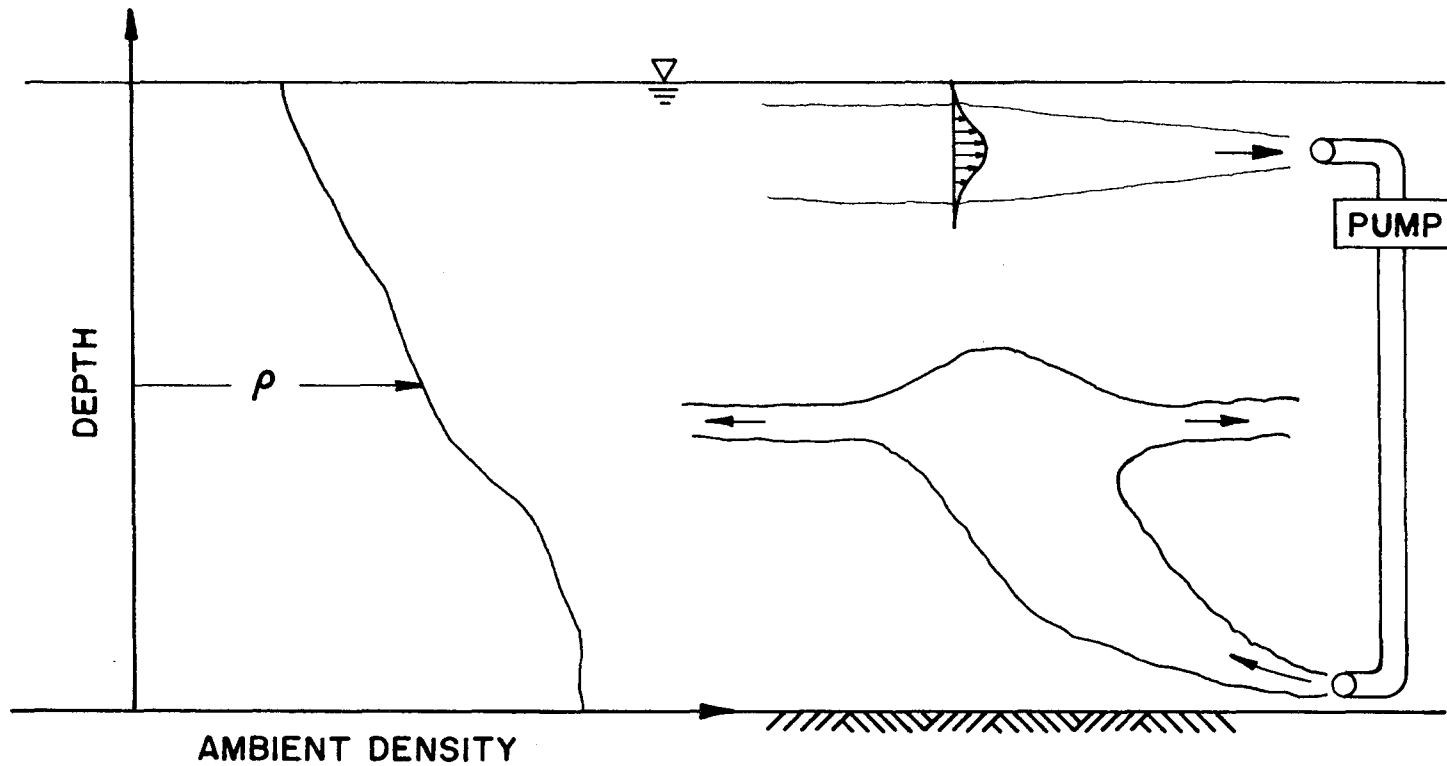


Figure 2.1 Schematic diagram of a pumping system in a density-stratified impoundment

The characteristic behavior of a turbulent buoyant jet in a density-stratified environment, as contrasted with a buoyant jet in a uniform environment, is that it does not extend to the surface, but rather reaches a maximum height of rise at some lesser elevation. The initial positive buoyancy of the jet, and any initial vertical momentum it might have by virtue of being inclined upward, is eventually counter-balanced by the heavier fluid (or negative buoyancy) that it entrains as it rises. When the fluid reaches the point of zero vertical momentum or the maximum height of rise, it possesses negative buoyancy with respect to the density of the ambient fluid at that elevation and consequently flows downward and spreads horizontally, intruding into the ambient fluid at approximately its level of neutral buoyancy. The essential function of the buoyant jet in the pumping system is to entrain fluid from the environment along its trajectory and to deliver this fluid to a different elevation in the environment at a volume rate of flow several times the initial rate. A more complete discussion of the mechanics of the buoyant jet is given in Sect. 2.2.4.

The withdrawal of fluid from a stratified environment differs from withdrawal from an environment of uniform density in that fluid is removed from distinct layers of the environment and not from all parts of it. The essential characteristic of this feature of the pumping system is that withdrawal of fluid from the impoundment is restricted to a zone of limited elevations and densities. A more complete discussion of the withdrawal layer is given in Sect. 2.2.5.

In addition to the gross features of the pumping system described above, several other phenomena may affect the density structure of the impoundment. Turbulent diffusion will be enhanced by shear at the interface of the intruding layer and the ambient fluid at the level of neutral buoyancy. Circulation patterns may be established by the entrainment of fluid by the jet.

### 2.1.2 Relative Importance of Various Features

That lakes and reservoirs generally remain density-stratified for long periods during the summer, as previously discussed, is evidence that naturally generated fluid motions do not cause rapid mixing. Extreme natural processes can act to change the density structure of the impoundment rapidly. However, impoundments which experience such frequent and rapid natural mixing are unlikely candidates for artificial mixing. The gravitational stability of the stratified impoundment makes the impoundment more conducive to horizontal fluid motions than to vertical ones. These horizontal motions contribute to vertical mixing by shearing, but this effect seems small.

While natural processes continually act to alter the density structure of the impoundment, an effective pumping system can also alter it. This study of the response of the impoundment to the pumping system supposes that the mixing due to the pumping system can be uncoupled from the natural mixing. Therefore, barring extreme natural mixing phenomena, the mixing will be governed largely by the buoyant jet and selective withdrawal created by the pumping system.

## 2.2 DEVELOPMENT OF ONE-DIMENSIONAL MODEL AND GOVERNING EQUATIONS

The purpose of the simulation technique is to predict in a gross way the changes in density stratification during the mixing process. In particular, the time history of the density-depth profiles is sought. This is accomplished by developing a simple model of the pumping system and impoundment, which retains the components deemed essential to predicting the gross behavior. As a result, the complex fluid mechanical details are ignored or presented in crude fashion with the expectation that they will have little effect on the overall response of the impoundment to the mixing. The success of such simplification can be determined only by comparing the simulation model with experimental data.

### 2.2.1 General Assumptions

The following assumptions are made for the simple simulation model. They can be altered or made less restrictive should the need for more complex models be indicated by the results of this study.

a) The stratified lake or reservoir is considered to be a closed system. Mass is conserved and no fluxes of energy are allowed through the impoundment boundaries, except those of the pumping system. Since the only influence on the density structure of the impoundment to be considered is the pumping system, the problem is an initial value problem. That is, the density-depth profiles for a given pumping system are determined by the initial density-depth profile. In the



physical problem, where the density stratification is due to temperature, this assumption will be valid if the mixing proceeds much more rapidly than changes in the heat budget. This will not always be the case. However, the present analysis isolates the effect of the pumping system from all variable external conditions.

b) The surfaces of constant density (or isopycnic surfaces) of the stratified impoundment are assumed to be horizontal planes. This implies that the densities at a given elevation are the same throughout the impoundment. The problem is now one-dimensional in that at a given time during the mixing process the only variation in density occurs vertically. The assumption is strictly correct under static conditions, as guaranteed by hydrostatic equilibrium. Although it is obviously not correct directly in the buoyant jet, return flow layers, or withdrawal layer, it is assumed correct for the impoundment in a gross sense during mixing for the purpose of the simulation.

The assumption of horizontal isopycnic surfaces has been used in other studies of the temperature structure of lakes and reservoirs. Orlob and Selna (35) and Wunderlich and Elder (57) have made similar assumptions for studies of lake and reservoir temperatures under natural and regulated conditions. While the assumption itself was not rigorously tested, predictions of temperature structure using it have agreed well with field data.

c) The relationship between the horizontal cross-sectional area of the impoundment and the depth is assumed to be known. This information permits the analysis, though one-dimensional, to be applied to

impoundments with shapes which are not necessarily prismatic. Thus, for the purpose of the simulation, the impoundment is viewed as stack of horizontal layers of differing shape and area, each of which contains fluid of constant density throughout.

d) The buoyant jet and withdrawal layer, the main features of the pumping system, are assumed to be the only components of the mixing process that require modeling in the simulation. As discussed in Sect. 2.1, other features exist, but they are assumed of secondary importance or too complex to model. The mechanics of the buoyant jet and withdrawal layer themselves are treated in a three-dimensional manner, although their effects on the impoundment are treated in the one-dimensional manner assumed above. That is, the physical impoundment is separated conceptually into two regions: Region 1 is the stratified impoundment exclusive of the buoyant jet and withdrawal layer. It is viewed in a one-dimensional sense with the density at any elevation the same throughout the impoundment at that elevation. Region 2 consists of the buoyant jet and the withdrawal layer. The behavior of these elements is governed in part by the density profile in Region 1. Changes in Region 1 represent the response of the impoundment to mixing and are governed by the transfer of fluid between the two regions.

### 2.2.2 Model and Equations

A schematic diagram of the stratified impoundment as viewed in the one-dimensional sense is shown in Fig. 2.2. The horizontal cross-sectional area,  $A$ , is a function of  $y$ , the vertical elevation

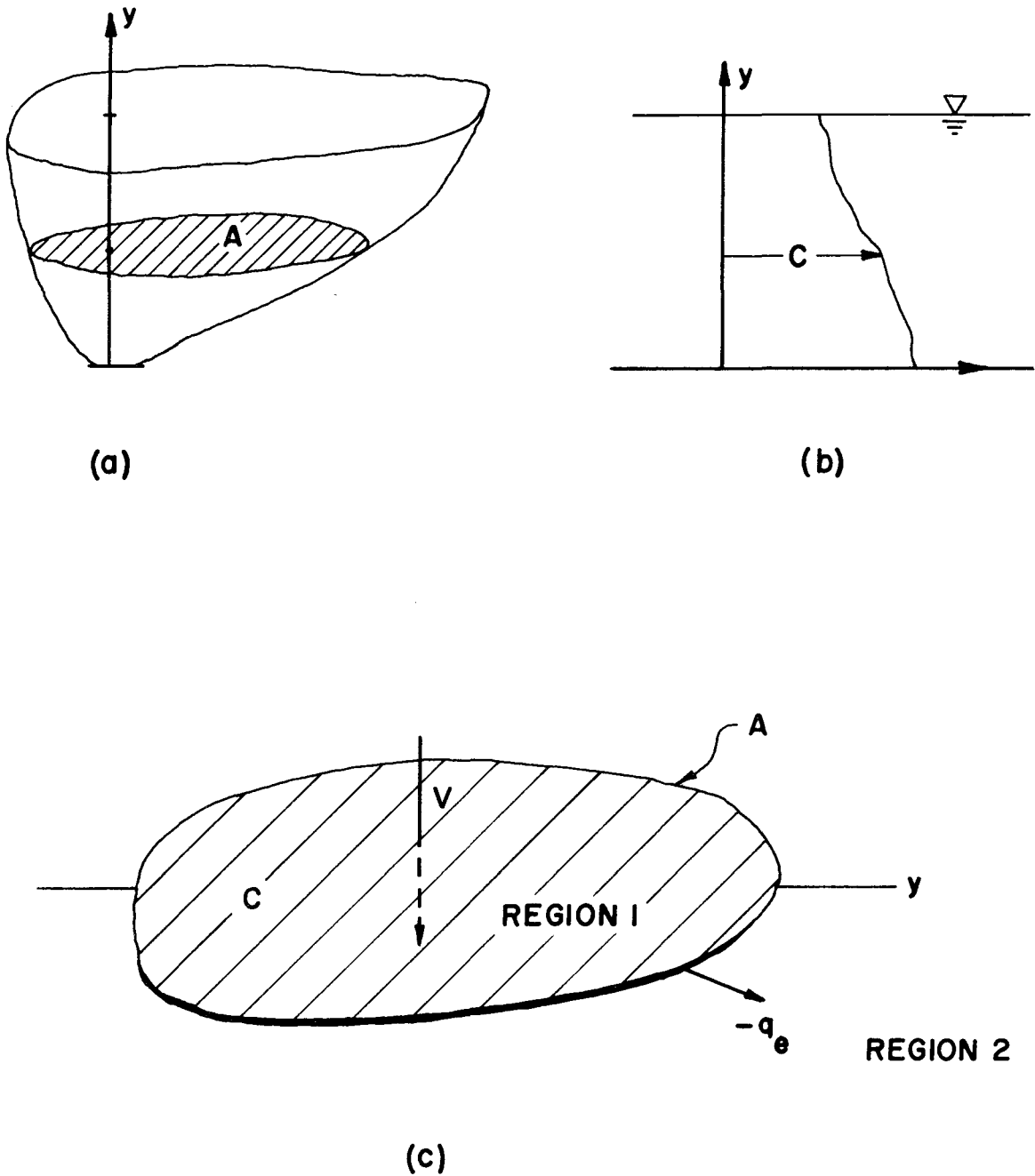


Figure 2.2 Sketch of impoundment: (a) horizontal cross-sectional area,  $A$ , (b) vertical profile of density-stratifying agent,  $c$ , (c) elemental section

with datum at the bottom of the impoundment. Fig. 2.2b shows an instantaneous vertical profile of the density-stratifying agent,  $c$ , either a concentration of mass or temperature. The stratifying agent,  $c$ , is both a function of elevation,  $y$ , and a function of time,  $t$ .

The pumping system causes fluid to be removed, in effect, from the impoundment (Region 1) at various elevations and then to be injected back into the impoundment at other elevations. The withdrawal layer and buoyant jet (Region 2) remove or entrain fluid from the impoundment as a whole. This fluid is transported by the enlarging buoyant jet until it is discharged back into the impoundment as a whole at its neutrally buoyant level. The volume rate of flow per unit depth into or from the impoundment at a given elevation is  $q_e(y, t)$ . It is positive for fluid transported into the impoundment (Region 1) and negative for fluid extracted.

Discharge of fluid into and from the impoundment at various elevations and the conservation of total mass require the fluid at some elevations to be moved up at a given time and at other elevations moved down. The effective transport velocity characterizing this vertical movement is  $v(y, t)$ .

Fig. 2.2c shows schematically a horizontal cross-section of the impoundment at elevation  $y$  with area  $A$ , density-stratifying agent,  $c$ , and the flow per unit depth from Region 1 to Region 2,  $q_e$ .

Continuity requires that:

$$\frac{\partial(vA)}{\partial y} = q_e(y, t) \quad . \quad (2.1)$$

Conservation of the density-stratifying agent,  $c$ , requires that:

$$A \frac{\partial c}{\partial t} + \frac{\partial}{\partial y} (cvA) = cq_e \quad . \quad (2.2)$$

Eq. (2.2) is correct over the depth so long as the value of  $c$  associated with the fluid discharged into or from the impoundment at the elevation  $y$  is the same as the value of  $c$  at that elevation in the impoundment.

This condition is satisfied in Regions 1 and 2 in terms of the density of the fluid, for fluid is discharged into and from the impoundment from the withdrawal layer and jet only at elevations of equal density.

Combining Eq. (2.1) and Eq. (2.2) and simplifying leads to the following two governing equations:

$$\frac{\partial}{\partial y} (vA) = q_e \quad , \quad (2.1)$$

$$\frac{\partial c}{\partial t} + v \frac{\partial c}{\partial y} = 0 \quad . \quad (2.3)$$

It can be shown that Eqs. (2.1) and (2.3) follow from the full continuity and tracer conservation equations for an incompressible stratified fluid by integrating over the horizontal area, neglecting vertical diffusion in the impoundment (Region 1) and assuming small density differences to exist.

The continuity equation relates the vertical transport velocity,  $v$ , to the transport from Region 2 to Region 1,  $q_e$ , at a given time. The discharge,  $q_e$ , is a function of the density profile in the impoundment at a given time, as well as a function of elevation. Determination of  $q_e$  as a function of  $y$  at a given time requires the knowledge of the behavior of the buoyant jet and withdrawal layer (Region 2) in the density profile in the impoundment (Region 1) at that time.

### 2.2.3 Physical View of the Governing Equations

The solution of Eqs. (2.1) and (2.3) requires a knowledge of the vertical distribution of  $q_e$ , the discharge per unit depth to or from the impoundment (Region 1), at a given time. An example of the vertical distribution of  $q_e$  at a particular time during mixing is given in Fig. 2.3. The flows created by the pumping system are shown schematically in Fig. 2.3a, and the corresponding distribution of  $q_e$  is shown in Fig. 2.3b.

The entrainment of the jet (Region 2) from the impoundment (Region 1) is negative and is shown between elevations A and C. The detailed distribution of  $q_e$  over this zone is governed by the jet mechanics and is given in Sect. 2.2.4. Elevation C is the level of neutral buoyancy, and the zone between elevations B and D contains the positive return flow from the jet into the impoundment. There is no transport of fluid from jet or withdrawal layer (Region 2) to the impoundment (Region 1) between elevations D and E. Selective withdrawal creates the negative transport from the impoundment between elevations E and F. The specific shape of the  $q_e$  distribution in this zone is given in Sect. 2.2.5. There is no further transport between regions from the top of the withdrawal layer, F, to the surface, G.

Continuity requires that

$$\int_A^G q_e \, dy = 0 \quad . \quad (2.4)$$

The integration of  $q_e$  over the withdrawal layer, E to F, yields  $-Q_j$ , the discharge pumped from top to bottom. Similarly, integration of  $q_e$

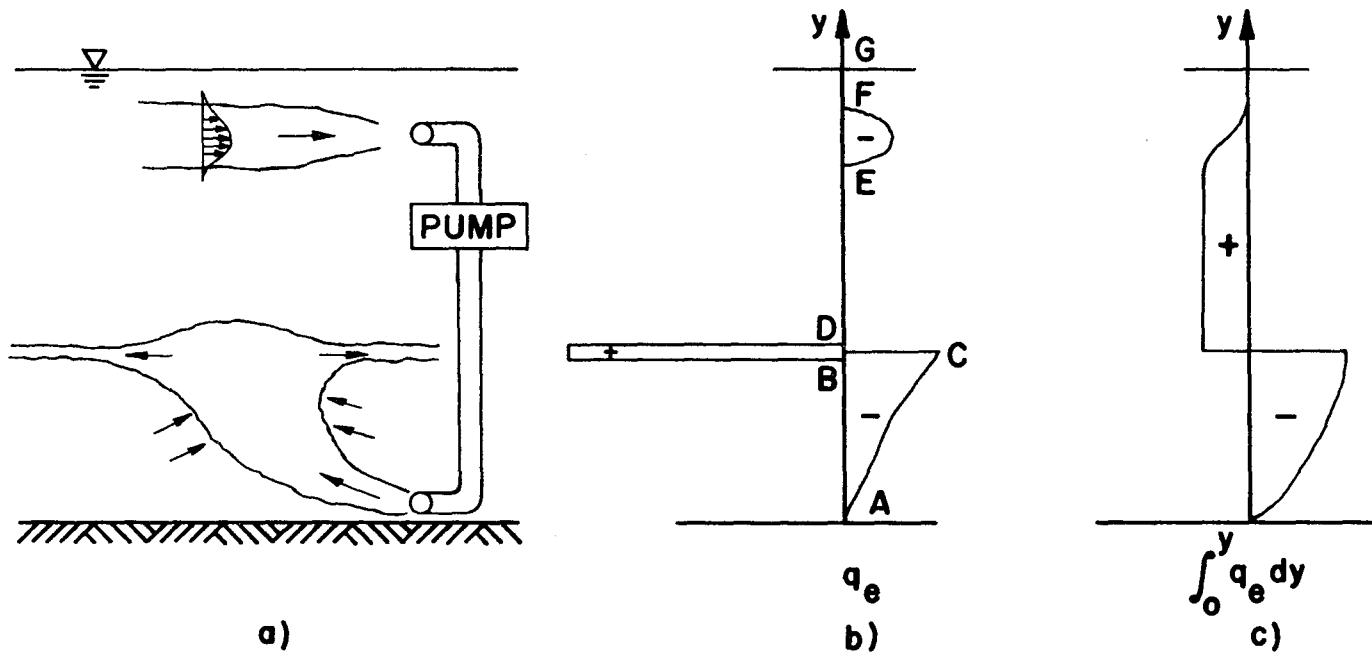


Figure 2.3 Pumping system (a) with typical distributions of  $q_e$  (b) and integrated  $q_e$  (c)

over the zone between elevations C and D yields  $+Q_j$ . The integration of  $q_e$  from elevation A to elevation C equals zero, as the discharge into the impoundment between B and C is just that fluid which was entrained from the impoundment by the jet between elevations A and C.

The solution to Eq. (2.3) requires that the vertical transport velocity,  $v(y, t)$  be known. The transport velocity at any elevation  $y$  for a particular time is given by the integration of Eq. (2.1)

$$\frac{\partial(vA)}{\partial y} = q_e, \quad (2.1)$$

$$v(y) = \frac{1}{A(y)} \int_0^y q_e(\xi) d\xi. \quad (2.5)$$

Given the distribution of  $q_e$  over the depth at a particular time, the transport velocity is found by Eq. (2.5), and the distribution of  $vA$  is shown in Fig. 2.3c. The transport velocity above the level of neutral buoyancy (elevation C) is positive (or upward) and below is negative (or downward).

Sect. 2.2.4 and 2.2.5 contain the detailed descriptions of the buoyant jet and selective withdrawal mechanics necessary to present the distributions of  $q_e$  and  $v$  in quantitative terms.

#### 2.2.4 Buoyant Jet Mechanics Involved to Obtain $q_e$

The determination of the discharge or entrainment from the impoundment into the rising round buoyant jet requires detailed knowledge of the buoyant jet. The trajectory must be found so that the entrainment  $q_e$  is known as a function of elevation. The elevation at



which the density of the fluid in the buoyant jet is equal to that in the ambient fluid of the impoundment (i. e. the level of neutral buoyancy) must be known to locate the zone over which flow discharged back into the impoundment. The velocity and width of the buoyant jet must be known as a function of elevation to make the calculation of  $q_e$ , the fluid entrained from the impoundment.

The mechanics of buoyant jets and plumes in uniform or linearly stratified environments have been formulated and verified experimentally by several investigators. Vertical plumes (zero initial momentum) in a uniform environment have been studied by Schmidt (42) and by Morton, Taylor, and Turner (34). Vertical and horizontal buoyant jets (initial momentum) or forced plumes in a uniform environment have been studied by Abraham (1). Vertical buoyant jets in a linearly stratified environment have been studied by Morton (33). The general case of a buoyant jet inclined at any angle in a linearly stratified environment has been studied by Fan (18) and Fan and Brooks (19). Detailed explanations of the studies mentioned above and of additional theoretical and experimental studies can be found in Fan (18).

The integral technique introduced by Morton, Taylor, and Turner (34) to solve the problem of the simple plume and used by Fan (18) to solve the problem of an inclined buoyant jet in a linearly stratified environment is followed here. An abbreviated description of this technique, as it was applied by Fan (18) for the case of a linearly stratified environment is given here as a preface to the extension to the case of an inclined buoyant jet in an arbitrarily stratified environment. The solution to the latter is required for the mixing problem.

Fig. 2.4 shows schematically a turbulent, round buoyant jet inclined at the origin at an angle  $\theta_0$  with the horizontal. The environment is linearly stratified. The general assumptions of the analysis are:

- 1) The fluids are incompressible.
- 2) The Boussinesq assumption requires that variations of density throughout the flow field are small relative to the reference density chosen. Thus, variations in density are neglected in inertia terms but included in gravity terms.
- 3) The density of the fluid is assumed to be a linear function of either mass concentration (e.g. salt) or temperature for the range of variation.
- 4) The flow is fully turbulent. This means that the analysis holds only in the zone of established flow and must be corrected to account for the zone of flow establishment near any finite size source.
- 5) The longitudinal turbulent transport is small relative to longitudinal convection.
- 6) The pressure throughout the flow field is hydrostatic.
- 7) The curvature of the jet trajectory is small.
- 8) The velocity profiles are similar at all cross-sections normal to the jet trajectory. Also, the profiles for buoyancy and concentration of a tracer are assumed similar. The similarity assumption is met by using axisymmetric Gaussian profiles, as follows:

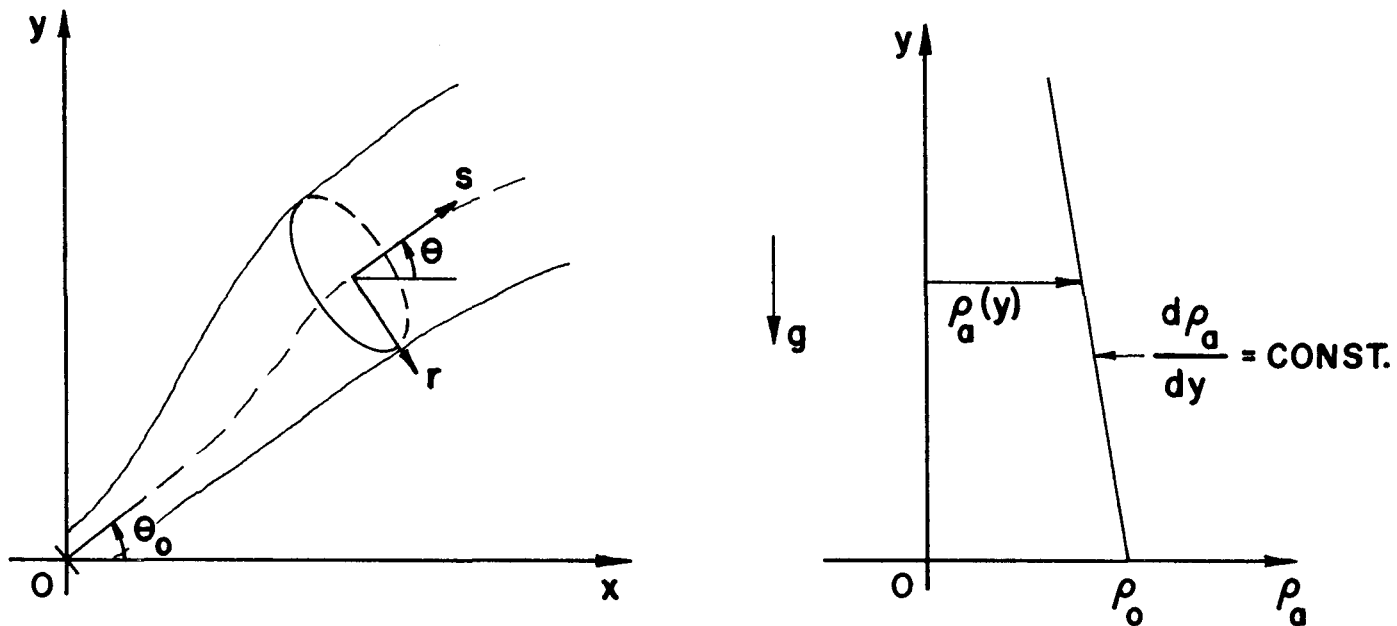


Figure 2.4 Definition sketch for a buoyant jet in a linearly stratified environment

$$\text{Velocity: } u_*(s, r) = u(s) e^{-r^2/b^2} \quad (2.6)$$

$$\text{Buoyancy: } \frac{\rho_a^*(s, r) - \rho^*(s, r)}{\rho_o} = \frac{\rho_a(s) - \rho(s)}{\rho_o} e^{-r^2/(\lambda b)^2} \quad (2.7)$$

$$\text{Tracer: } c_1^*(s, r) = c_1(s) e^{-r^2/(\lambda b)^2} \quad (2.8)$$

The terms  $u_*$ ,  $\rho_a^*$ ,  $\rho^*$  and  $c_1^*$  are the velocity, ambient density, density in the jet, and the concentration in the jet, respectively, and are related to the center line values  $u(s)$ ,  $\rho_a(s) - \rho(s)$ ,  $c_1(s)$  by the Gaussian form. The tracer  $c_1$  is present in the jet only. The nominal half width of the jet is  $\sqrt{2}b$  ( $=2\sigma$ ), and  $1/\lambda^2$  is the turbulent Schmidt number, assumed constant. The reference density is  $\rho_o = \rho_a(0)$ .

- 9) The entrainment relation or volume flux derivative is given by the equation:

$$dQ/ds = 2\pi\alpha ub \quad (2.9)$$

where  $Q$  is the volume flux and  $\alpha$  is a coefficient of entrainment, assumed constant.

Using these assumptions, the conservation equations for mass, momentum, buoyancy, together with the geometric relations, are evaluated using the integral technique of Morton, Taylor, and Turner (34). This method yields the following equations (Fan, 18):

$$\text{Continuity} \quad \frac{d}{ds} (ub^2) = 2\alpha ub \quad (2.10)$$

$$\text{x-Momentum} \quad \frac{d}{ds} \left( \frac{u^2 b^2}{2} \cos \theta \right) = 0 \quad (2.11)$$

$$\text{y-Momentum} \quad \frac{d}{ds} \left( \frac{u^2 b^2}{2} \sin \theta \right) = g \lambda^2 b^2 \frac{(\rho_a - \rho)}{\rho_o} \quad (2.12)$$

$$\text{Buoyancy} \quad \frac{d}{ds} \left[ u b^2 (\rho_a - \rho) \right] = \frac{1 + \lambda^2}{\lambda^2} b^2 u \frac{d\rho_a}{ds} \quad (2.13)$$

$$\text{Tracer} \quad \frac{d}{ds} (c_1 u b^2) = 0 \quad (2.14)$$

$$\text{Geometry} \quad \frac{dx}{ds} = \cos \theta \quad (2.15)$$

$$\frac{dy}{ds} = \sin \theta \quad (2.16)$$

where the seven variables  $u$ ,  $b$ ,  $\theta$ ,  $c_1$ ,  $(\rho_a - \rho)$ ,  $x$ , and  $y$  are functions of  $s$  only.

Although closed form solutions to these equations are not possible, they can be solved by quadrature. For the case of a linearly stratified environment,  $\frac{d\rho_a}{dy} = \text{constant}$ . For this case Fan (18, 19) has normalized these equations and presented nondimensional solutions, obtained by quadrature, as functions of two nondimensional parameters.

While linearly stratified environments often occur or are closely approximated in many situations, many instances exist in which the stratification is clearly not linear. In the simulation model an initially linear density profile will be shortly made nonlinear by the mixing process. In order to find the behavior of a buoyant jet, and hence its entrainment from the impoundment in the mixing simulation, the behavior of a buoyant jet in any stable arbitrary stratification must be determined.

A method of solution for the case of a buoyant jet in an arbitrary density stratification has been determined (17). Since the density gradient  $d\rho_a/dy$  is no longer constant with elevation and along the jet trajectory, the equations cannot be normalized as in the case of linear stratification. The solution is found in dimensional parameters. The equations for quadrature are obtained by simplifying Eqs. (2.10) to (2.16) and are:

$$\frac{du}{ds} = \frac{2g\lambda^2}{u} \frac{(\rho_a - \rho)}{\rho_o} \sin \theta - \frac{2u\alpha}{b} , \quad (2.17)$$

$$\frac{db}{ds} = 2\alpha - \frac{b}{u^2} g\lambda^2 \frac{(\rho_a - \rho)}{\rho_o} \sin \theta , \quad (2.18)$$

$$\frac{d\theta}{ds} = \frac{2g\lambda^2}{u^2} \frac{(\rho_a - \rho)}{\rho_o} \cos \theta , \quad (2.19)$$

$$\frac{d(\rho_a - \rho)}{ds} = \frac{1 + \lambda^2}{\lambda^2} \sin \theta \frac{d\rho_a}{dy} - \frac{2\alpha}{b} (\rho_a - \rho) , \quad (2.20)$$

$$\frac{dx}{ds} = \cos \theta , \quad (2.21)$$

$$\frac{dy}{ds} = \sin \theta , \quad (2.22)$$

$$c_1 u b^2 = \text{constant} = c_{1o} u_o b_o^2 . \quad (2.23)$$

Since the integration of these equations by quadrature is a step-wise calculation along the trajectory,  $s$ , it is possible to vary the density gradient,  $\frac{d\rho_a}{dy}$ , in Eq. (2.20) to match the local ambient density gradient at the elevation corresponding to that point on the trajectory. Therefore, the calculation of the jet parameters proceeds with continual adjustment of the ambient density gradient with changes in elevation.

The calculation is accomplished using a computer subroutine which employs the Runge-Kutta-Gill method of integration with an automatic control of the truncation error. A more detailed description of the calculation technique is given in Ref. (17).

Initial values for the jet parameters and values for the constants  $\alpha$  and  $\lambda$  are required to begin the calculation. Fan (18) found that an entrainment coefficient,  $\alpha = 0.082$ , and a spreading ratio,  $\lambda = 1.16$ , were satisfactory for his work with buoyant jets in a linearly stratified environment. While the technique proposed above for nonlinearly stratified environments has not been compared extensively with experiments, a comparison with an experiment by Hart (20) for a vertical buoyant jet is shown in Fig. 2.5. The values  $\alpha = 0.082$  and  $\lambda = 1.16$  were used and the width (2b), maximum height of rise (point b), and neutrally buoyant level (point a) are predicted quite well.

Since the solution outlined above is valid only in the zone of established flow (fully turbulent region), the initial values for b and  $(\rho_a - \rho)$  must be corrected to account for the zone of flow establishment. For simple nonbuoyant momentum jets this zone was found by Albertson et al. (2) to extend 6.2 source diameters from the source. Fan (18) showed that conservation of momentum between the source and zone of established flow requires that the initial value of b be  $D/\sqrt{2}$ , where D is the source diameter, and the initial value of  $(\rho_a - \rho)$  be  $(1 + \lambda^2)/2\lambda^2$  times the value at the source (17). While most buoyant jets associated with the mixing process described herein are initially horizontal so that

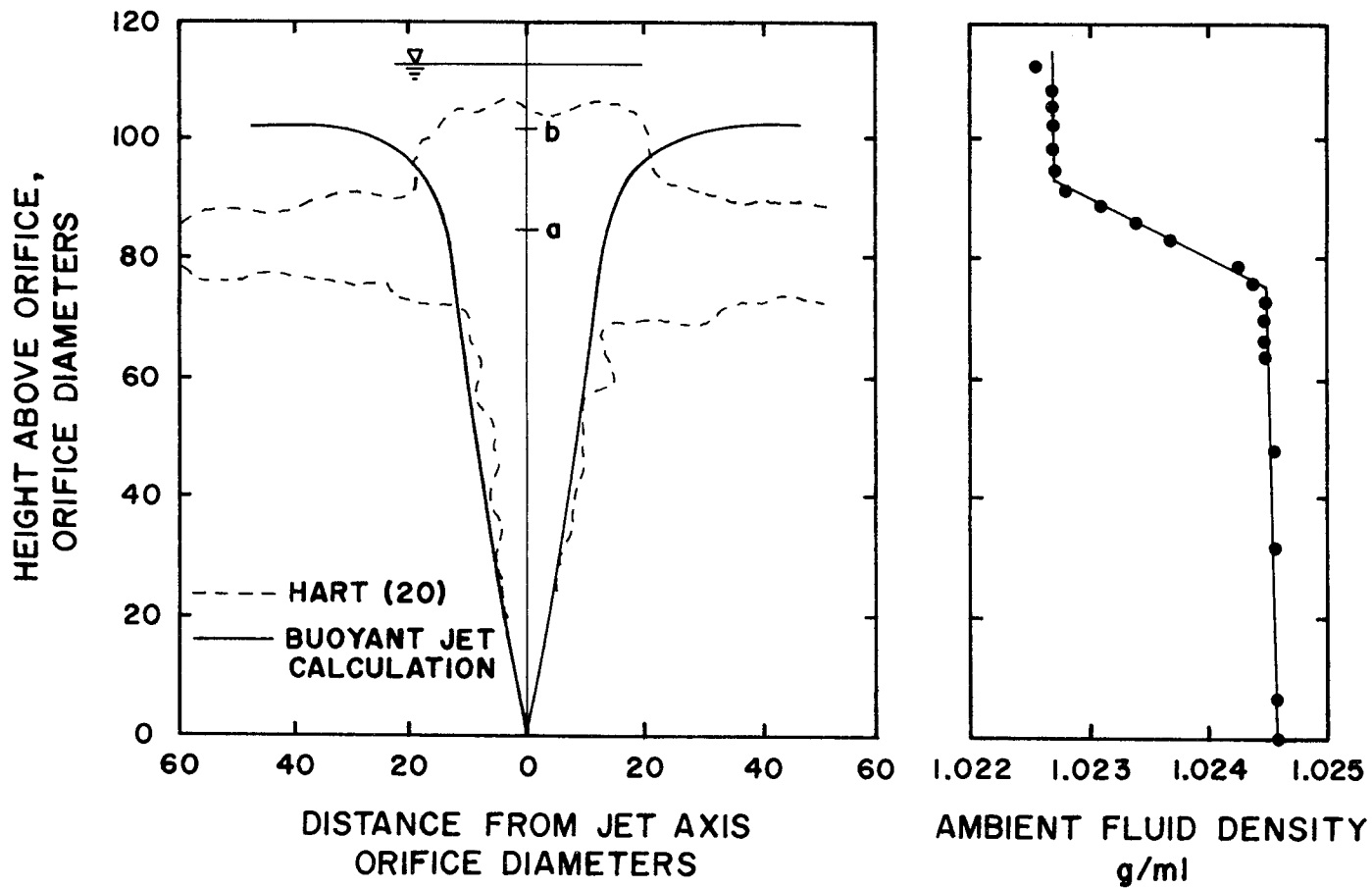


Figure 2.5 Comparison of buoyant jet theory for nonlinearly stratified environment with Hart's experiment (20)



the zone of flow establishment does not require a correction to the vertical coordinates calculated, it should be recognized that for jets with an initial angle of inclination,  $\theta_0$ , the calculation begins at  $y = 6.2 D \sin \theta_0$  instead of  $y = 0$ .

The purpose of the calculation of the buoyant jet parameters  $u$  and  $b$  is to allow the computation of the jet entrainment and thus the discharge per unit depth,  $q_e$ , from the impoundment. The volume flux in the buoyant jet at any  $y$  is:

$$\int_0^\infty 2\pi u_* r dr = \pi u b^2 . \quad (2.24)$$

The entrainment into the jet (Region 2),  $-q_e$ , is the change in volume flux during a change in distance

$$\frac{d}{ds} (\pi u b^2) = 2\pi u b = -q_e , \quad (2.25)$$

as given in Eq. (2.9). However, the integrated form of Eq. (2.1) is required to obtain  $v(y)$  at a given time for the solution of Eq. (2.3):

$$v(y) = \frac{1}{A(y)} \int_0^y q_e(\xi) d\xi . \quad (2.5)$$

The integral on the right hand side of Eq. (2.5)

$$\int_0^y q_e(\xi) d\xi , \quad (2.26)$$

is the summation of all the jet entrainment up to the elevation  $y$ . This is simply the volume flux at  $y$  minus the initial fluid discharged, i. e.

$$\int_0^y q_e(\xi) d\xi = -\pi u(y) b^2(y) + Q_j , \quad (2.27)$$

where  $Q_j$  is the jet discharge at the origin.

Therefore,

$$v(y) = - \frac{1}{A(y)} \left[ \pi u(y) b^2(y) - Q_j \right] , \quad (2.28)$$

over the trajectory of the buoyant jet only.

Calculation of the buoyant jet trajectory and parameters provides information as to the elevation at which fluid is discharged back into the impoundment and the rate at which this occurs. As previously discussed, and shown in Fig. 2.5 and 2.6, the buoyant jet reaches a maximum height of rise at which the fluid in the jet is negatively buoyant with respect to the ambient fluid at that elevation. This is the elevation of zero vertical momentum and is predicted well by jet mechanics, although the similarity assumptions break down. The fluid sinks back slightly to its level of neutral buoyancy and spreads horizontally into the impoundment. Although mixing occurs as the fluid reaches this elevation, the level of neutral buoyancy can be approximated by that elevation at which the center line density in the rising jet is equal to the density of the environment. For the simulation model the level of neutral buoyancy ( $\ell_{nb}$ ) is defined as the elevation at which

$$\rho(y) = \rho_a(y) , \quad (2.29)$$

jet (Region 2)      impoundment (Region 1)

and the rate at which fluid is discharged to the impoundment as

$$\pi u(y_{\ell_{nb}}) b^2(y_{\ell_{nb}}) . \quad (2.30)$$

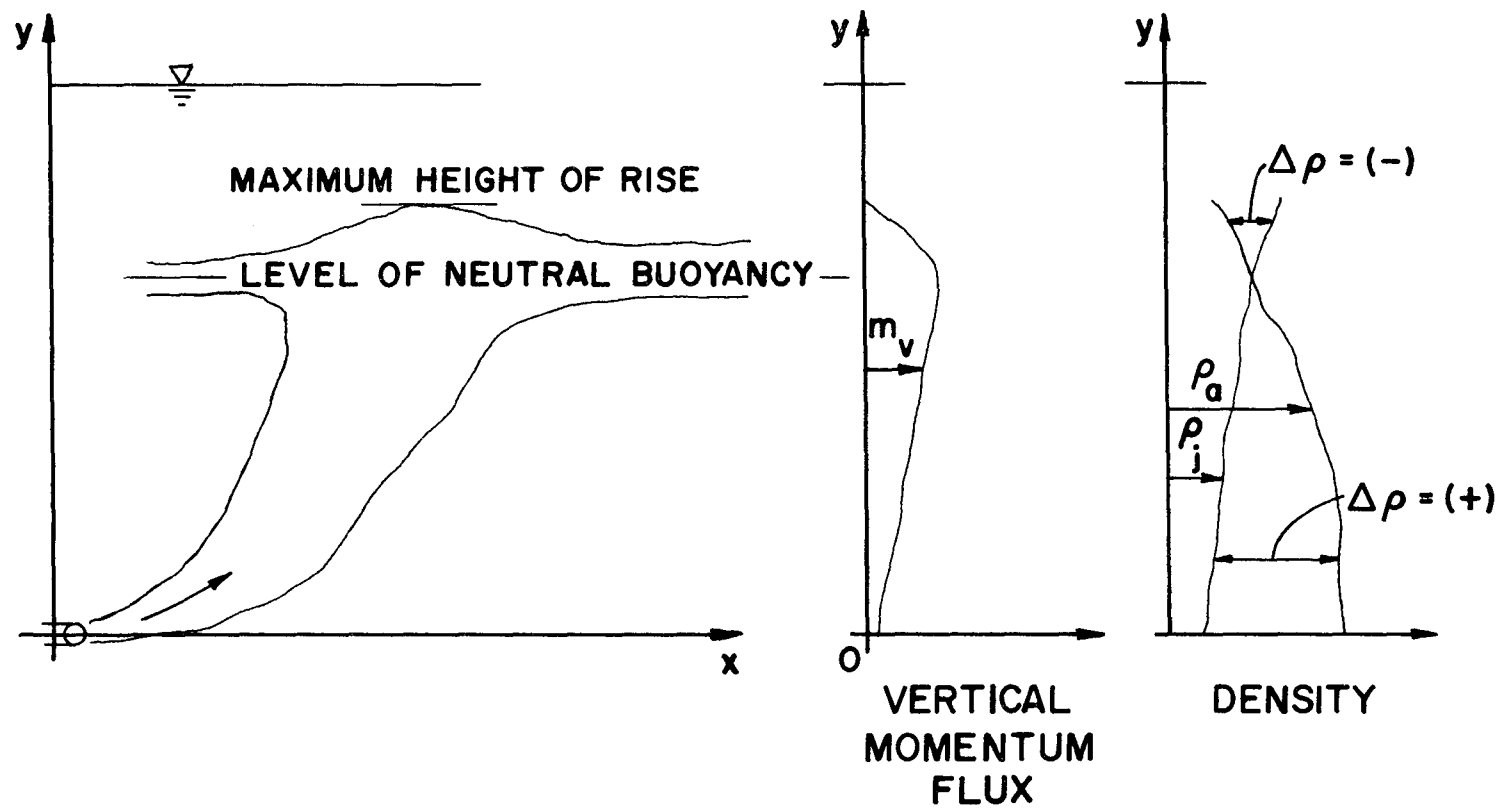


Figure 2.6 Sketch of buoyant jet vertical momentum flux,  $m_v$ , and center line density,  $\rho_j$ , in ambient density profile,  $\rho_a$

### 2.2.5 Selective Withdrawal Mechanics Involved to Obtain $q_e$

The extent of the selective withdrawal layer and the distribution of discharge from the impoundment in the layer are required to determine  $q_e$  for the simulation in this region.

A detailed account of the development of theoretical models for selective withdrawal in discretely stratified and continuously stratified impoundments is given by Brooks and Koh (8). The case of a continuously stratified impoundment is representative of the type of stratified situation often encountered in lakes and reservoirs. The special case of a weak, linear stratification was studied by Koh (27) and others, as this assumption makes the problem mathematically tractable.

Experiments were performed by Debler (16) to confirm the predictions of Yih (59) and others for the inviscid, nondiffusive selective withdrawal from a linearly stratified impoundment. The flow is considered to be two-dimensional. The thickness of the withdrawal layer,  $\delta$ , for these experiments can be expressed as:

$$\frac{\delta}{a} = 2.7 \pm 0.2 \quad , \quad (2.31)$$

where

$$a = \left( \frac{q^2}{g\epsilon} \right)^{\frac{1}{4}} \quad (2.32)$$

$$\epsilon = - \frac{1}{\rho_0} \frac{d\rho}{dy} a = \text{constant} \quad (2.33)$$

$g$  is the gravitational acceleration,  $q$  is the discharge per unit width, and  $\epsilon$  is constant. This solution indicates no growth in the thickness of

the withdrawal layer with distance from the source, but the inviscid, nondiffusive conditions under which it was found make it essentially a near-sink solution.

Koh (26, 27) studied the case of viscous, diffusive selective withdrawal from a linearly stratified impoundment. The steady equations of motion are linearized for the perturbation solution, and the solution is limited to low speed laminar-linear flow. The principal features of the solution are a similarity solution for the velocity distribution across the withdrawal layer and a withdrawal layer thickness that increases as the one-third power of the distance upstream from the outlet. Laboratory experiments in which linear density profiles were created using both salt and temperature were performed. The theoretical results were verified and extended beyond the limits of the theory using the experimental results.

Brooks and Koh (8) point out that selective withdrawals associated with lakes or reservoirs are likely to be turbulent due to their large scale or large Reynolds numbers. If turbulent resistance and mixing are neglected, an inviscid analysis results and, as suggested above, applies only near the outlet. However, vertical mixing may be important away from the outlet. Brooks and Koh (8) modified and extended Koh's results for a viscous, diffusive flow to the case of a turbulent, diffusive flow. Incorporation of turbulent exchange coefficients to replace the molecular viscosity and diffusion coefficients as well as some notions about self-generated turbulent flows lead to

results amenable to large scale flows. These changes do not affect the similarity solution for the velocity distribution across the withdrawal layer, but they do provide new estimates of the layer thickness. Again, these results apply to two-dimensional flows in linearly stratified impoundments. The solutions for two zones beyond the region in which the inviscid solution would apply are as follows (8):

$$\text{for } 2.7 < \frac{\delta}{a} < 13.7$$

$$\frac{\delta}{a} = 8.4 k_2^{\frac{1}{4}} \left( \frac{x}{a} \right)^{\frac{1}{4}} \quad (2.34)$$

$$\text{for } \frac{\delta}{a} > 13.7$$

$$\frac{\delta}{a} = 7.14 k_2^{\frac{1}{3}} \left( \frac{x}{a} \right)^{\frac{1}{3}} \quad (2.35)$$

where  $a$  is defined by Eq. (2.32) and  $x$  is the distance from outlet. The coefficient  $k_2$  is a constant of proportionality used in defining a turbulent diffusion coefficient  $E_m$  as follows:

$$E_m = k_1 u_{\max} \delta = k_2 q \quad (2.36)$$

where  $u_{\max}$  is the maximum velocity in the flowing layer of thickness  $\delta$ .  $E_m$  is defined using  $u_{\max}$  and  $\delta$  as the characteristic velocity and length scale, respectively.

Though  $k_2$  is regarded as a universal constant for flow in turbulent withdrawal layers, its value is yet undetermined. Brooks and Koh present solutions based on a range of values for  $k_2$  from  $10^{-2}$  to  $10^{-4}$ , (see Fig. 2.7), and an application to a field study resulted in a

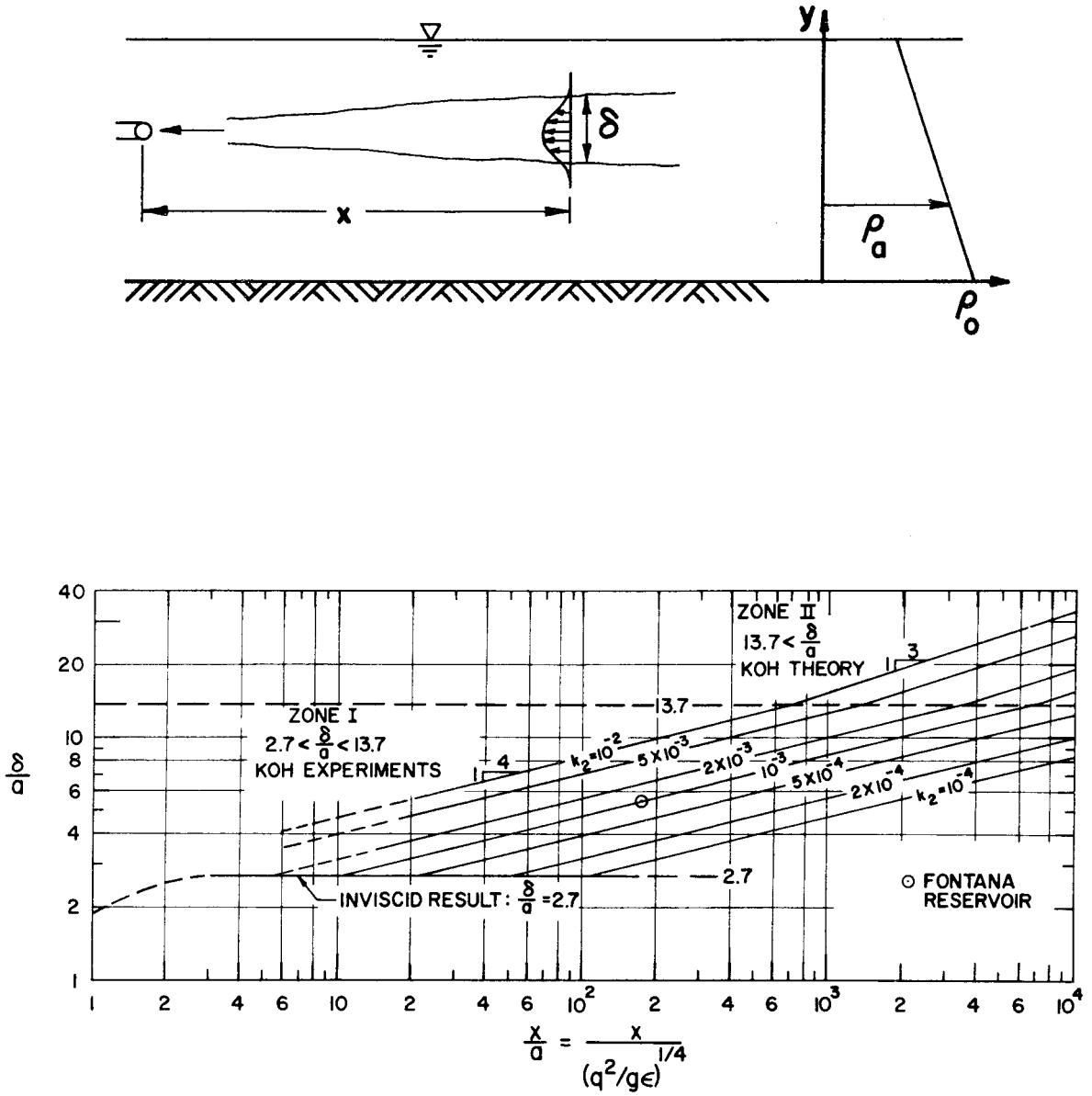


Figure 2.7 Definition sketch for turbulent withdrawal layer and solutions of Brooks and Koh (8)

value for  $k_2$  of  $10^{-3}$ . This produced a value of  $E_m$  of the order  $8 \text{ cm}^2 / \text{sec}$  which is within the region of values often calculated for the vertical diffusion of heat in lakes (35). Additional field data from studies on Tennessee Valley Authority reservoirs (51, 58), while too limited to confirm the theory, indicate that  $k_2$  is of the order of  $10^{-3}$ .

The theoretical descriptions of withdrawal layers discussed to this point have required that the density profile in the impoundment be linear. Since linear density profiles are not always present or approximated in lakes and reservoirs, there is strong interest in understanding the behavior of withdrawal layers in nonlinear, continuous density stratification. Theoretically, the analysis of the nonlinear case is quite difficult.

Wood (55) has shown that similarity solutions for the velocity in the withdrawal layer exist when fluid is withdrawn from a reservoir into a contracting channel. Other studies (5, 24) using laboratory experiments as a guide have produced semi-empirical or trial and error solutions for withdrawal layer thickness. Lack of reliable field data has hindered verification of these techniques.

Changes in the density profile due to selective withdrawal are usually small relative to changes due to entrainment by the buoyant jet. This is so because the thickness of the withdrawal layer is usually a smaller portion of the depth than the vertical extent of the jet, and the discharge from the layer may be one or more orders of magnitude less than that eventually delivered by the jet (Eq. 2.27). For these reasons,



a rather simplistic model of the withdrawal layer is utilized in the simulation to calculate  $q_e$  for the withdrawal region. A more sophisticated approach is possible but not necessarily warranted.

The withdrawal layer is assumed to be two-dimensional with the discharge per unit width defined as the pumped discharge divided by the average width of the impoundment at the elevation of the intake. While this assumption is not valid near the intake, limited field studies (51, 53) show some justification for it away from the intake. For a given density profile, the withdrawal layer thickness,  $\delta$ , is estimated by assuming a linear density gradient based on the gradient at the elevation of the center line of the outlet. A thickness near the outlet is calculated using the solution to the inviscid case given by Eq. (2.31). The thickness of a turbulent withdrawal layer at the greatest distance,  $x$ , in the impoundment from the outlet is calculated using Eq. (2.34) or (2.35) from Brooks and Koh (8). A value for  $k_2$  is assumed of the order  $10^{-3}$ . These two values for the thickness of the withdrawal layer are assumed to bound the range of the growing layer. For the purpose of the one-dimensional simulation, the mean of these two values is used to represent, in a gross way, that part of the vertical profile over which selective withdrawal occurs.

The velocity distribution across a withdrawal layer of this thickness follows the similarity solution found by Koh (26) for the region of forward flow. It is symmetric about the center line of the withdrawal layer. Fig. 2.8 shows Koh's similarity solution for velocity, calculated numerically, for half the withdrawal layer thickness. This distribution

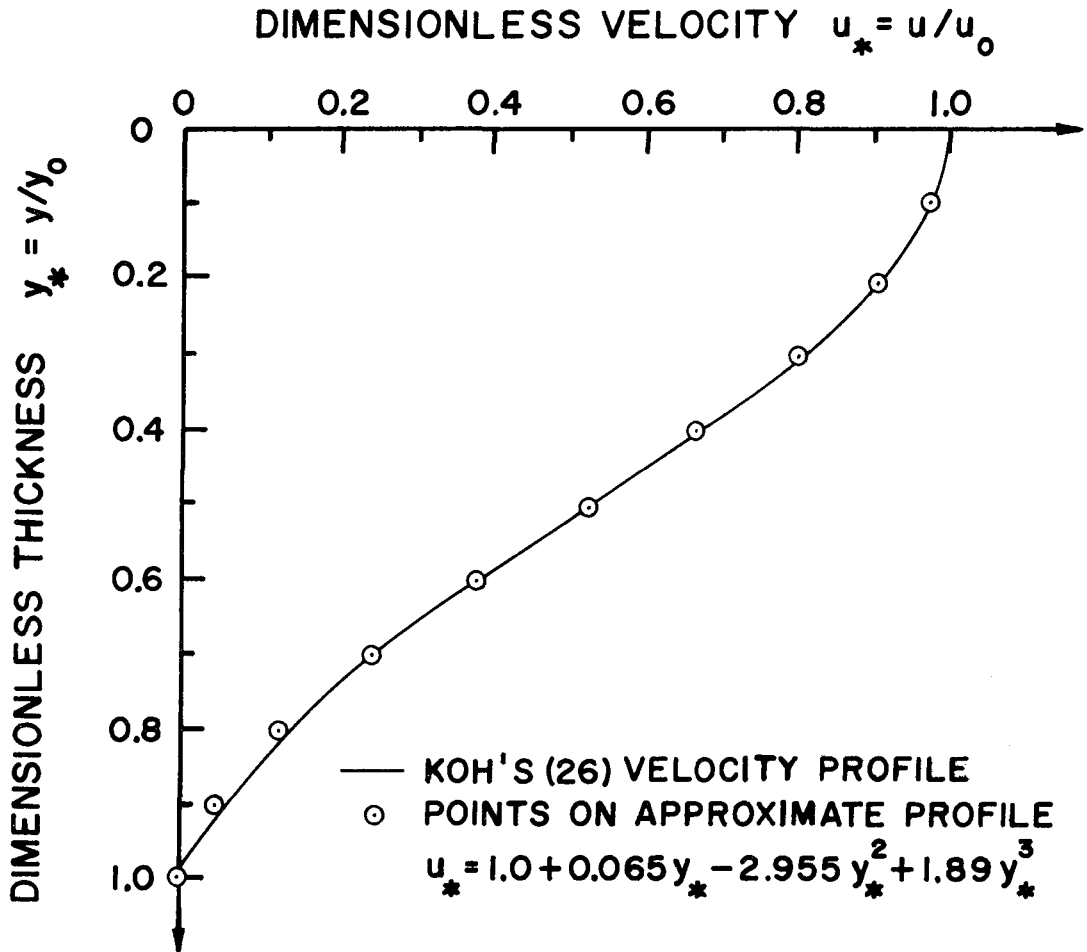


Figure 2.8 Normalized velocity profile for half of withdrawal layer, Koh's (26) theory and approximate profile

can be approximated by means of the polynomial

$$u_* = 1. + .065 y_* - 2.955 y_*^2 + 1.89 y_*^3 , \quad (2.37)$$

where

$$u_* = u/u_o$$

$$y_* = y/y_o$$

$y_o$  and  $u_o$  are the layer half thickness and center line velocity, respectively, and  $y$  is measured from the layer center line. The discharge per unit depth from the impoundment through the withdrawal layer,  $-q_e$ , is simply  $u$  times the average width at that elevation.

As noted in Sect. 2.2.3, the integrated form of  $q_e$  or the vertical transport velocity,  $v$ , is of primary interest for solution of the governing equations. Recall that

$$v(y) = \frac{1}{A(y)} \int_0^y q_e(\xi) d\xi . \quad (2.5)$$

For the calculation of  $v(y)$  in the withdrawal layer, this integral can be divided into two integrals: one from  $y = 0$  to the bottom of the withdrawal layer,  $y_E$ , and one from the bottom of the withdrawal layer to any elevation in the layer:

$$v(y) = \frac{1}{A(y)} \int_0^{y_E} q_e(\xi) d\xi + \frac{1}{A(y)} \int_{y_E}^y q_e(\xi) d\xi . \quad (2.37)$$

However, as shown in Sect. 2.2.3, the first integral is simply the total pumped discharge,  $Q_j$ , and

$$v(y) = \frac{Q_j}{A(y)} + \frac{1}{A(y)} \int_{y_E}^y q_e(\xi) d\xi. \quad (2.38)$$

The total discharge from the impoundment (Region 1) into the withdrawal layer (Region 2) is known, a priori, to be  $-Q_j$ , whereas for the buoyant jet case it must be calculated for each density profile.

Using the normalized velocity profile for the withdrawal layer (Eq. (2.37)), the second term on the right side of Eq. (2.38) becomes, for the lower half of the withdrawal layer

$$-\frac{Q_j}{A(y)} B \int_1^{y_*} u_*(\xi_*) (1) d\xi_*. \quad (2.39)$$

The constant B is necessary because the full velocity profile calculated by Koh has a small region of reverse flow which is neglected in this formulation. Choosing  $B = 0.96$  makes the value of Eq. (2.39) equal to

$$-0.5 \frac{Q_j}{A(y)} \text{ at } y_* = 0 \text{ which is the center of the withdrawal layer.}$$

Therefore, for the lower half of the withdrawal layer

$$v(y_*) = \frac{Q_j}{A(y)} \left[ 1. - 0.96(1-y_*) - 0.03125(1-y_*^2) + 0.94575(1-y_*^3) - 0.4545(1-y_*^4) \right] \quad (2.40)$$

and for the upper half of the withdrawal layer

$$v(y_*) = \frac{Q_j}{A(y)} \left[ 0.5 - 0.96(1-y_*) - 0.03125(1-y_*^2) + 0.94575(1-y_*^3) - 0.4545(1-y_*^4) \right] \quad (2.41)$$

as shown in Fig. 2.9.

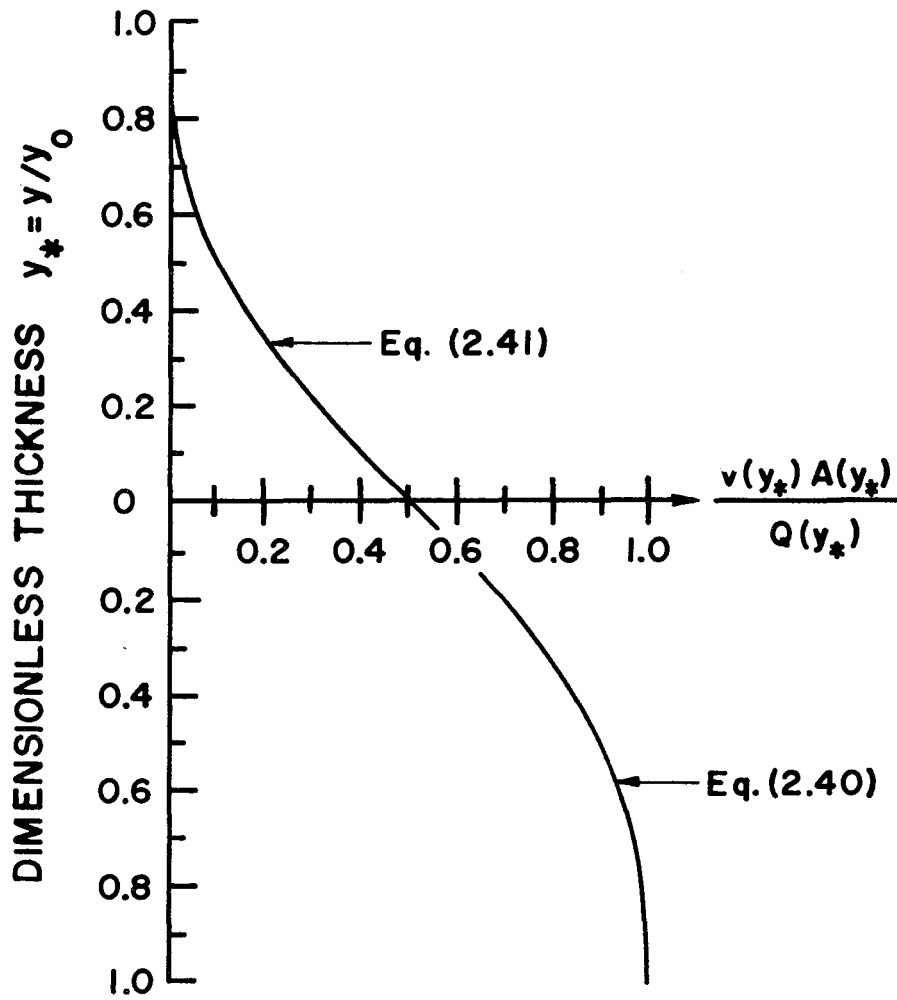


Figure 2.9 Normalized integrated entrainment from the withdrawal layer

Now, given the calculated withdrawal layer thickness,  $2y_0$ , the pump discharge,  $Q_j$ , and the area-depth relationship  $A(y)$ , one can calculate the transport velocity,  $v(y)$ , at a given time in the zone of selective withdrawal.

#### 2.2.6 Summary

Sections 2.2.4 and 2.2.5 provide the descriptions of the buoyant jet and withdrawal layer which are required in the solution of the governing equations. The physical descriptions of the distributions of  $q_e$  and  $v$  for a particular density profile have been made quantitative. Referring to Fig. 2.3, the transport velocity distribution between elevations A and C is given by Eq. (2.28). The integrated value of  $q_e$  between elevations C and E is constant, and  $v(y) = Q_j/A(y)$ . The transport velocity distribution within the selective withdrawal zone can be found using Eqs. (2.40) and (2.41).

### 2.3 SOLUTION OF GOVERNING EQUATIONS

The solutions to the equations governing the simulation model are the density profiles in the impoundment during mixing. A numerical solution to the governing equations, using the mechanics of buoyant jets and selective withdrawal described in Sect. 2.2, provides the profiles at any time during mixing for a given pumping system and initial profile.

#### 2.3.1 Method of Solution

The solutions of Eqs. (2.1) and (2.3) in closed-form are not possible. As shown in Sect. 2.2.4,  $q_e$ , the discharge into or from the impoundment, must be calculated numerically in the region of the

buoyant jet for a given density profile. Therefore, the vertical transport velocity,  $v$ , is not available in closed-form and is a function of the density profile,  $c$ , as well as elevation,  $y$ , and time,  $t$ . Solutions to the governing equations are found using numerical techniques. For the general case of an arbitrary, but gravitationally stable, initial density stratification, the governing equations cannot be normalized to produce a set of generalized solutions. Solutions for Eqs. (2.1) and (2.3) are found in terms of their physical dimensions.

### 2.3.2 Finite Difference Solution

A finite difference technique is employed for the numerical solution of the governing equations. An explicit scheme is used; that is, new values at a given point in time and space are expressed in terms of values calculated previously at points in time and space. The choice of the differencing scheme and the space-time grid is made after an examination of the truncation error incurred and the stability of a particular scheme. Minimizing the truncation error improves the approximation of the differential equation by the difference equation. Assuring a stable scheme guarantees that errors will not be amplified and that convergence to the solution is possible. A more rigorous explanation of these conditions is given by Richtmyer and Morton (39) and examples of their significance in calculations for nonlinear partial differential equations are given by Liggett and Woolhiser (31).

The transport velocity,  $v$ , can be found for a given density profile from Eq. (2.5), and the variable coefficient,  $v$ , in Eq. (2.3) for the density-stratifying agent,  $c$ , is then determined. Thus, the

starting values for  $v$  are available for this initial value problem. That the density profile must be known for  $v$  to be found dictates an explicit scheme for the difference form of Eq. (2.3). The explicit scheme employed to solve Eq. (2.3) is shown in Fig. 2.10. The intersections of the time and space lines are the points at which  $v$  and  $c$  are calculated. The local space step or interval is  $h$  and the local time step is  $k$ .

The differential equation

$$\frac{\partial c}{\partial t} + v \frac{\partial c}{\partial y} = 0 \quad (2.3)$$

is approximated by the following difference equation (for  $v > 0$ ):

$$\frac{c_{i,j+1} - c_{i,j}}{k} + v_{i-1,j} \frac{c_{i,j} - c_{i-1,j}}{h} = 0 \quad (2.42)$$

The first subscript refers to the space variable, in this case elevation, and the second subscript refers to time. This scheme is explicit because the value of  $c$  at time  $j+1$  is expressed in terms of values of  $c$  and  $v$  at time  $j$  for which they have been calculated previously. Similarly, for  $v < 0$  in Fig. 2.10:

$$\frac{c_{i,j+1} - c_{i,j}}{k} + v_{i+1,j} \frac{c_{i+1,j} - c_{i,j}}{h} = 0 \quad (2.43)$$

The truncation error for this scheme is the difference between Eqs. (2.3) and (2.42). A Taylor series expansion of  $c$  about the point  $(i, j)$  in the time and space variable yields



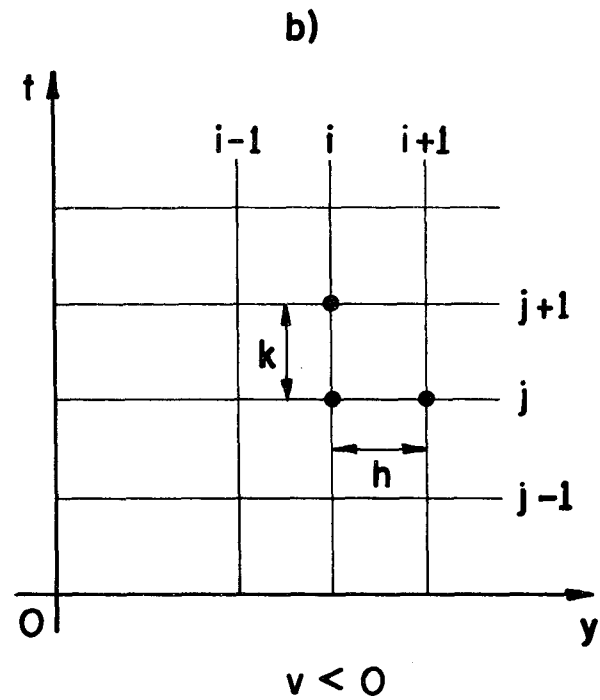
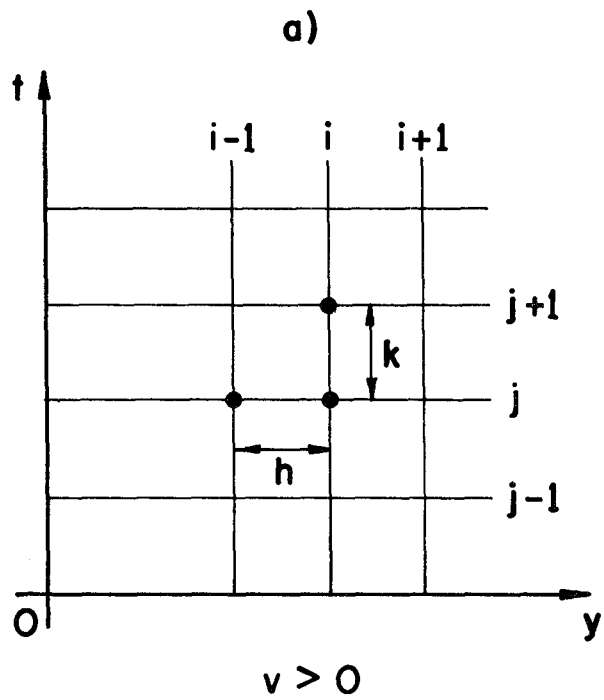


Figure 2.10 Finite difference schemes for: (a)  $v > 0$  and (b)  $v < 0$

$$c_{i,j+1} = c_{i,j} + \sum_{n=1}^{\infty} \frac{k^n}{n!} c_t^{(n)}, \quad (2.44)$$

and

$$c_{i-1,j} = c_{i,j} + \sum_{n=1}^{\infty} (-1)^n \frac{h^n}{n!} c_y^{(n)}, \quad (2.45)$$

where  $c_t^{(n)}$  and  $c_y^{(n)}$  are the  $n^{\text{th}}$  time and space derivatives, respectively. Substituting Eqs. (2.44) and (2.45) into Eq. (2.42) yields

$$\begin{aligned} & \frac{c_{i,j+1} - c_{i,j}}{k} + v_{i-1,j} \frac{c_{i,j} - c_{i-1,j}}{h} \\ &= \frac{1}{k} \sum_{n=1}^{\infty} \frac{k^n}{n!} c_t^{(n)} + \frac{v_{i-1,j}}{h} \sum_{n=1}^{\infty} (-1)^n \frac{h^n}{n!} c_y^{(n)}. \end{aligned} \quad (2.46)$$

Therefore,

$$\text{Truncation Error} = \frac{1}{k} \sum_{n=2}^{\infty} \frac{k^n}{n!} c_t^{(n)} + \frac{v_{i-1,j}}{h} \sum_{n=2}^{\infty} (-1)^n \frac{h^n}{n!} c_y^{(n)}. \quad (2.47)$$

The differential Eq. (2.3) requires that

$$c_t^{(n)} = \frac{\partial^{n-1}}{\partial t^{n-1}} \left( -v \frac{\partial c}{\partial y} \right). \quad (2.48)$$

The truncation error to order  $n=2$  using Eqs. (2.47) and (2.48) is

$$\text{Truncation Error} = \frac{1}{2} v_{i-1,j} \left[ (k v_{i-1,j}) - h \right] \frac{\partial^2 c}{\partial y^2} - \frac{k}{2} \left[ \frac{\partial y}{\partial t} \frac{\partial c}{\partial y} \right] . \quad (2.49)$$

The first term of the truncation error is identically zero if,

$$\frac{h}{k} = v_{i-1,j} . \quad \text{for } v > 0 . \quad (2.50)$$

In the second term in Eq. (2.49), the product  $\left[ \frac{\partial v}{\partial t} \frac{\partial c}{\partial y} \right]$  is usually small, although it is difficult to bound as  $\frac{\partial c}{\partial y}$  can be large and  $\frac{\partial v}{\partial t}$  is related to the density profile through the jet equations in a complicated way.

Thus, the time step,  $k$ , must be made sufficiently small, in addition to the relation given in Eq. (2.50), for the truncation error to be minimized.

Similarly, for regions where  $v < 0$ , the truncation error is minimized by choosing

$$\frac{h}{k} = |v_{i+1,j}| \quad \text{for } v < 0 \quad (2.51)$$

and  $k$  (i. e.  $\Delta t$ ) sufficiently small.

The stability of the difference scheme is investigated to assure that errors are not amplified in the numerical calculation. The solution to the initial-value differential Eq. (2.3) can be written as the Fourier series

$$c = \sum_{m=-\infty}^{\infty} A_m e^{im(y-vt)} , \quad (2.52)$$

where:

$$A_m = \frac{1}{d} \int_0^d c_o(y) e^{im y} dy \quad (2.53)$$

and  $c_0(y)$  is the initial distribution of  $c$ . Similarly a Fourier series solution for the difference equation can be found. Consider the expression  $c_{\ell j} = A \xi^\ell e^{imjh}$ , where  $A$ ,  $\xi$ , and  $m$  are constants;  $h = \Delta y$ , the space step,  $i = \sqrt{-1}$ ; and  $j$ ,  $\ell$  are the positions in space and time, respectively. If the expression  $c_{\ell, j}$  is substituted into the difference Eq. (2.42), it satisfies the equation provided that  $\xi$  is given by

$$\xi = \xi(m) = 1 - v \frac{k}{h} (1 - e^{-imh}) . \quad (2.54)$$

And thus,

$$c_{\ell, j} = \sum_{m=-\infty}^{\infty} A_m [\xi(m)]^\ell e^{imjh} \quad (2.55)$$

gives the exact solution to the difference equation, if  $A_m$  is defined by Eq. (2.53).

Because Eq. (2.55) is formulated by separating the space and time variables, each harmonic grows independently of the others as time goes on.  $\xi(m)$  is the growth factor for the amplitude of the  $m^{\text{th}}$  harmonic for a time interval,  $k$ , and the corresponding factor for the differential equation solution is  $e^{-imvk}$ . A comparison of the two growth factors shows that they agree through first order terms:

$$\begin{aligned} \xi(m) &= 1 - vkim - \frac{vkhm^2}{2} + \dots \\ e^{-imvk} &= 1 - vkim - \frac{vmk^2}{2} + \dots \end{aligned} \quad (2.56)$$

For any harmonic the two factors can be made to agree to a given accuracy by choosing  $k$  and  $h$  sufficiently small; however there will always exist a harmonic, some high value of  $m$ , for which the growth factors disagree significantly. The Fourier series solution for the differential equation is assumed absolutely convergent. Therefore for a chosen accuracy for the solution, harmonics above a sufficiently high order are negligible in the true solution. These high order harmonics can be falsified in the approximate or difference solution so long as they do not become amplified to the extent that they are no longer negligible. Therefore, if

$$\max_m |\xi(m)| \leq 1 \quad (2.57)$$

no harmonic is amplified, otherwise some harmonic is amplified without limit as time,  $\ell$ , increases.

It can be shown that Eq. (2.57) reduces to:

$$v \frac{k}{h} \leq 1 \quad \text{for } v > 0 \quad (2.58)$$

and

$$|v| \frac{k}{h} \leq 1 \quad \text{for } v < 0 \quad (2.59)$$

Eqs. (2.50) and (2.51) from the truncation error analysis and Eqs. (2.58) and (2.59) from the stability analysis require that

$$\frac{h}{k} = \frac{\Delta y}{\Delta t} = v_{i-1,j} \quad \text{for } v > 0 \quad (2.60)$$

$$\frac{h}{k} = \frac{\Delta y}{\Delta t} = |v_{i+1,j}| \quad \text{for } v < 0 \quad (2.61)$$

This condition means that the ratio of the space interval to time interval must equal the vertical transport velocity locally  $\left(\frac{\Delta y}{\Delta t} = |v|\right)$ . Requiring these relations for the difference equations, Eqs. (2.42) and (2.43) become:

$$c_{i,j+1} = c_{i-1,j} \quad \text{for } v > 0 \quad (2.62)$$

$$c_{i,j+1} = c_{i+1,j} \quad \text{for } v < 0 \quad (2.63)$$

Now, these simple relations indicate that the density-stratifying agent,  $c$ , at a given elevation and time is moved upward (or downward, if  $v < 0$ ) exactly one space interval,  $\Delta y$ , in time  $\Delta t$ . This result is sound physically, for this is the distance through which a parcel of fluid containing  $c$  would move in time  $\Delta t$ . In addition, from the point of view of the numerical calculation, it minimizes the accumulation of truncation error which occurs for stable schemes with  $\frac{\Delta y}{\Delta t} < v$  and which appears as the "pseudo-dispersion" pointed out by Bella and Dobbins (3).

For a given density profile at a given time, the vertical transport velocity varies with elevation,  $y$ . Hence if the time step,  $\Delta t$ , is kept constant during the calculation, the space step,  $\Delta y$ , must vary with elevation. The result is a time-space grid on which time intervals are regular and space intervals are irregular. This is illustrated schematically in Fig. 2.11. The irregular space intervals differ for each time step as each new density profile results in new values of  $v$ .

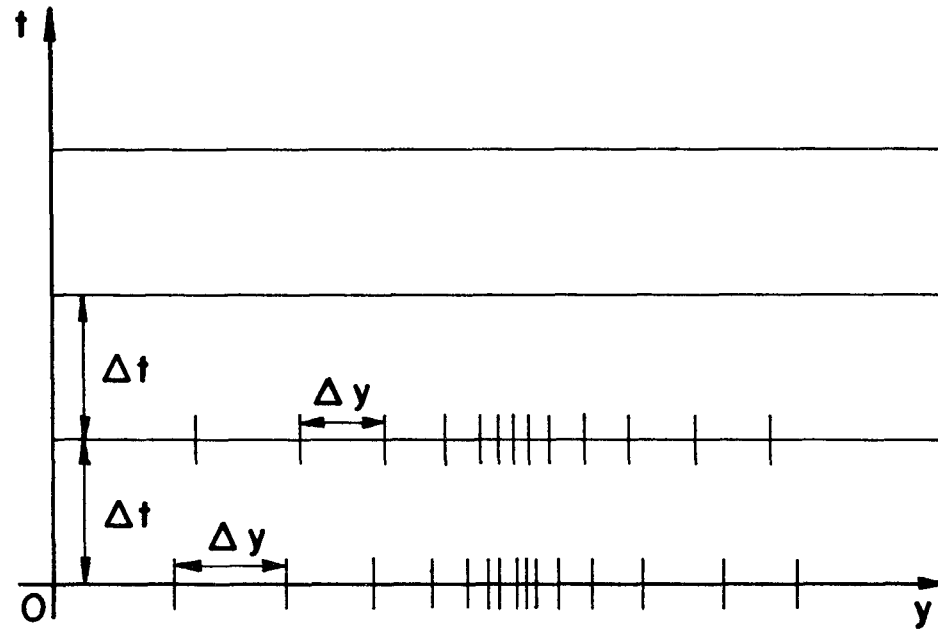


Figure 2.11 Irregular space intervals,  $\Delta y$ , at each time interval,  $\Delta t$

Eq. (2.3) can be viewed as a kinematic wave equation. It has one set of characteristics in the time-space plane with slopes  $\frac{dy}{dt} = v$  along which  $c = \text{constant}$ . The numerical calculation scheme giving Eqs. (2.62) and (2.63) essentially defines these characteristics. Lines in the  $t - y$  plane which connect points of constant  $c$  trace out these characteristics.

### 2.3.3 Outline of Computation Technique

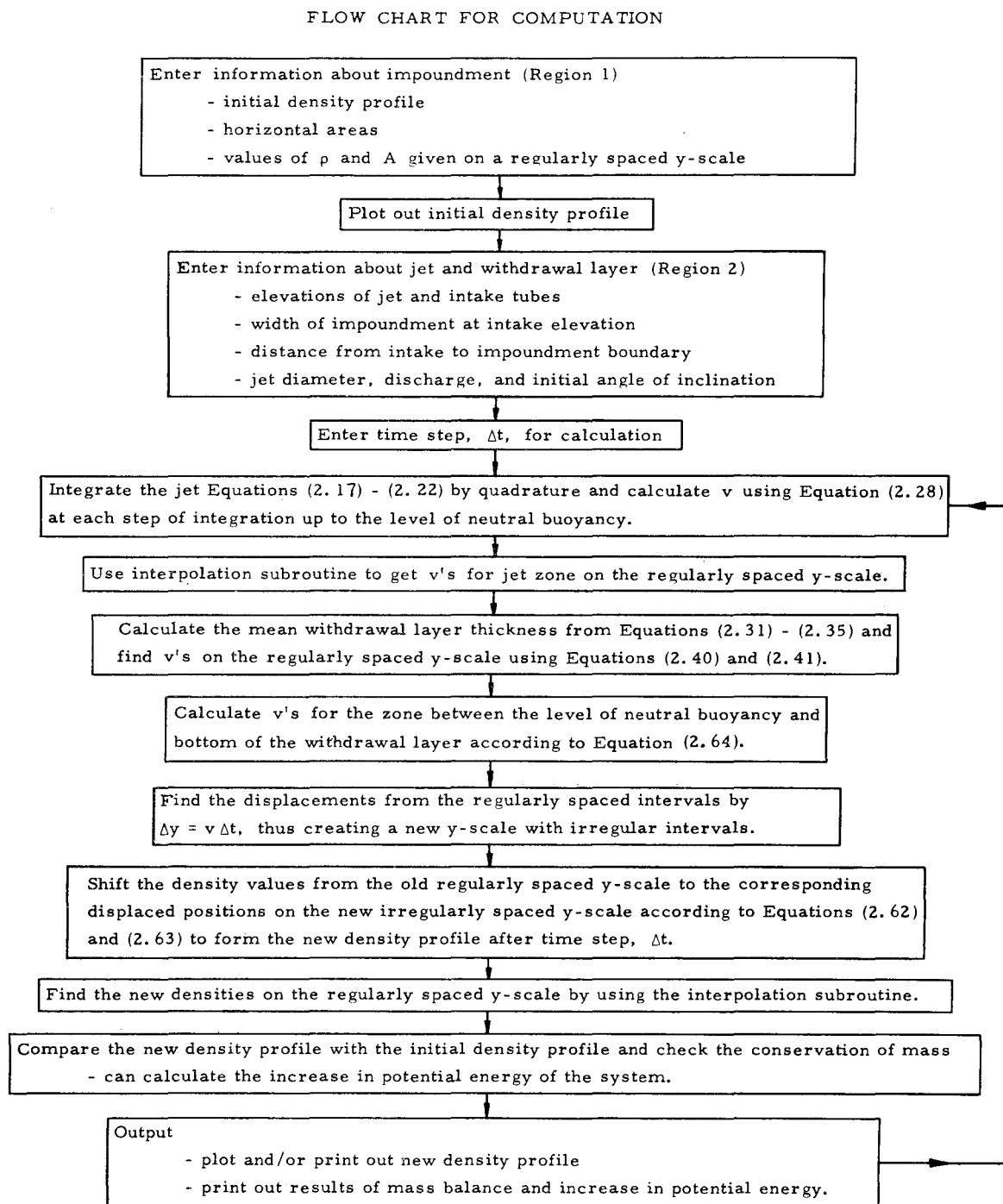
Simulation of mixing by a pumping system involves the synthesis of the numerical calculation scheme and the knowledge of the buoyant jet and withdrawal layer mechanics described previously. The essential ingredients of the simulation have been developed, and how they are combined for the computer program is presented here. The general structure of the program is described rather than its intricate details. A flow chart (Fig. 2.12) shows the basic elements of the computation. A listing of the program is given in the Appendix.

The initial density profile in the impoundment (Region 1) is introduced by giving density values at uniformly spaced intervals on the elevation axis. These intervals are chosen small enough so that any gravitationally stable density profile can be approximated. The values of the horizontal cross-sectional area of the impoundment,  $A$ , are also introduced on this  $y$ -axis. The elevation of the intake tube and discharge jet are specified relative to this axis.

The jet diameter, initial angle of inclination (usually zero) and discharge are specified. The reference density,  $\rho_0$ , is chosen as the ambient density at the elevation of the jet, and the initial density of the



Figure 2.12 Outline of computation procedure



jet discharge is the ambient density at the elevation of the intake tube, corrected for dilution in the zone of flow establishment. With these initial data, the jet trajectory and parameters are calculated as described in Sect. 2.2.4. The integration proceeds along the jet trajectory in intervals equal to or smaller than intervals on the vertical axis at which density data are specified. This allows the local ambient density gradient to be continually adjusted in the equations. But it means that the local vertical transport velocity in the impoundment (Region 1) due to jet entrainment (Region 2) is calculated (Eq. (2.28)) at irregularly spaced elevations.

The calculation of the jet parameters continues until the difference between the center line density of the jet and the ambient fluid at that elevation is zero (Eq. (2.29)) or has just changed sign. This elevation is the location of the level of neutral buoyancy. It is assumed that this is the terminal level of the fluid in the jet, although, physically, fluid with negative buoyancy overshoots this level before reaching approximately this position. It is convenient for later calculations to have the values of the integrated jet entrainment known at regularly spaced elevations. An interpolation subroutine uses the integrated jet entrainment values calculated along the jet trajectory to find the values of jet entrainment and vertical transport velocity at regularly spaced intervals from the level of the jet up to the level of neutral buoyancy.

The calculation of entrainment from the impoundment (Region 1) by the withdrawal layer requires an estimate of its extent. The thickness of the withdrawal layer is approximated by the mean of the inviscid

flow thickness, Eq. (2.31), and the turbulent flow thickness Eq. (2.34) or Eq. (2.35), as discussed in Sect. 2.2.5. The two-dimensional discharge,  $q$ , required for these equations is obtained by dividing the pump discharge by the average width of the impoundment at the elevation of the withdrawal tube. The required density gradient is chosen to be that gradient which exists in the impoundment at the elevation of the withdrawal tube. The calculation of the turbulent flow thickness requires the distance from the withdrawal tube to the point for which the calculation is made. The distance between the withdrawal tube and the impoundment boundary toward which it is directed is used. The mean of the inviscid flow thickness and turbulent flow thickness is rounded off to an even number of space intervals on the  $y$ -scale. The vertical transport velocity in the impoundment (Region 1) due to the withdrawal layer (Region 2) is calculated at each of these intervals using Eqs. (2.40) and (2.41).

Between the level of neutral buoyancy of the jet and the bottom of the withdrawal layer (between elevations C and E in Fig. 2.13), no transport of fluid occurs between the impoundment (Region 1) and the jet or withdrawal layer (Region 2). The integration of  $q_e$  from  $y = 0$  to any elevation in this zone equals  $Q_j$ , since the return flow to the impoundment (between elevations B and D) is simply the total volume flux entrained by the jet from the impoundment (between elevations A and C) plus the jet discharge,  $Q_j$ . The vertical transport velocity in the impoundment in this zone is then

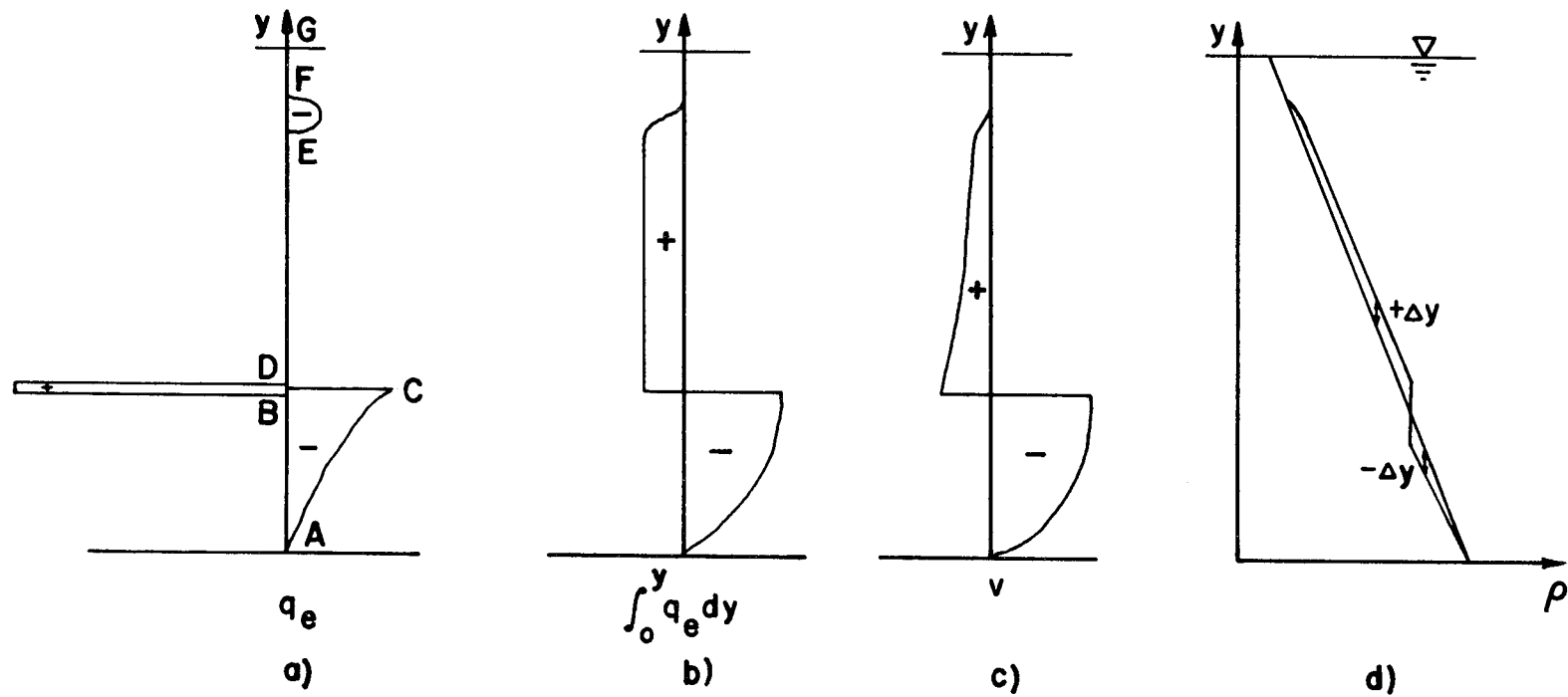


Figure 2.13 Sketch of vertical distributions of: (a)  $q_e$ ,  
(b) integrated  $q_e$ , (c)  $v$ , and (d)  $\Delta y$

$$Q_j/A(y) \quad (2.64)$$

and it is calculated at each of the regularly spaced intervals on the y-scale in this zone.

From the top of the withdrawal layer to the surface (between elevations F and G), there is no transport between Region 1 and Region 2. The integration of  $q_e$  from  $y = 0$  to the top of the withdrawal layer equals zero, and further integration to the surface does not change the integration. Therefore, the vertical transport velocity between elevations F and G (Fig. 2.13) is zero.

Now the values of vertical transport velocity are known at regularly spaced points on the y-axis. The velocities below the level of neutral buoyancy are negative and those above it are positive. The irregularly spaced displacements,  $\Delta y = v \Delta t$ , are calculated for a fixed time interval,  $\Delta t$ . A value of  $\Delta y$  is calculated at each regularly spaced point on the y-axis, as shown in Fig. 2.14. The distance  $\Delta y$  is above the regularly spaced points, if  $v$  is positive, and below them, if  $v$  is negative. A new set of irregularly spaced points on the y-axis is defined by the points  $\Delta y$  away from the regularly spaced points. The densities at these new points are those which existed at the regularly spaced points before the increase in time,  $\Delta t$ , as described in Sect. 2.3.2. These density values are assigned to the new irregularly spaced points.

The physical significance of this shifting of density values from the regularly spaced points to points  $\Delta y$  away is made clear by looking at the level of neutral buoyancy. At this point (see Fig. 2.14) the

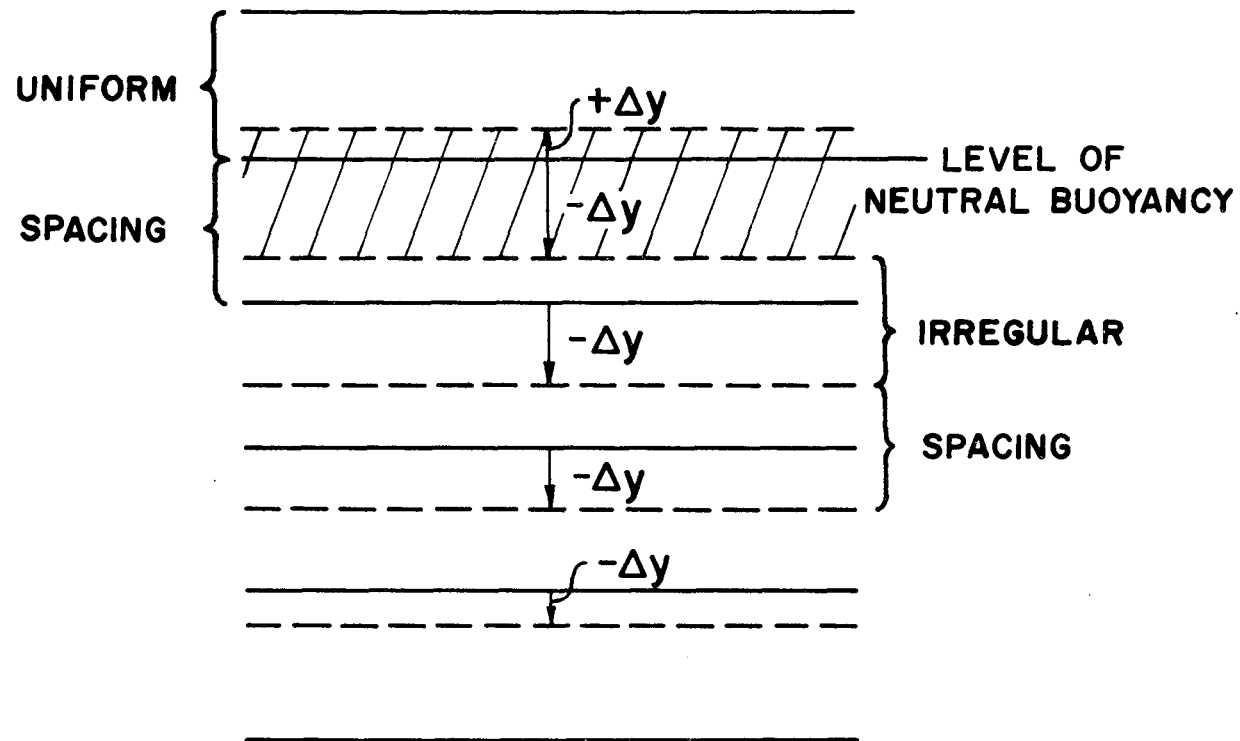


Figure 2.14 Sketch of displacements,  $\Delta y$ , from uniform spacing to form irregular spacing

separation of the positive and negative velocities occurs. The negative (downward)  $\Delta y$  is such that the volume included between the level of neutral buoyancy and this new elevation is just that required to contain the total fluid entrained by the jet in time  $\Delta t$ . The positive (upward)  $\Delta y$  is such that the volume included between the level of neutral buoyancy and this new elevation is just that required to contain the fluid discharged by the pump in time  $\Delta t$ . Since the density value shifted to each of these new points after time  $\Delta t$  is that which existed at the level of neutral buoyancy, a region of constant density is formed between these points. This region corresponds exactly to the volume of fluid delivered by the jet in time  $\Delta t$  to the level of neutral buoyancy (Eq. (2.30)) and whose density was assumed to be the same as that of the ambient fluid at this elevation (Eq. (2.29)).

The density values for time  $\Delta t$  after the start of mixing are now known at irregular intervals on the  $y$ -axis. They are found at regular intervals by using an interpolation subroutine. The change in the density profile in time interval  $\Delta t$  is shown schematically in Fig. 2.13d. The calculation can now recycle and begin computations based on the new density profile. However, before recycling a check of the mass balance for the system is made by comparing the density profile just calculated to the initial density profile.

## 2.4 FLEXIBILITY OF COMPUTER SIMULATION

Several extensions of and additions to the simulation technique are possible. The basic structure of the simulation is such that changes are possible in the description of the buoyant jet or withdrawal

layer. Should one wish to consider a buoyant plume (no initial momentum) in place of a buoyant jet, the trajectory and entrainment calculations for a simple plume could replace those for the buoyant jet. Similarly, a more detailed model of withdrawal layer entrainment taking into account nonlinear density profiles, three-dimensional effects, or drag along the bottom (53) might replace the simple model presented here. A better approximation of the level of the spreading jet could be incorporated into the simulation.

Additional modifications to the simulation model may make it possible to include factors which were neglected in the model presented here. Vertical diffusion of heat and mass might be included. The calculation of the redistribution of a conservative, non-reacting tracer substance due to mixing is described in Chapter 3. This technique might be used to model temperature profiles, and thus permit the inclusion of the nonlinear temperature-density relation in the simulation. Coupling a comprehensive heat balance simulation (as studied for natural impoundments (14, 15, 35, and 57)) to the mixing simulation would yield a better approximation to the actual mixing process in the field.





## CHAPTER 3

## MIXING OF A TRACER SUBSTANCE

## 3.1 EFFECT OF MIXING ON A TRACER

The vertical redistribution of the chemical and biological constituents of an impoundment due to mixing has a strong influence on the water quality. Transport of dissolved chemical constituents in a reduced state to regions with higher dissolved oxygen content results in oxygenation and probably in precipitation from solution. Similarly, transport of water with high concentrations of dissolved oxygen to regions of low concentrations of oxygen may satisfy some of the oxygen demand there. Nutrients transported to the upper regions of the impoundment may stimulate the growth of the phytoplankton population. Also the mixing may result in a redistribution of phytoplankton for which temperature and light conditions either stimulate or retard growth. As the vertical profiles of the various chemical and biological constituents seldom resemble the density profile before mixing, the distributions of these substances during mixing are different from the density profiles produced. Moreover, the reactions among the various constituents during mixing are likely to modify their profiles in addition to the alterations caused by physical mixing.

### 3.2 SIMULATION OF THE MIXING OF A CONSERVATIVE, NON-REACTING TRACER

The redistribution of a conservative, non-reacting tracer due only to the physical mixing process is considered as a first approximation to the complex processes involved. Such a tracer represents a dissolved chemical or biological substance which has little effect on the density of the solution relative to the effect of temperature. The tracer remains in solution without combining with other substances. In keeping with the simulation model for density-stratifying substances, the tracer is assumed to have the same concentration at a given elevation throughout the impoundment (exclusive of the jet and withdrawal zones) at a given time. The distribution of the tracer concentration,  $c_s$ , is therefore one-dimensional and is expressed as a vertical profile (Fig. 3.1). The vertical profile of the tracer concentration at the start of pumping may have any shape.

The tracer concentration  $c_s$  is now included in the analysis for the density-stratifying agent,  $c$  (Sect. 2.2.2). The analysis is changed only by the addition of a conservation relation for the tracer,  $c_s(y, t)$ . Conservation of the tracer requires that:

$$A \frac{\partial c_s}{\partial t} + \frac{\partial (c_s v A)}{\partial y} = c_s * q_e \quad (3.1)$$

Eq. (3.1) is similar to Eq. (2.2) for the density-stratifying agent except that the right side of Eq. (3.1) has the term  $c_s * q_e$ . The term  $c_s * q_e$  represents the flux of tracer put into or taken from the impoundment



(Region 1) by the jet and withdrawal region. For the case of the density-stratifying agent, the concentration in that term is the same as the concentration on the left side of the equation because fluid is always taken from or put into the impoundment at the same density as exists at that elevation in the ambient fluid. In the case of the tracer, concentrations in fluid taken from the impoundment by withdrawal and jet entrainment are those which exist in the ambient fluid. That is,

$$c_s^*(y, t) = c_s(y, t) \quad (3.2)$$

for elevation  $A \leq y \leq \text{elevation } C$   
 and elevation  $E \leq y \leq \text{elevation } F$  (see Fig. 3.1) .

However, the concentration of tracer in the fluid returned to the impoundment by the jet at the level of neutral buoyancy is not necessarily the same concentration of tracer that exists in the ambient fluid at that elevation. That is,

$$c_s^*(y, t) \neq c_s(y, t) \quad (3.3)$$

for elevation  $B \leq y \leq \text{elevation } D$  (see Fig. 3.1) .

The concentration of tracer in this fluid depends on the concentrations of of tracer in the fluid withdrawn at the intake and in that entrained by jet from the impoundment. The concentration of tracer in the fluid returned to the impoundment by the jet at the level of neutral buoyancy ( $y_{\ell nb}$ ) for particular density and tracer profiles is:

$$c_s^*(y_{\ell nb}, t) = \frac{\int_0^{y_{\ell nb}} c_s(y, t) q_e(y, t) dy + c_s(\text{intake}, t) Q_j}{\int_0^{y_{\ell nb}} q_e(y, t) dy + Q_j} \quad (3.4)$$

where:

$y_{\ell nb}$  = elevation of level of neutral buoyancy,

$q_e$  = volume rate of flow per unit depth entrained by jet,

$Q_j$  = jet discharge.

Since  $c_s^* = c_s$  for all elevations except the region where fluid is returned to the impoundment by the jet, Eq. (3.1) becomes

$$\frac{\partial c_s}{\partial t} + \frac{\partial(c_s v A)}{\partial y} = c_s q_e \quad (3.5)$$

for all  $y$  except between elevations B and D (Fig. 3.1). Combining the continuity relation, Eq. (2.1), with Eq. (3.5) yields

$$\frac{\partial c_s}{\partial t} + v \frac{\partial c_s}{\partial y} = 0, \quad (3.6)$$

for all  $y$  except between elevations B and D. Eq. (3.6) is analogous to Eq. (2.3) which is the governing equation for the density-stratifying agent. Therefore, the finite difference solution to Eq. (2.3) now predicts the local displacements of the tracer profile also. Although the solution for tracer concentrations in the region of flow returned to the impoundment is not analogous to that for density, the concentration for this region is readily calculated using Eq. (3.4).

The computation technique requires little modification to accomodate tracer profiles, as all of the changes in the tracer concentration profiles are due to the same local displacements calculated for the density profile (with the exception of the concentration calculated

by Eq. (3.4)). The technique outlined in Sect. 2.3.3 is followed. Any initial profiles for tracer substances can be provided as input to the calculation. As mixing proceeds, the modified tracer profiles are calculated at progressive time intervals.

An example of the effect of mixing upon the profile for a single tracer is shown in Fig. 3.2. Profiles of tracer concentration and density are shown for two times during mixing as well as the initial profiles. The discontinuities in the slope of the tracer profiles during mixing are due to the fact that the tracer concentration in the fluid discharged by the jet into the impoundment at the level of neutral buoyancy is not the same concentration that exists in the ambient fluid at that elevation. These discontinuities are smoothed out in the lower regions of the impoundment as the level of neutral buoyancy occurs at greater elevations.

### 3.3 TEMPERATURE AS A TRACER AND THE NONLINEAR TEMPERATURE-DENSITY RELATIONSHIP

The simulation technique was developed with the assumption that the density of the fluid is a linear function of salt concentration or of temperature (see Sect. 2.2.4). The assumption is valid for salt concentrations over a large range (0-70 grams/liter), but the assumption begins to break down for temperature over a range of  $10^{\circ}\text{C}$  at certain parts of the nonlinear temperature-density relationship (36). In particular, the range of temperatures ( $10^{\circ}\text{C}$  -  $30^{\circ}\text{C}$ ) often encountered in temperature-stratified lakes and reservoirs is large enough to make the assumption of a linear temperature-density relation invalid.

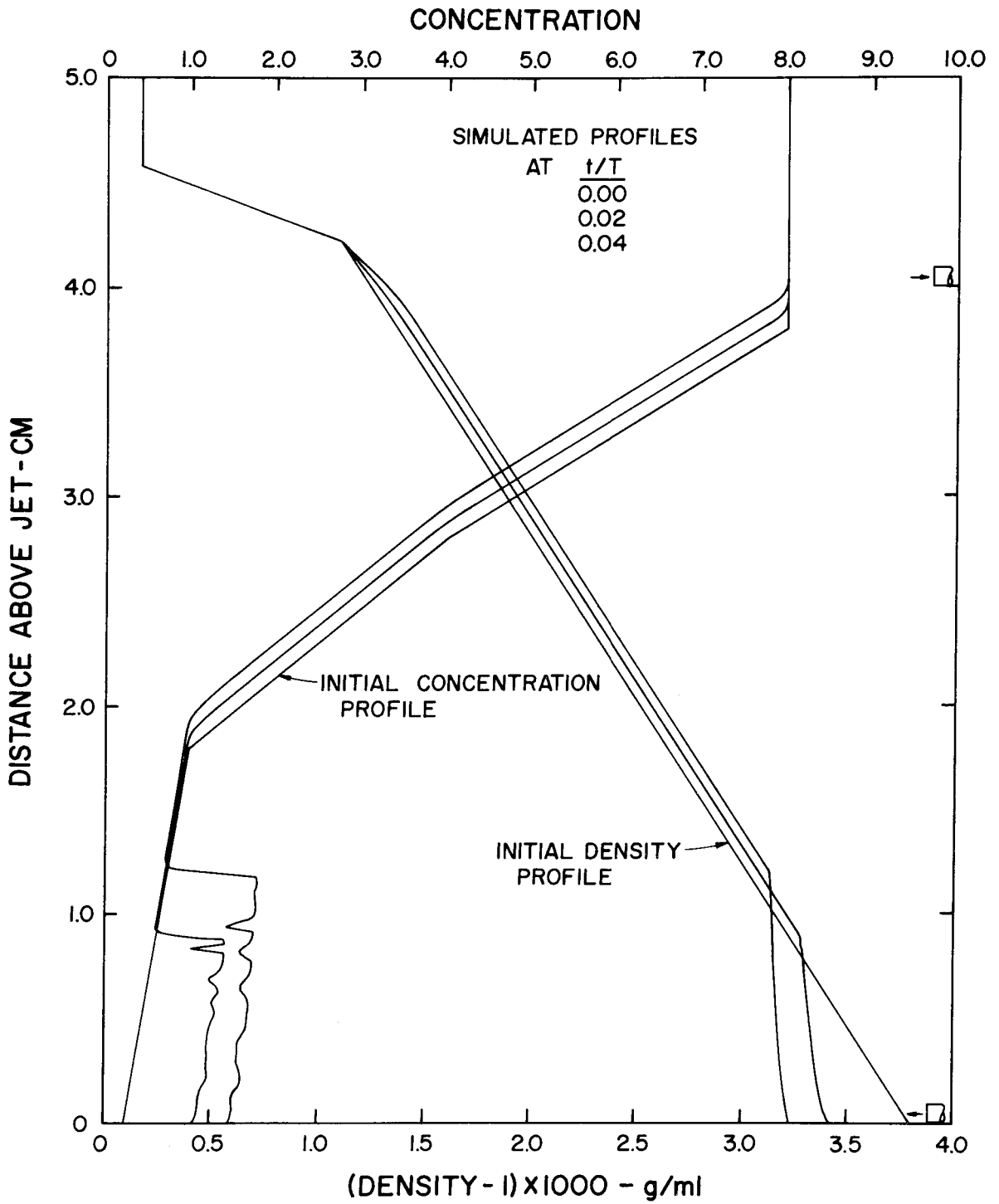


Figure 3.2 Example of simulated redistribution of a tracer due to mixing



The effect of this assumption on the simulation results can be determined by using temperature as a tracer substance in the simulation. When the assumption of a linear temperature-density relationship is valid, the profiles of temperature are directly proportional to the density profiles. However, it was found that for surface temperatures about 30°C and bottom temperatures about 10°C the temperature profiles during mixing exhibited discontinuities at the level of neutral buoyancy. That is, the temperature of the fluid delivered to the impoundment by the jet of this elevation was not the temperature of the ambient fluid. The temperature profile records this anomaly because the buoyant jet mechanics are such that buoyancy (based on density) flux is conserved while heat flux is not.

The simulation technique can be modified to account for the nonlinear temperature-density relation and to conserve heat (adiabatic mixing). The nonlinear temperature-density relation

$$\rho = \phi(T^0) \quad (3.7)$$

is made available by providing values at fixed intervals of temperature and using an interpolation subroutine. The initial temperature profile is converted to a density profile using Eq. (3.7). The buoyant jets mechanics (Sect. 2.2.4) are changed to conserve heat flux instead of buoyancy flux (based on density). Temperature is introduced in analogy to buoyancy (see Eq. (2.7)):

$$T_a^{0*}(s, r) - T^{0*}(s, r) = (T_a^0 - T^0) e^{-r^2/(\lambda b^2)}, \quad (3.8)$$

where:  $T_a^0$  = temperature of the ambient fluid

$T^0$  = temperature of the jet.

The conservation of buoyancy flux (Eq. (2.13)) is replaced by

$$\frac{d}{ds} \left[ u b^2 (T_a^0 - T^0) \right] = \frac{1+\lambda^2}{\lambda^2} b^2 u \frac{dT_a^0}{ds} , \quad (3.9)$$

and the density difference,  $(\rho_a - \rho)$ , required for the buoyancy force in the jet dynamics is calculated from the temperatures

$$(\rho_a - \rho) = \phi(T_a^0) - \phi(T^0). \quad (3.10)$$

The jet equations, simplified for quadrature (Eqs. (2.17) to (2.23)), remain the same with the exception of Eq. (2.20) for  $(\rho_a - \rho)$  which is replaced by:

$$\frac{dT^0}{ds} = (T_a^0 - T^0) \frac{2\alpha}{b} - \frac{1}{\lambda^2} \sin \theta \frac{dT_a^0}{dy} , \quad (3.11)$$

and

$$(\rho_a - \rho) = \phi(T_a^0) - \phi(T^0). \quad (3.10)$$

With the exception of these changes, the simulation is carried out as described in Chapter 2.

Although the assumption of a linear temperature-density relationship is valid where "small" temperature differences are involved, care must be exercised in the application of the simulation technique to temperature-stratified impoundments as the temperature

difference between the fluid at the surface and bottom may be large enough to make this assumption invalid. If this is the case, the simulation should be modified to conserve heat and account for the nonlinear temperature-density relationship as outlined above. This procedure was employed for simulations of the mixing of temperature-stratified lakes in the analysis of some field experiments in Chapter 5.

### 3.4 EXTENSION OF THE TECHNIQUE TO REACTING TRACER SUBSTANCES

The simulation of the mixing of a conservative, non-reacting tracer substance predicts the redistribution of the tracer due to physical mixing, but in many cases reactions would occur among substances before the mixing was completed. A more useful approximation to the situation which exists when reactions are possible makes use of the simulation developed for a non-reacting tracer. Since the calculation proceeds for fixed time intervals, it is proposed that the calculation be halted after a given number of time intervals. The profiles of reacting substances at this time can provide the concentrations required to make calculations of chemical reactions among the various tracer substances. These calculations may change the total mass of given substance in solution and/or alter the concentration profile for that substance. The new concentration profiles which result from these reactions may then be entered into the simulation program, the density profile remaining as it was when the simulation was halted.

The mixing simulation is continued for the given time interval, and then it is stopped to allow the reactions to be recalculated. Thus, in a stepwise manner the simulation for the non-reacting tracers may be used to provide an approximation to the actual situation where substances react during mixing.



## CHAPTER 4

## LABORATORY EXPERIMENTS

## 4.1 PURPOSE OF EXPERIMENTS

Laboratory experiments were conducted in which density-stratified impoundments were mixed by pumping. The objectives of these laboratory experiments were:

- 1) to confirm the validity of the simulation model and its ability to predict the gross behavior of the mixing process;
- 2) to demonstrate those phenomena associated with the mixing process which are not modeled by the simulation technique; and
- 3) to investigate the effect of scale on the mixing process.

The experimental procedure is discussed in Sect. 4.2 and the experimental results and discussion of these results are given in Sects. 4.3 and 4.4, respectively.

## 4.2 EXPERIMENTAL PROCEDURE

Experiments were carried out in three laboratory impoundments of different shapes and sizes. Density stratification was produced in these impoundments by using salt (NaCl) water solutions. Mixing was accomplished by using a laboratory pump connected to the intake and discharge tubes in the tank. Concentration profiles were recorded at regular time intervals during the mixing process.

#### 4.2.1 Description of the Experimental Apparatus

The three laboratory impoundments used were a 2-meter tank, a 9-meter flume, and a 40-meter flume. The two flumes were closed off near their ends to form tanks and were horizontal for all experiments. Instrument carriages were mounted on each tank to hold conductivity probes. Stationary instrument holders were used for positioning jet and withdrawal tubes and additional conductivity probes. Each tank had a glass-walled section permitting observation of the jet and withdrawal tubes. The laboratories in which the tanks were located were temperature-controlled. The physical dimensions of the impoundments are shown below:

<u>Tank</u>	Dimensions in Meters		
	<u>Length</u>	<u>Width</u>	<u>Depth</u>
2-meter tank	2.23	1.08	0.61
9-meter flume	8.67	0.61	0.55
40-meter flume	36.32	1.10	0.40

The arrangement of a typical laboratory mixing experiment is shown schematically in Fig. 4.1 and photographically in Fig. 4.2. Copper tubes were bent to provide horizontal intake and discharge. The circulating pump was a Jabsco laboratory pump, Model P-6-M6, run by a 1/8-horsepower electric motor. The discharge was determined with a Fischer-Porter Tri-Flat Tube Flowrator (No. 3-F-3/8-5). Both glass and steel spheres were used in the Flowrator to achieve the necessary range of discharge measurements ( $5\text{-}29\text{ cm}^3/\text{sec}$ ). The

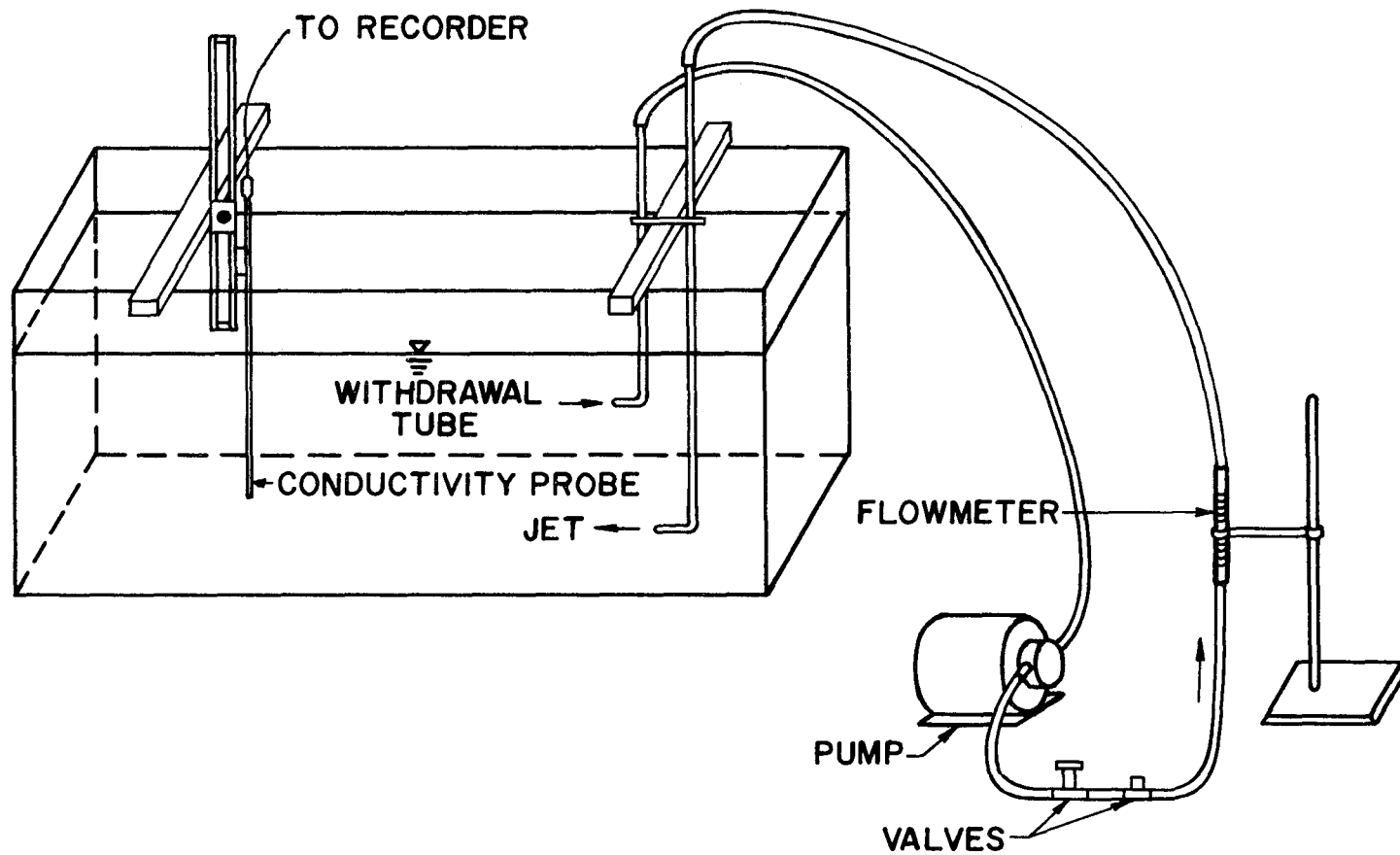
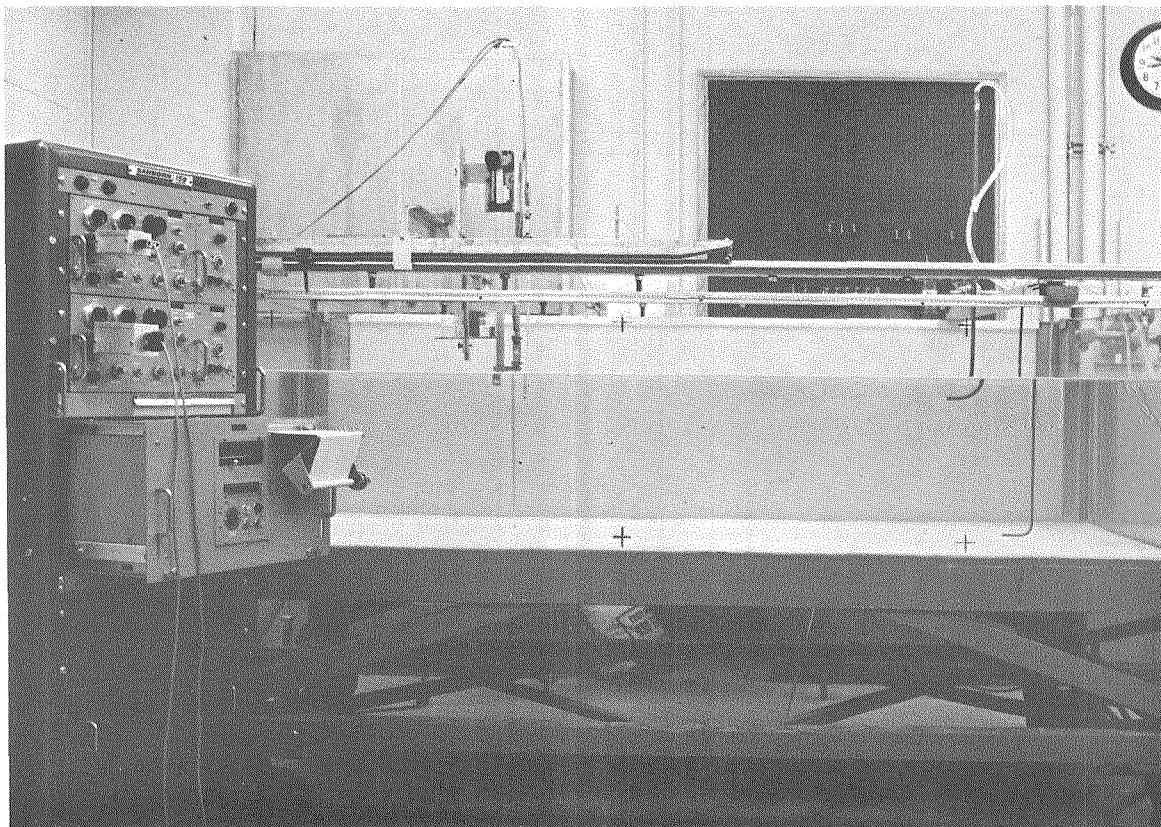


Figure 4.1 Schematic diagram of experimental setup





10704

Figure 4.2 Photograph of experimental set up (2m tank)

flowmeter was calibrated with various salt solutions, and the discharge measurements were found to vary less than 1% over the range of salt concentrations (0.2-10 g/l) and temperatures encountered in the experiments. Since this variation was small, the discharge was not adjusted during an experiment, though the density of the fluid discharged through the flowmeter did change slightly during mixing.

The positions of the withdrawal tube and jet discharge tube in the tank were varied. In all experiments the tubes were aligned one above the other in the same vertical plane. In most of the experiments the jet tube was positioned near the bottom of the tank and the withdrawal tube was above it, near the surface. In the other experiments the positions of the tubes were reversed. The intake and outlet tubes were directed along the longitudinal center line of the tank near one end or at the center (Fig. 4.1). Specific data regarding the location of the tubes, the hydraulic parameters, and initial density profiles for each experiment are given in Tables 4.1 and 4.2, Fig. 4.9 and in Sect. 4.3.

#### 4.2.2 Density Stratification

Density-stratified environments were created in the laboratory impoundments by using specially prepared salt water solutions to achieve density differences and employing several mixing and filling techniques to produce vertical density gradients.

The shape of the density-depth profile was dependent on the manner in which the tank was filled. Density profiles in lakes and reservoirs often exhibit a two-layer shape, that is, one region of

Table 4.1 Summary of Laboratory Mixing Experiments

Exper. Number	Tank	Area of Tank	Method of Stratification (1)	Total Depth	Distance between jet & intake	Jet Discharge	Jet Diameter	Initial Density Diff. Jet & Intake	Initial Density of Jet	Temp. of Water	Jet Froude Number	Plume Parameter	Shape Factor	Characteristic Time	Reference
		A cm <sup>2</sup>		d <sub>t</sub> cm	d cm	Q cc/sec	D cm	$\Delta\rho$ 10 <sup>-3</sup> g/ml	$\rho_0$ g/ml	°C	F Eq. (6.4)	P Eq. (6.6)	S Eq. (6.7)	T = $\Psi/Q$ hr	Figure Numbers
1	2m	24,000	2-layer	50.0	45.0	10.85	0.480	6.73	0.99834	21.0	33.7	$3.12 \times 10^{-4}$	11.9	27.6	---
2	2m	24,000	A	47.8	40.4	10.85	0.480	3.95	1.00008	20.9	44.0	$5.32 \times 10^{-4}$	14.7	24.8	---
3	2m	24,000	A	33.7	18.7	12.25	0.480	3.52	0.99943	21.6	52.7	$4.37 \times 10^{-3}$	68.6	10.2	---
4	No Experiment														
5	2m	24,000	A	45.8	38.1	12.25	0.480	2.44	1.00163	21.5	63.2	$8.83 \times 10^{-4}$	16.5	20.7	4.10
6	2m	24,000	A	43.3	35.6	12.25	0.480	4.43	1.00354	22.0	47.0	$7.78 \times 10^{-4}$	18.9	19.4	4.11
7	2m	24,000	A	44.6	41.4	12.25	0.849	3.03	1.00200	23.3	13.7	$6.46 \times 10^{-4}$	14.0	22.5	4.12
8	2m	24,000	A	43.2	30.0	3.07	0.213	2.94	1.00180	23.0	110.1	$3.68 \times 10^{-4}$	26.7	65.2	4.13
9	2m	24,000	B	45.7	40.0	23.94	0.849	4.90	1.00370	21.5	21.0	$1.08 \times 10^{-3}$	15.0	11.1	4.14
10	2m	24,000	B	43.0	35.0	20.78	0.849	2.44	1.00294	21.5	25.8	$1.86 \times 10^{-3}$	19.6	11.2	4.15, 4.16
11	9m	52,852	B	42.8	35.6	28.45	0.849	3.05	1.00355	20.5	31.6	$2.18 \times 10^{-3}$	41.7	18.4	---
12	9m	52,852	B	45.0	35.7	27.02	0.849	3.44	1.00426	20.7	28.3	$1.94 \times 10^{-3}$	41.5	19.4	4.17, 4.18
13	9m	52,852	B	43.3	35.8	23.94	0.849	2.46	1.00370	18.7	29.6	$2.01 \times 10^{-3}$	41.2	22.0	4.19, 4.20
14	9m	52,852	B	45.0	36.3	23.94	0.849	2.78	1.00315	19.7	27.9	$1.83 \times 10^{-3}$	40.1	22.2	4.21, 4.22
15	9m	52,852	B	46.0	35.4	23.94	0.849	2.28	1.00051	19.0	30.7	$2.14 \times 10^{-3}$	42.1	21.7	4.23
16	9m	52,852	B	25.1	20.0	8.78	0.849	2.00	1.00243	20.0	12.0	$3.51 \times 10^{-3}$	132.1	33.4	4.24
17	40m	399,520	B	24.6	19.0	28.45	0.849	4.79	1.00472	(2)	25.2	$8.36 \times 10^{-3}$	1106.7	74.1	4.25, 4.26, 4.27
18	40m	399,520	B	24.3	19.0	28.45	0.849	3.61	1.00367	(2)	29.1	$9.63 \times 10^{-3}$	1106.7	74.1	4.28, 4.29, 4.30

Notes:

- (1) A - Continuous filling method  
B - Towed plate method

- (2) See Table 4.3 for detailed measurements.

uniform density upon another. A two-layer system was used for one experiment. It was produced by simply spreading a layer of tap water carefully on a layer of salt solution.

The density profiles produced for all of the other experiments were continuous. Such stratification is common in natural impoundments. For many of the experiments density profiles were nearly linear. Any continuous stratification of arbitrary shape was acceptable as an initial density profile for the numerical simulation of the mixing process.

Stratification for many of the experiments in the 2-meter tank was accomplished by a technique allowing continuous filling (Fig. 4.3). A 600 liter polyethylene tank was filled with salt solution of concentration,  $c_0$ . It was equipped with a propeller stirring device to keep it well-mixed. Tap water with concentration  $c_1$  was discharged into this tank from a second tank at a constant rate. From this well-mixed tank was withdrawn salt solution of concentration  $c$ . A mass balance for the well-mixed tank shows that, if the discharge of tap water into the tank is one-half of the discharge from the tank, the resulting concentration  $c$  will vary linearly in time from  $c_0$  to  $c_1$ . These discharge conditions were met by using flow meters and valves for some cases. When the well-mixed tank and tap water supply tank had equal cross-sectional areas, a siphon between them satisfied this discharge condition. The salt solution taken from the well-mixed tank was discharged into the 2-meter tank by way of a floating radial spreader (see Fig. 4.4) which was used to minimize the mixing during spreading.

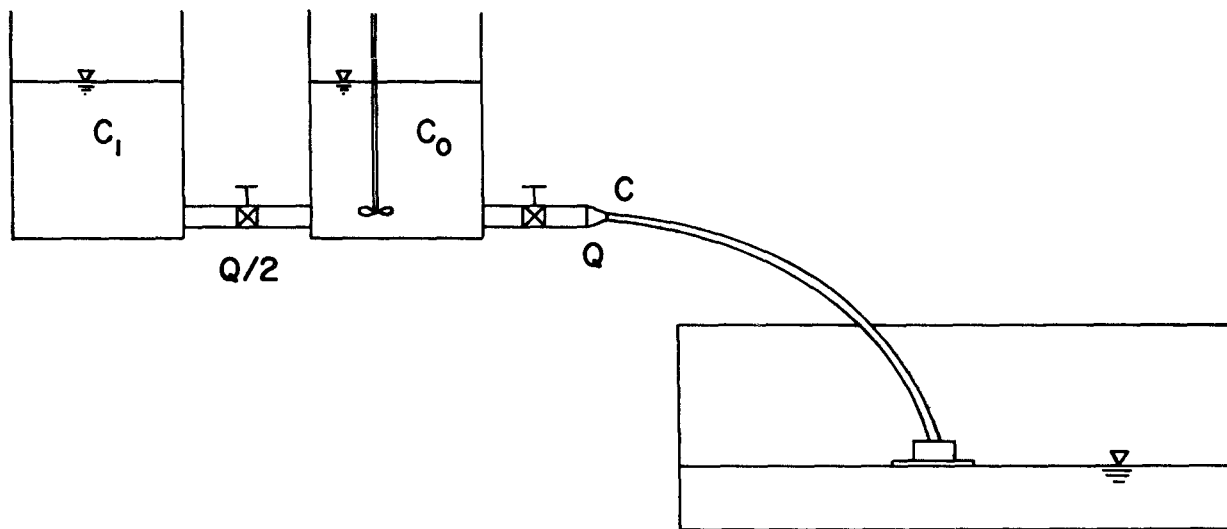
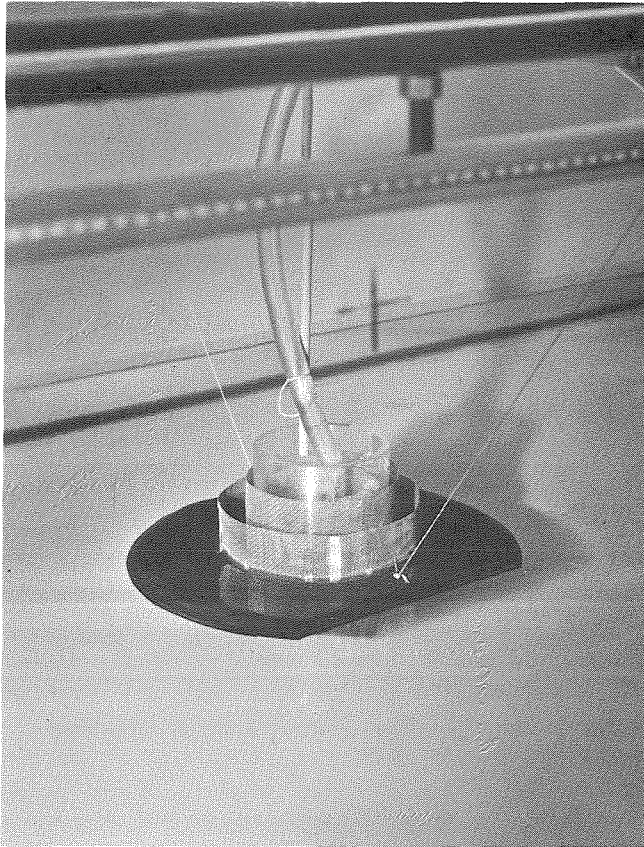


Figure 4.3 Definition sketch of continuous filling technique



10702

Figure 4.4 Photograph of surface spreading device

The density profiles generated by this continuous filling technique exhibited continuous density variation from bottom to top.

Deviation from linear density-depth profiles was often the result of filling so rapidly that the stirred tank did not remain well-mixed and mixing was induced by rapid spreading in the tank.

Stratification for experiments in the 9-meter flume, the 40-meter flume and some experiments in the 2-meter tank was accomplished by a technique better suited for containers of large volume than the continuous filling technique. This technique for generating linear profiles has been reported by Clark, Stockhausen, and Kennedy (12). It exploits the fact that the turbulent wake created by a moving plate perpendicular to the plane of discontinuity in a two-layer density profile, generates a density-depth profile which is nearly linear (Fig. 4.5).

The two-layer density profile was formed in either of two ways. The first, described previously, involved simply spreading the less dense layer upon the denser layer or injecting the denser fluid under a less dense layer. This method of achieving a two-layer system may require much time, when large volumes are involved. Also, it may result in a surface of density discontinuity between layers which is not horizontal, if the spreading or injection of fluid causes considerable mixing between layers. A second method was found to be more efficient. The tank was divided in two by a temporary dam. The regions on either side of this dam were filled with tap water to depth required for the mixing experiment. To one side was added the amount of salt required to produce a salt solution of the maximum density

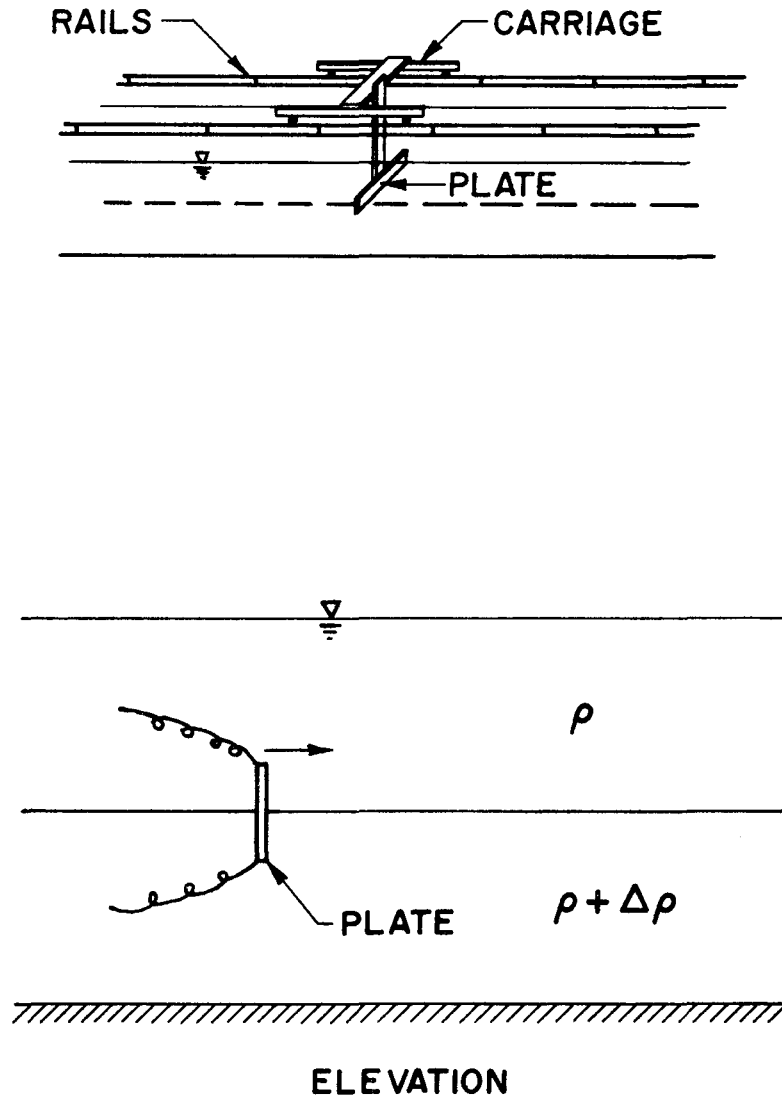


Figure 4.5 Sketch of arrangement of plate towed through a two-layer system



desired for the experiment. After this region had been mixed to uniformity by manual agitation with paddles, the dam was lifted and the resulting density underflow formed the required two-layer system.

Since each tank was equipped with an instrument carriage mounted on rails for longitudinal traverses, the mixing plate was attached to the carriage with a single vertical strut (Fig. 4.5). The plates were approximately one centimeter shorter in length than the widths of the tanks in which they were used. They were 10 centimeters wide and 0.6 centimeters thick. The plate was positioned across the width of the tank, as shown in Fig. 4.5, with its center line at the interface of the two-layer system. The carriage and plate were moved along the tank manually in the 2-meter tank and 9-meter flume, and by an electric motor in the 40-meter flume. The plate was moved at approximately 30 cm/sec in cases of depths of the order of 40 centimeters and at approximately 10 cm/sec in cases of depths of the order of 20 centimeters.

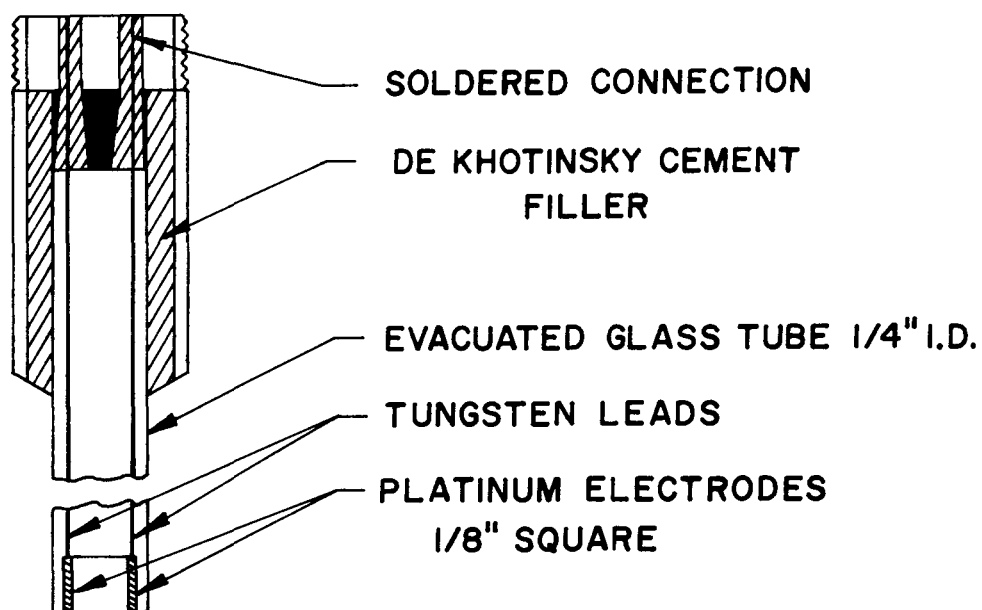
After the plate was towed through the two-layer system, the tank was left undisturbed for two to five hours to allow turbulent mixing to die out and hydrostatic equilibrium to be reached. The density profiles generated by this technique varied continuously from top to bottom and, in several cases, were nearly linear.

#### 4.2.3 Determination of Density Profiles

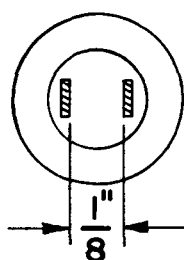
The salt solutions were made using tap water and Morton Culinox Food Grade Salt "999". The value of the density of the fluid in grams/milliliter was inferred from the salt concentration and temper-

ature of the fluid using convenient tables prepared by Owens (36), based on data in International Critical Tables. The concentration of the salt solution was determined by measuring the conductivity of the fluid with conductivity probes calibrated with a set of standard solutions. The concentration of salts in the tap water (inferred from conductivity measurements) varied among the experiments and was always less the equivalent NaCl concentration of 1 gram/liter. The maximum concentration of salt solution used was 10 grams/liter. Comparisons of density measurements using a pycnometer with tabulated density values show good agreement.

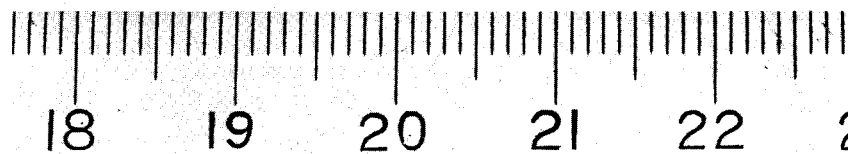
The conductivity probes used were of two similar types. One type, developed at the Massachusetts Institute of Technology, consisted of platinum plate electrodes 0.32 centimeters x 0.32 centimeters x 0.76 millimeters placed 0.32 centimeters apart at the base of a glass tube. This type of probe is shown in Fig. 4.6 and described by Koh (26). A second type of probe of similar design was constructed for this study. The electrodes were of the same size and spacing, but they were connected to short pure platinum wires which were silver soldered to copper wire leads which extended to the electrical connector at the top of the probe. These leads were insulated from one another by plastic tubing from the electrodes to the connector, and the glass tube containing them was not evacuated. Probes of both types measured approximately 50 centimeters from electrodes to connector. The electrodes were cleaned initially in chromic-sulfuric acid and platinized in the standard manner (44). The electrodes were kept in



LONGITUDINAL SECTION



CROSS SECTION



IMM

6689

Figure 4.6 Conductivity probe (from Koh (26) )

distilled water when not in use and cleaned before each use in sulfuric acid by electrolysis. Platinization was repeated during the course of the investigation whenever reduced sensitivity was detected. No difference in the quality of performance was discerned between the two types of probes.

The conductivity measurements were recorded by means of a two channel Sanborn 150 recorder with 1100 AS Carrier Pre-Amplifier. The probes were connected to the recorder through an external half-bridge circuit as shown in Fig. 4.7.

The probes were calibrated by means of a set of standard salt solutions which varied in concentration from 0.125 to 10.0 grams/liter (a density range of 0.99811 to 1.00507 grams/milliliter at 21°C). A typical calibration curve is shown in Fig. 4.8. The calibration relation was nonlinear because the range of concentrations used was large. Since the time between successive measurements of the concentration profile in the tank was often hours, readjustment of the recorder's bridge was occasionally necessary. Therefore, calibration curves were obtained for each conductivity probe just prior to each measurement of a concentration profile. Following each profile measurement, the baseline or lowest concentration for which the probe had been calibrated was checked.

The probe was held by a small clamp which was attached to a vertically traveling scale with vernier reading to  $\pm 0.01$  centimeter. Vertical concentration profiles were measured by fixing the probe at uniform vertical intervals and recording the conductivity measurement

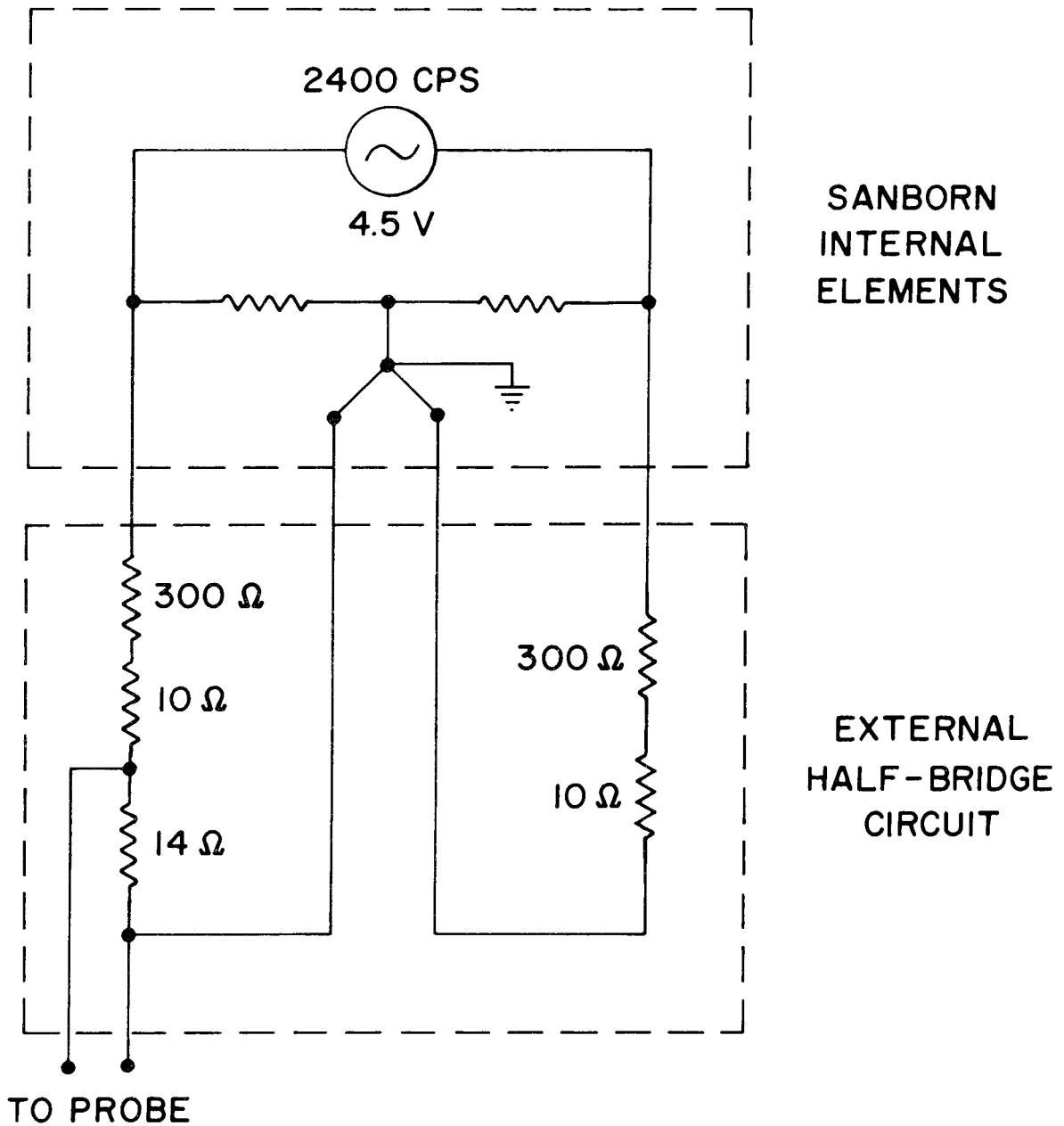


Figure 4.7 Circuit diagram for a conductivity probe used with a Sanborn recorder

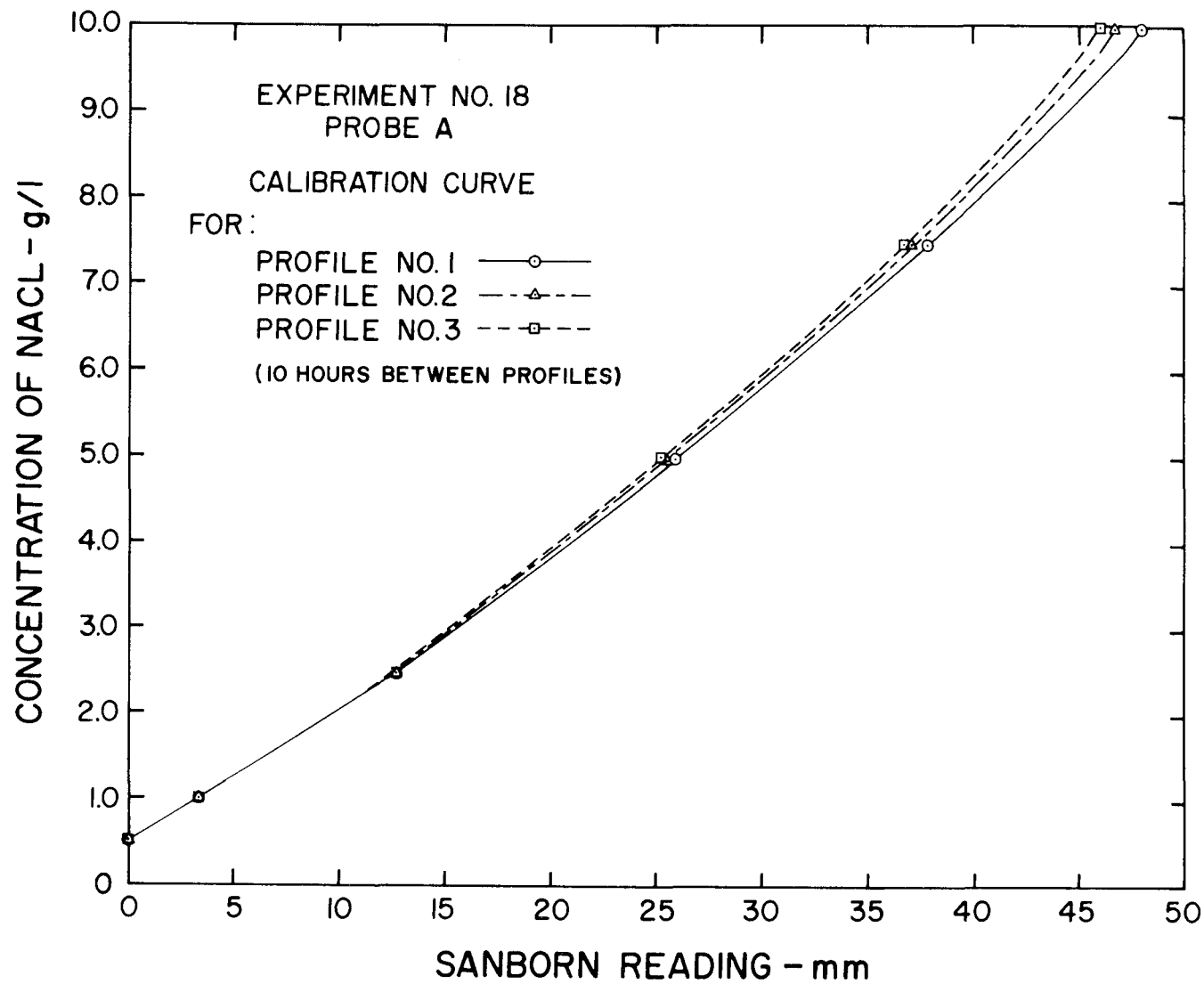
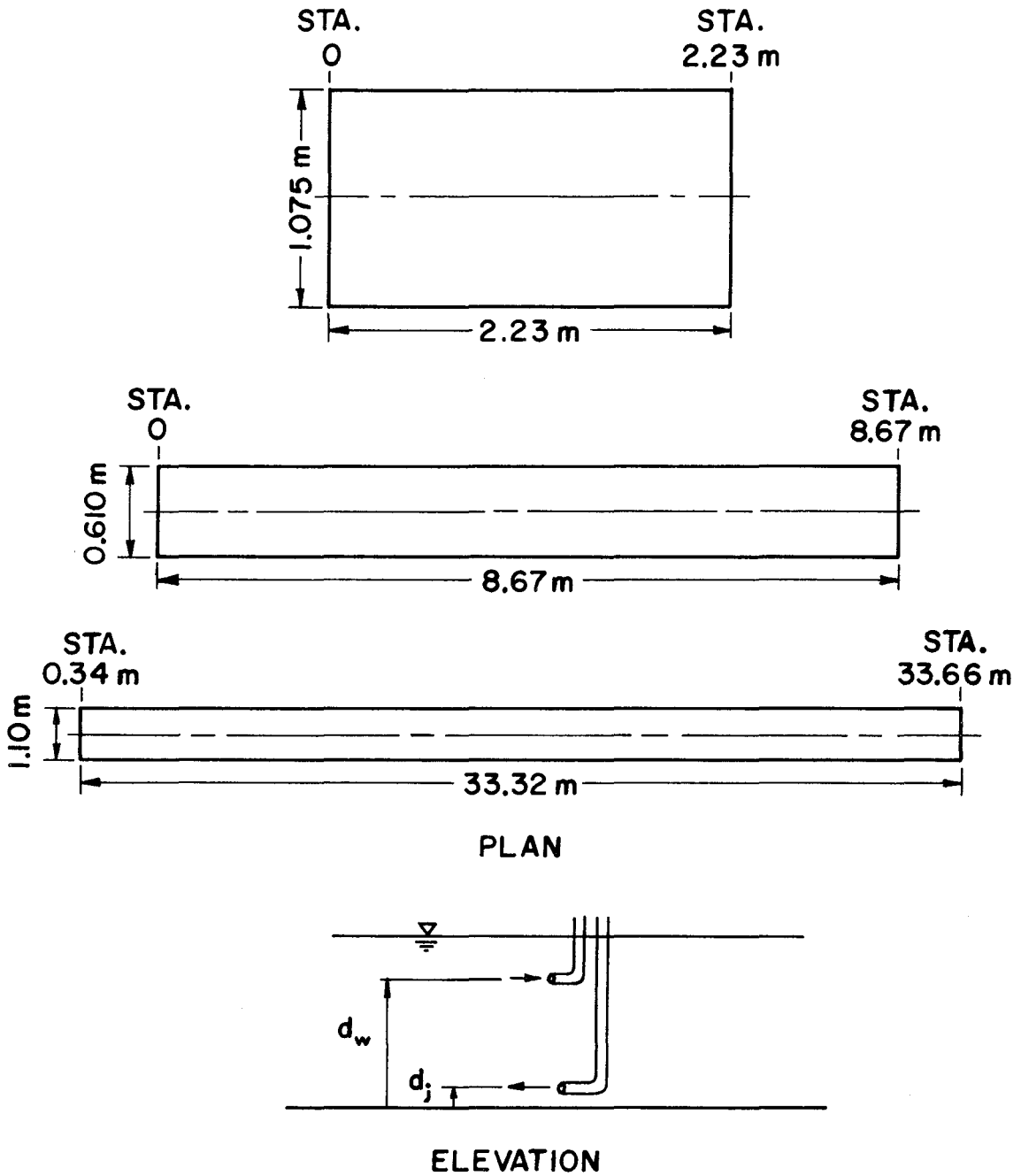


Figure 4.8 A typical set of calibration curves for a conductivity probe

at that position. Measurements were usually made from the surface downward. Since fluid was displaced by the probe's downward movement, a record of 30 to 40 seconds duration was made to allow relative equilibrium to be reached. Vertical profiles from the bottom upward were made occasionally to confirm the downward measurements, but the necessity of disturbing the upper region to get the probe to the bottom made this method less attractive. The length of time required to make sufficient measurements to delineate the concentration profile clearly was a function of the depth and detail of the density structure for each experiment. With the exception of the initial profile measured before pumping began, the time required was of the order of 10 to 15 minutes. This time interval was always small relative to the time required for significant and measurable changes in the density profile to occur.

Two conductivity probes were used simultaneously during several experiments so that lateral gradients in density might be observed as well as vertical distributions. The leads from each probe contained on-off switches. This allowed one probe to be off while the other was on and prevented any interaction of the electric fields. Thus, vertical profiles were measured, at two different locations in the tank with measurements made alternately at the same elevations within 30 to 40 seconds of each other. Fig. 4.9 and Table 4.2 indicate the locations of the probes relative to the jet and withdrawal tubes.



SCALES NOMINAL

Figure 4.9 Location sketch for the positions of conductivity probes and jet and intake tubes in laboratory tanks



Table 4.2 Summary of Locations of Jet and Intake Tubes and Vertical Density Profile Measurements

Locations of Jet and Profiles

Exper. Number	Tank	Location of Tube Stations on $\mathcal{C}_L$	$d_w$ cm from bottom	$d_j$ Fig. 4.9	Locations of Vertical Profile Measurements Stations on $\mathcal{C}_L$		
1	2 m	2.00 m	0.24	45.0	0.22 m		
2	2 m	2.10 m	3.8	44.2	0.30 m		
3	2 m	2.00 m	7.0	25.7	0.30 m		
4							
5	2 m	2.00 m	40.7	2.6	0.30 m		
6	2 m	2.00 m	38.0	2.4	0.30 m		
7	2 m	2.00 m	41.4	0.43	0.30 m		
8	2 m	2.10 m	30.0	0.11	0.10 m		
9	2 m	2.10 m	40.0	0.43	0.10 m	2.00 m off $\mathcal{C}_L$	
10	2 m	2.10 m	35.0	0.43	0.10 m	2.00 m off $\mathcal{C}_L$	
11	9 m	8.47 m	35.6	0.43	0.82 m	4.47 m	
12	9 m	8.40 m	35.7	0.43	1.25 m	4.50 m	
13	9 m	8.35 m	35.8	0.43	1.25 m	4.50 m	
14	9 m	5.67 m	36.3	0.43	0.98 m	8.10 m	
15	9 m	5.69 m	5.3	40.7	0.97 m	8.00 m	
16	9 m	8.35 m	20.0	0.43	1.10 m	4.50 m	
17	40 m	17.4 m	19.0	0.43	3.34 m	18.50 m	33.66 m
18	40 m	18.5 m	19.0	0.43	3.50 m	18.50 m	33.50 m

The temperature of the fluid in the tank was measured during each experiment with an 8-inch Weksler  $15^{\circ}$ - $32^{\circ}$ C mercury thermometer with divisions of  $0.1^{\circ}$ C. The temperatures of the fluid in the 2-meter tank and 9-meter flume were generally uniform and constant throughout the tanks. Detailed temperature measurements were made in the 40-meter flume where unsteady vertical and longitudinal temperature gradients were found to exist.

The density values inferred from the conductivity measurements reflect small variations in recorded conductivities, calibration curves, and temperature measurements. The accuracy of the density values is estimated to be  $\pm 1 \times 10^{-4}$  grams/milliliter. This estimate is for the relative densities of any one experiment. Although the absolute density values may be less accurate because tap water conductivities were assumed due only to concentrations of NaCl, the relative densities govern the mixing process.

## 4.3 EXPERIMENTAL RESULTS

### 4.3.1 Presentation of Typical Experimental Results

Results from several mixing experiments are presented in Figs. 4.10 to 4.30. The results are in the form of depth-density profiles at various times during the mixing process. The hydraulic data and locations of the probes, jet, and withdrawal tubes for each experiment are given in Tables 4.1 and 4.2, respectively.

The density profiles determined in the experiments are indicated by the data points. Each point represents the density, as inferred from the conductivity measurements, at a given elevation, location in

the tank, and time. A set of points for a given dimensionless time  $t/T$  defines the measured profile at that time. The dimensionless time is defined as  $t$ , the time elapsed since the start of pumping, divided by  $T$ , a characteristic time for the system. This characteristic time,  $T$ , is found by dividing the volume of the tank between the elevations of the jet and withdrawal tubes by the pump discharge. The density values are expressed in the form  $(\rho - I) \times 1000$ , where  $\rho$  is the density of the fluid and  $I$  is an arbitrary constant of order grams/milliliter which allows the product  $(\rho - I) \times 1000$  to be a positive number of order 1 gram/milliliter. This notation provides convenient expression of the densities and density differences encountered in the experiments.

Accompanying each set of experimental points is the density profile predicted by the simulation technique for that time. The measured initial density profile is provided as input to the simulation, and density profiles at any time after pumping begins are generated by the simulation technique. Only those density profiles at times corresponding to experimentally measured profiles are presented.

The vertical location and inside diameters of jet and withdrawal tubes are shown to scale on the density profiles. The results presented include experiments from the 2-meter tank (Experiments Nos. 5, 6, 7, 8, 9, and 10), 9-meter flume (Experiments Nos. 12, 13, 14, 15, and 16) and 40-meter flume (Experiments Nos. 17 and 18). For several experiments (Nos. 10, 12, 13, 14, 17, and 18) density profiles measured simultaneously at different locations with the tank are presented.

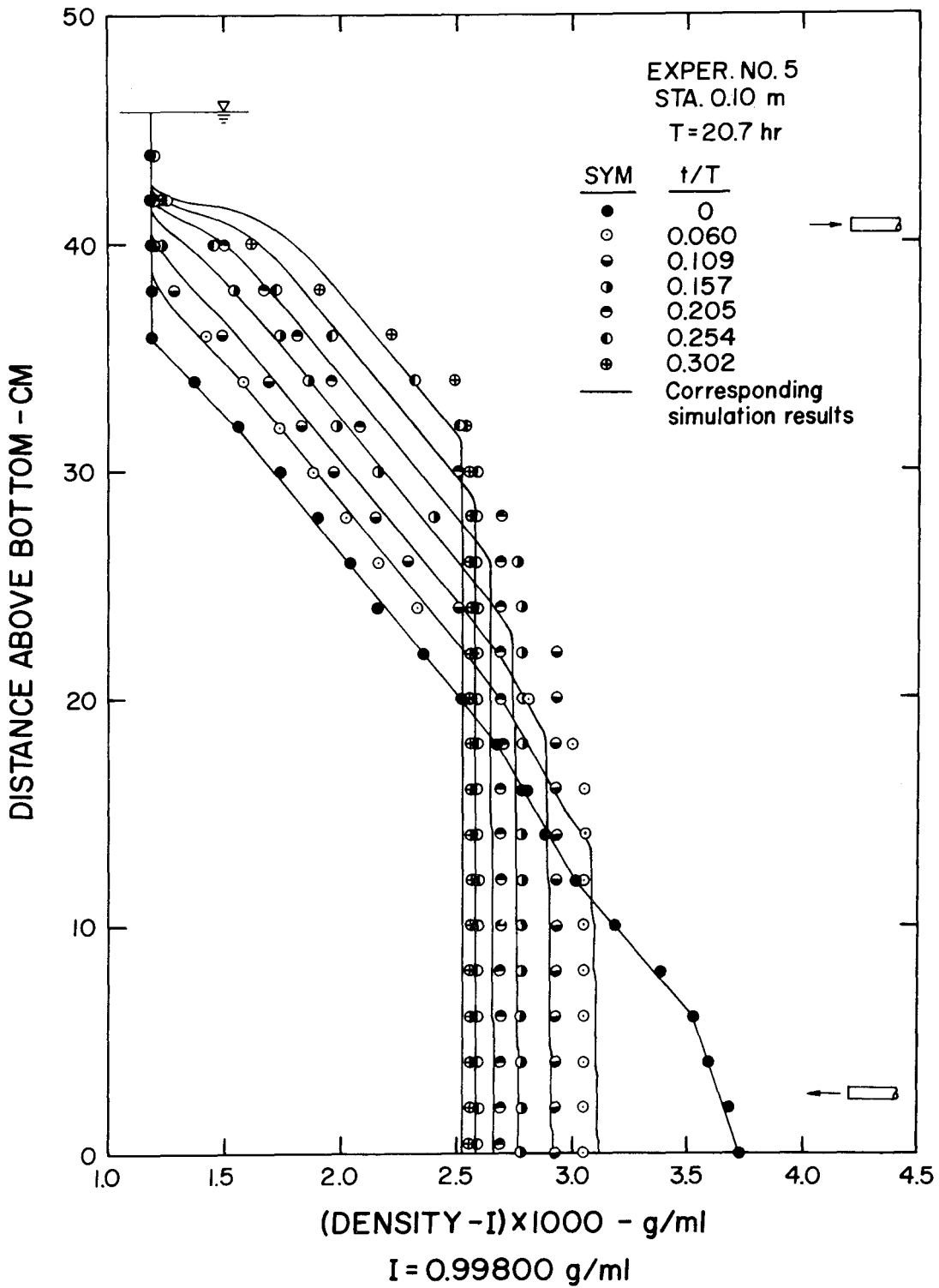


Figure 4.10 Measured and simulated density profiles for Experiment Number 5

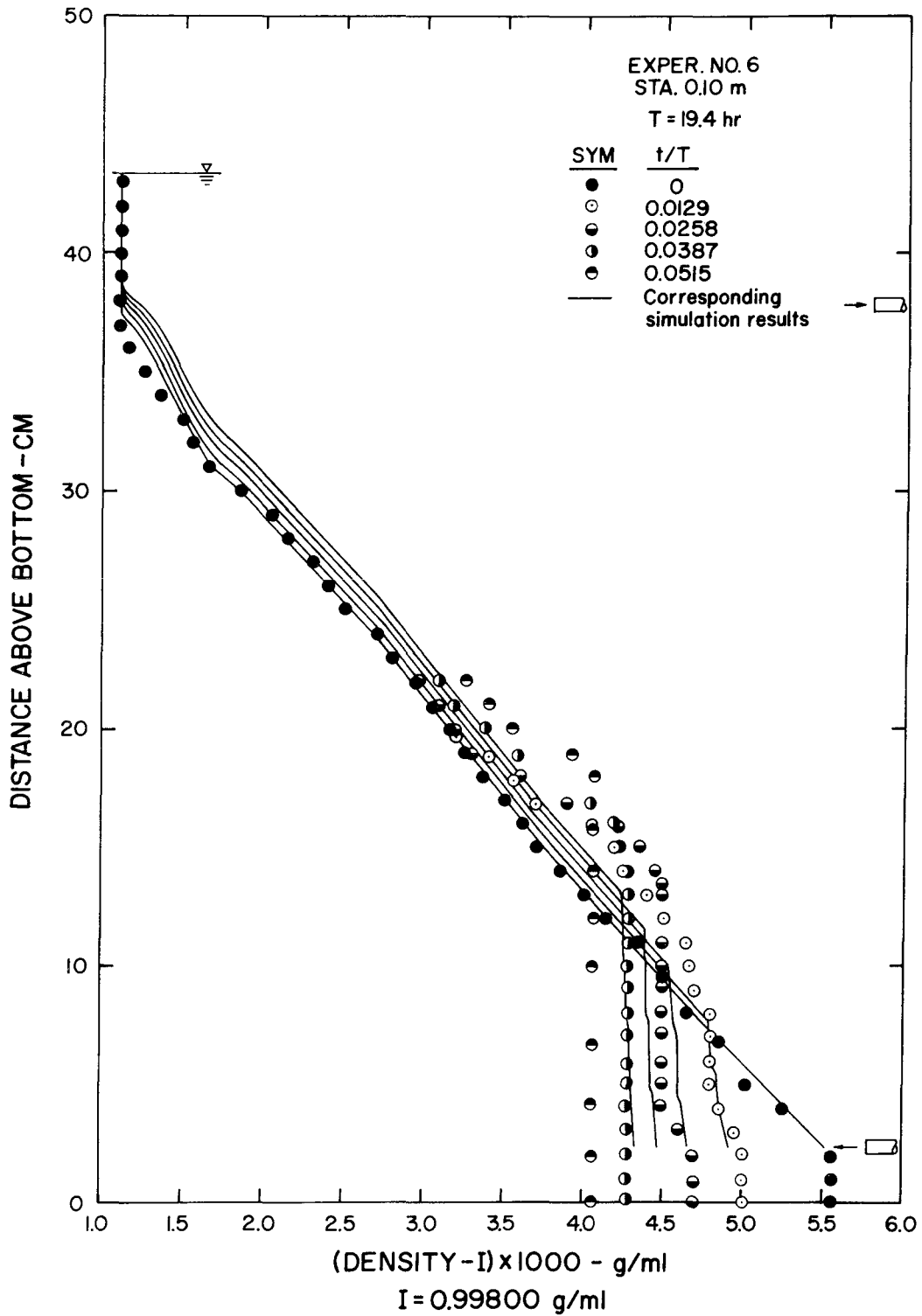


Figure 4.11 Measured and simulated density profiles for Experiment Number 6

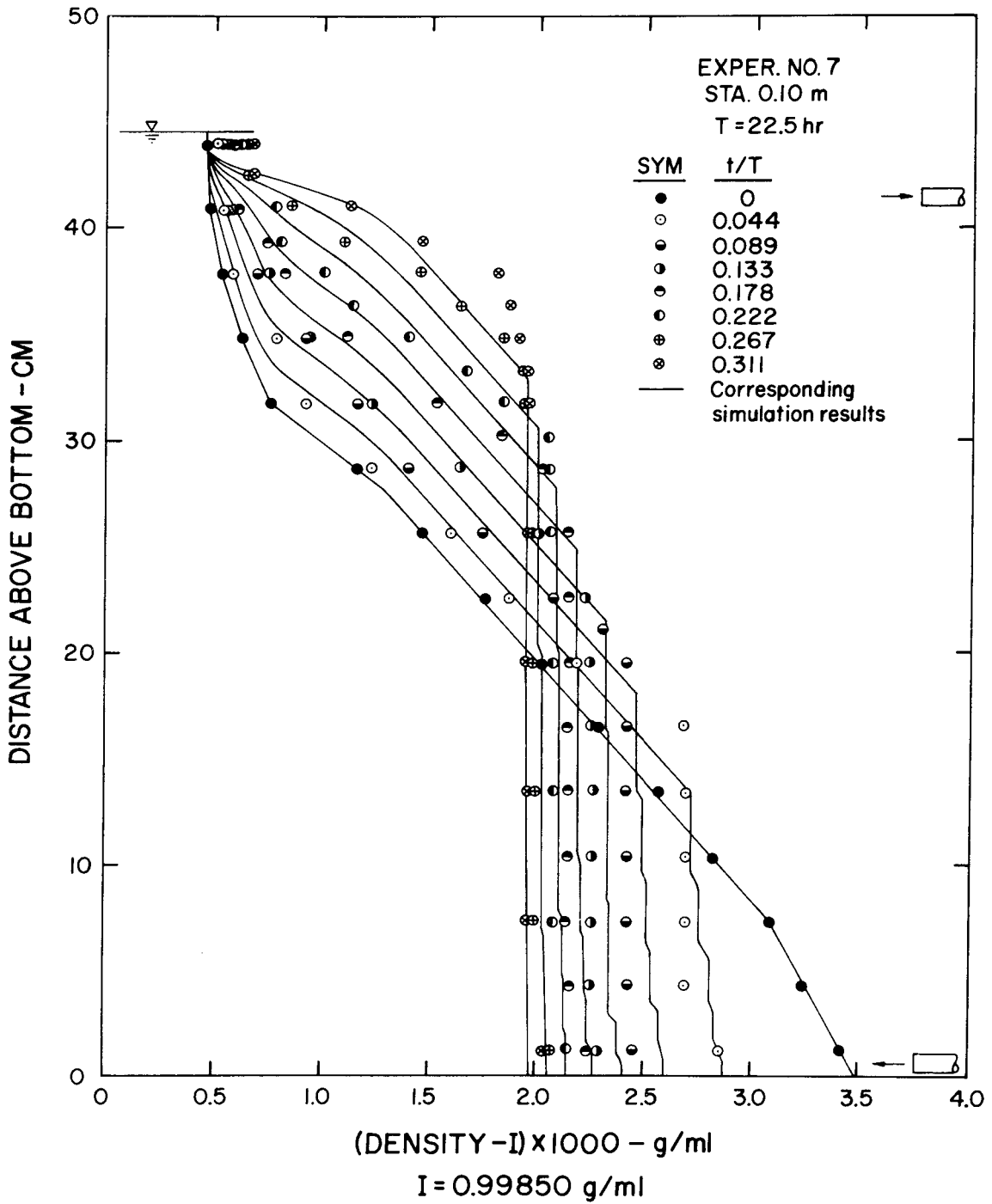


Figure 4.12 Measured and simulated density profiles for Experiment Number 7

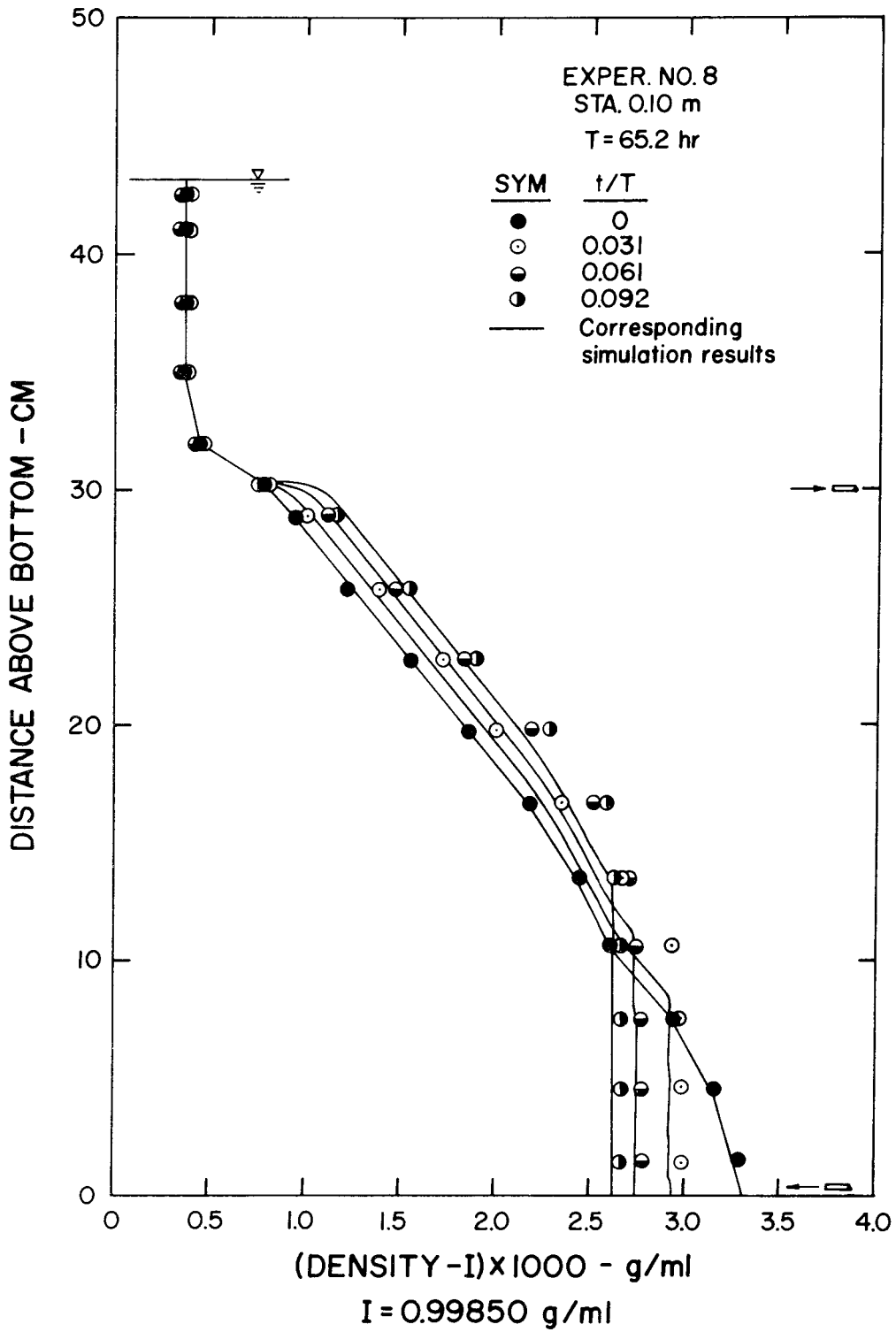


Figure 4.13 Measured and simulated density profiles for Experiment Number 8

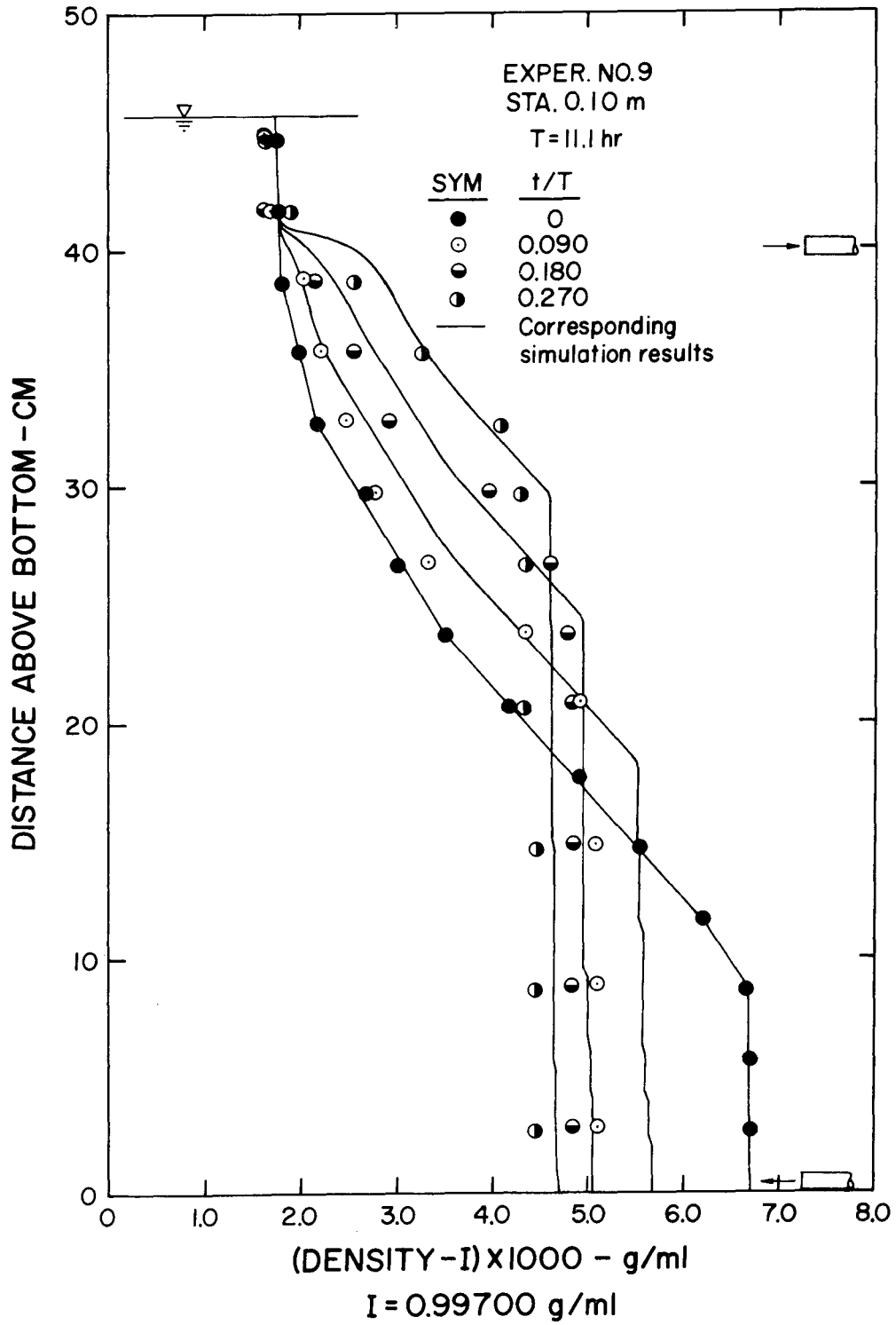


Figure 4.14 Measured and simulated density profiles for Experiment Number 9



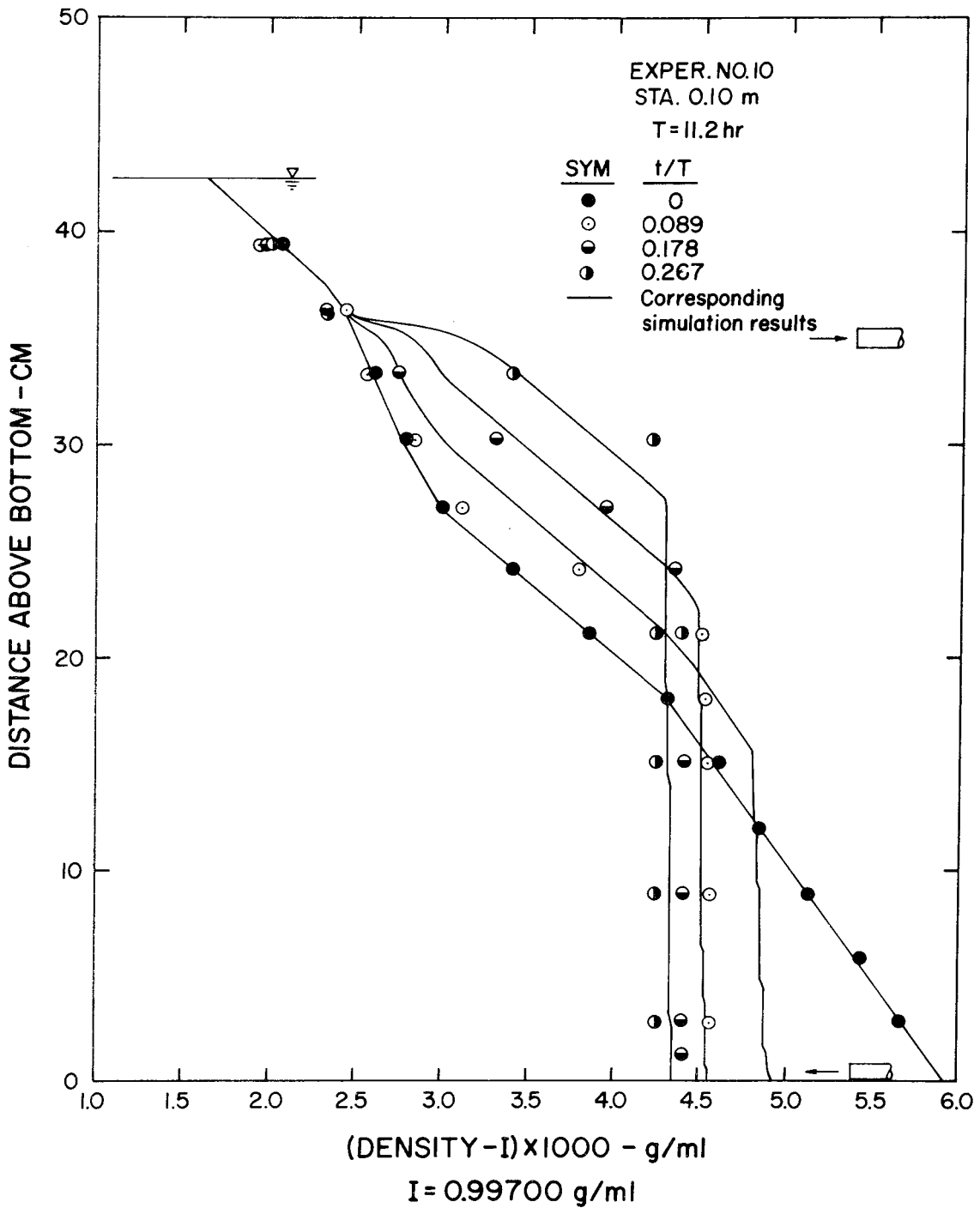


Figure 4.15 Measured and simulated density profiles for Experiment Number 10, at Station 0.10m

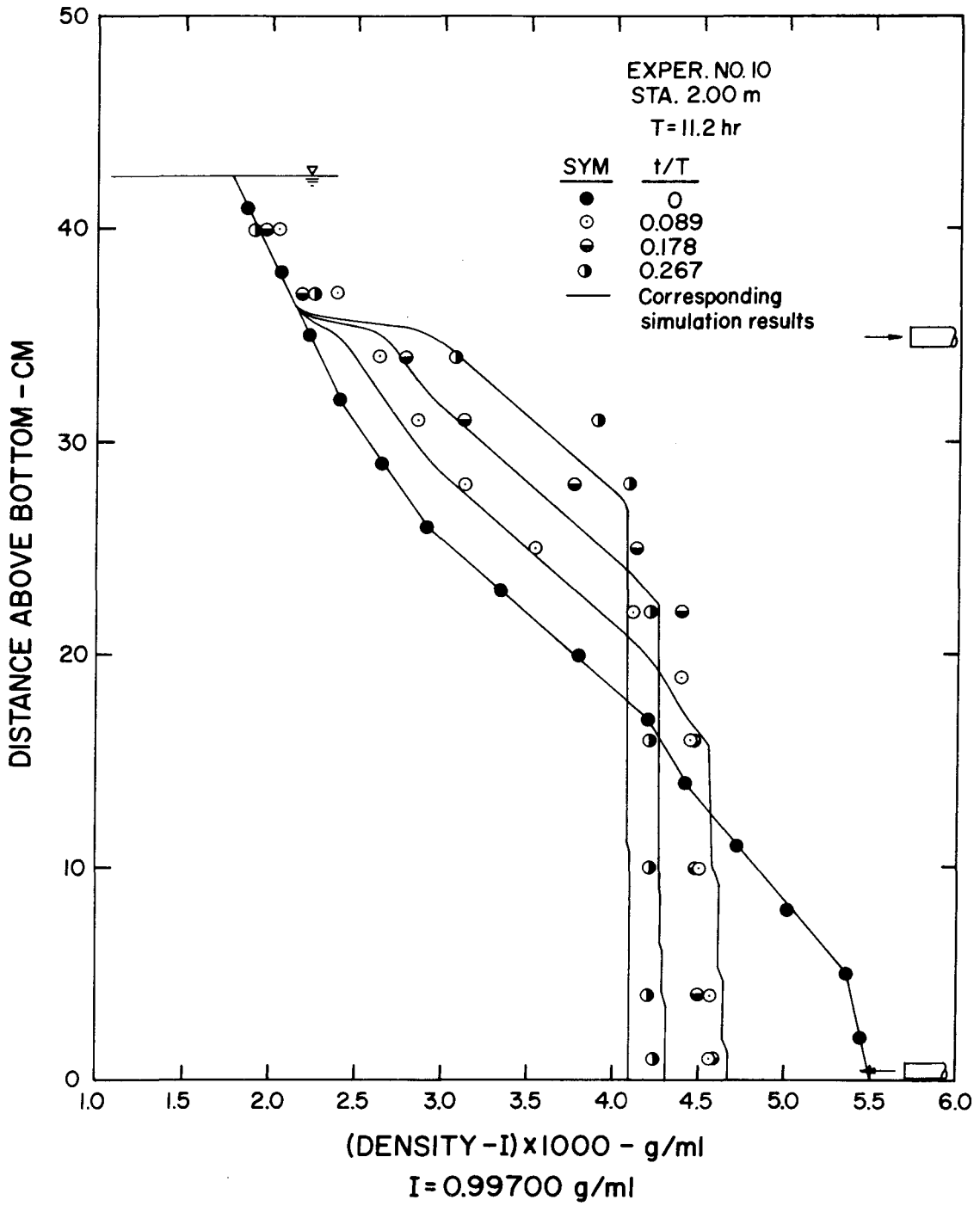


Figure 4.16 Measured and simulated density profiles for Experiment Number 10, at Station 2.00m

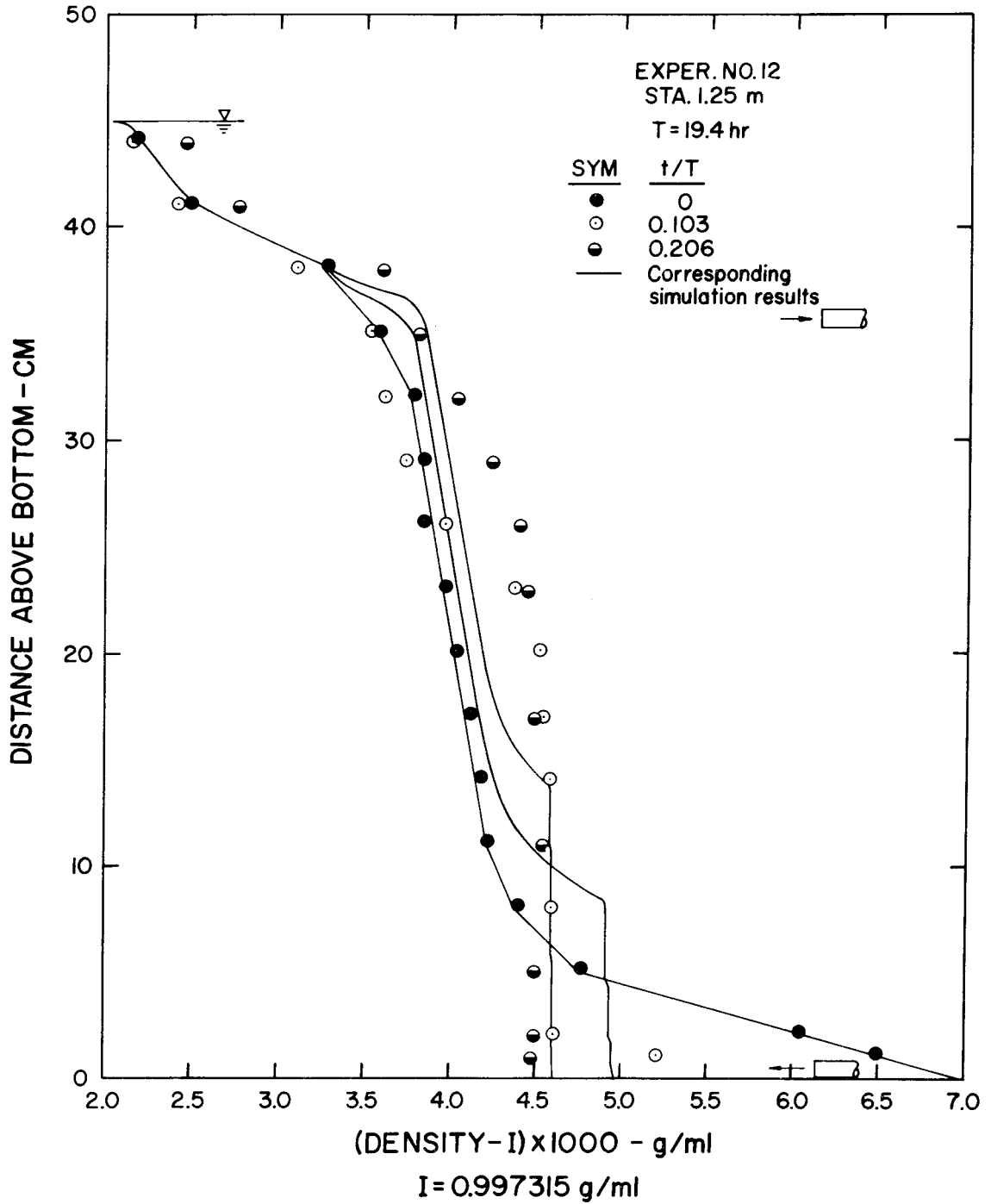


Figure 4.17 Measured and simulated density profiles for Experiment Number 12, at Station 1.25m

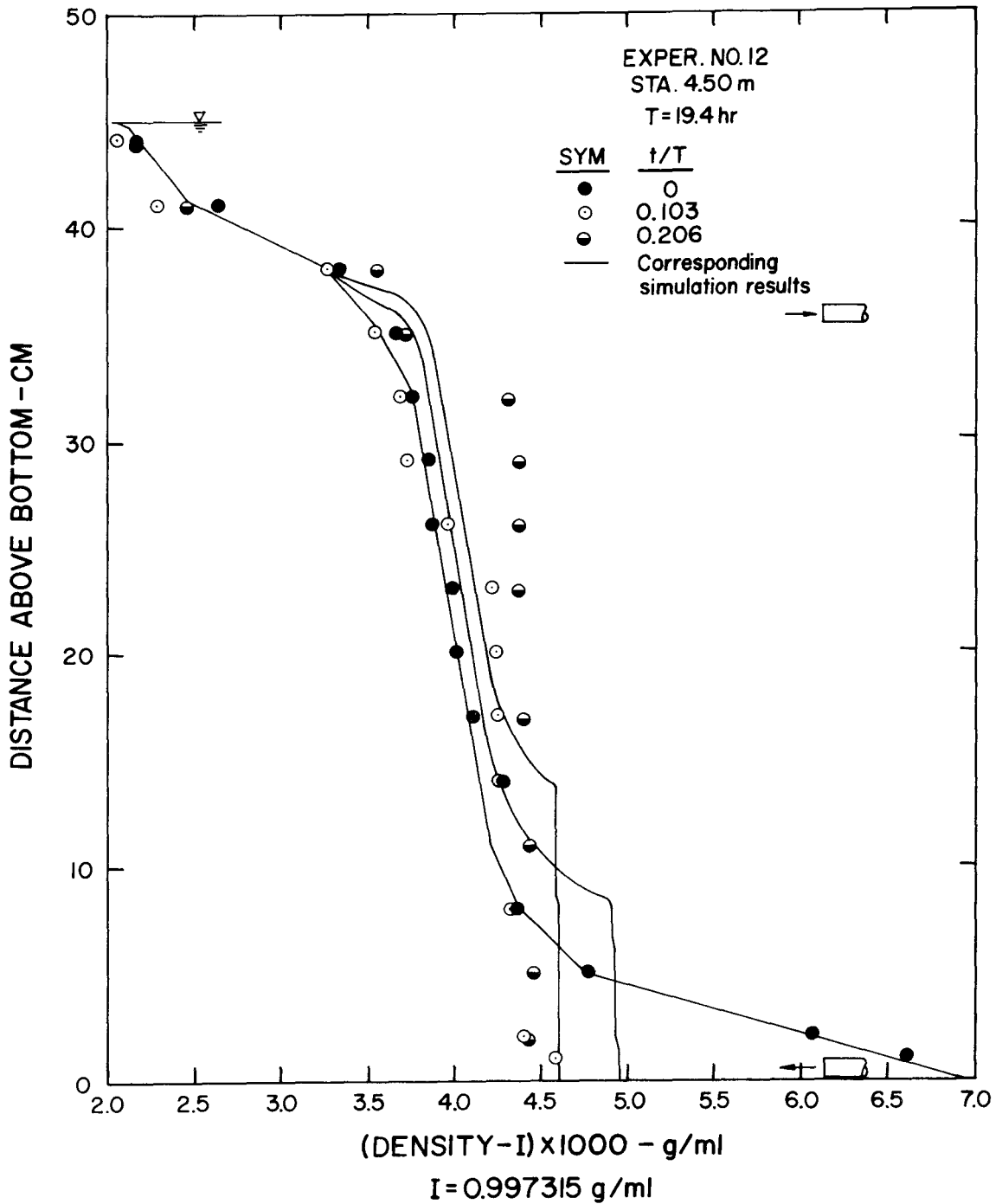


Figure 4.18 Measured and simulated density profiles for Experiment Number 12, at Station 4.50m

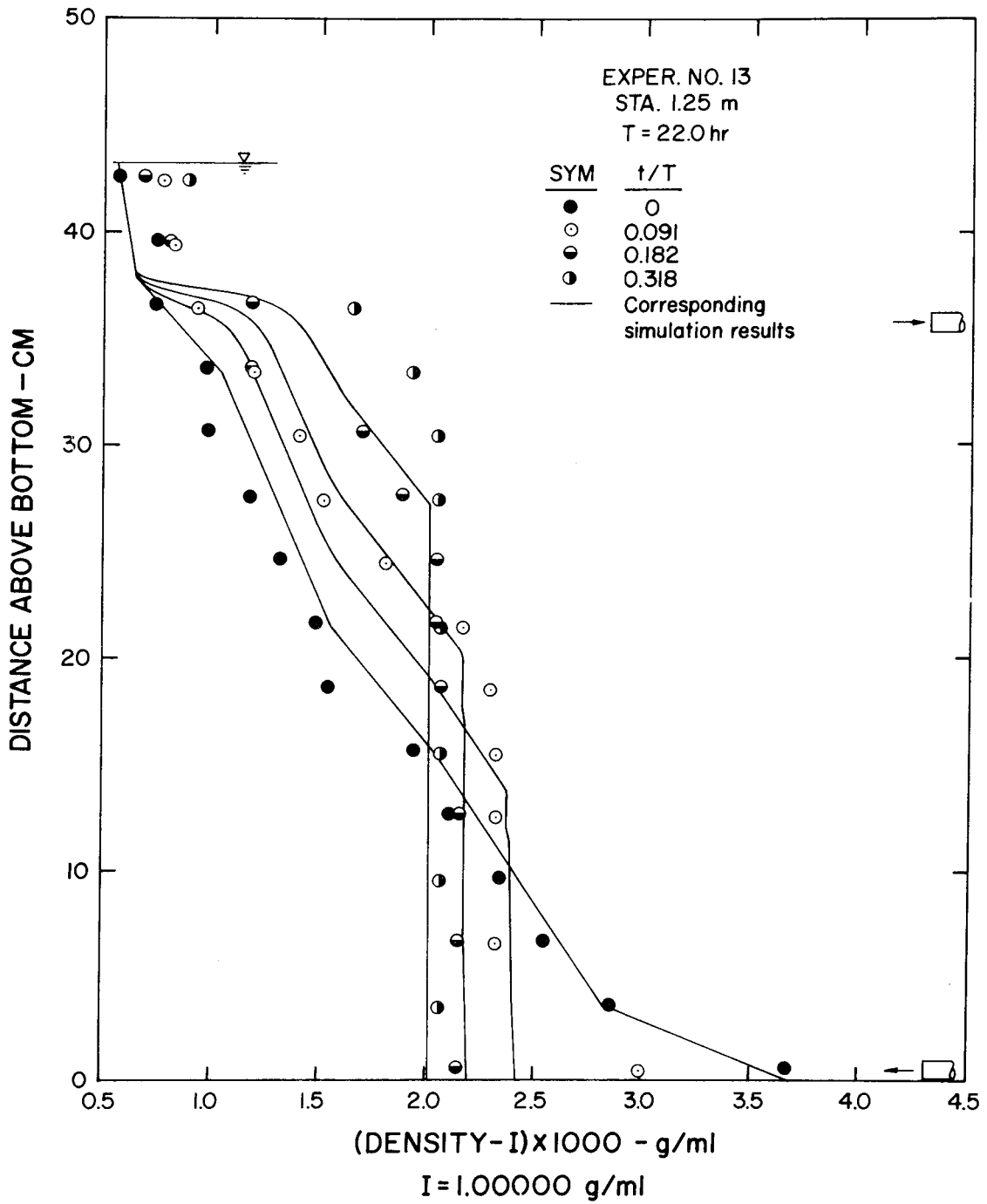


Figure 4.19 Measured and simulated density profiles for Experiment Number 13, at Station 1.25m

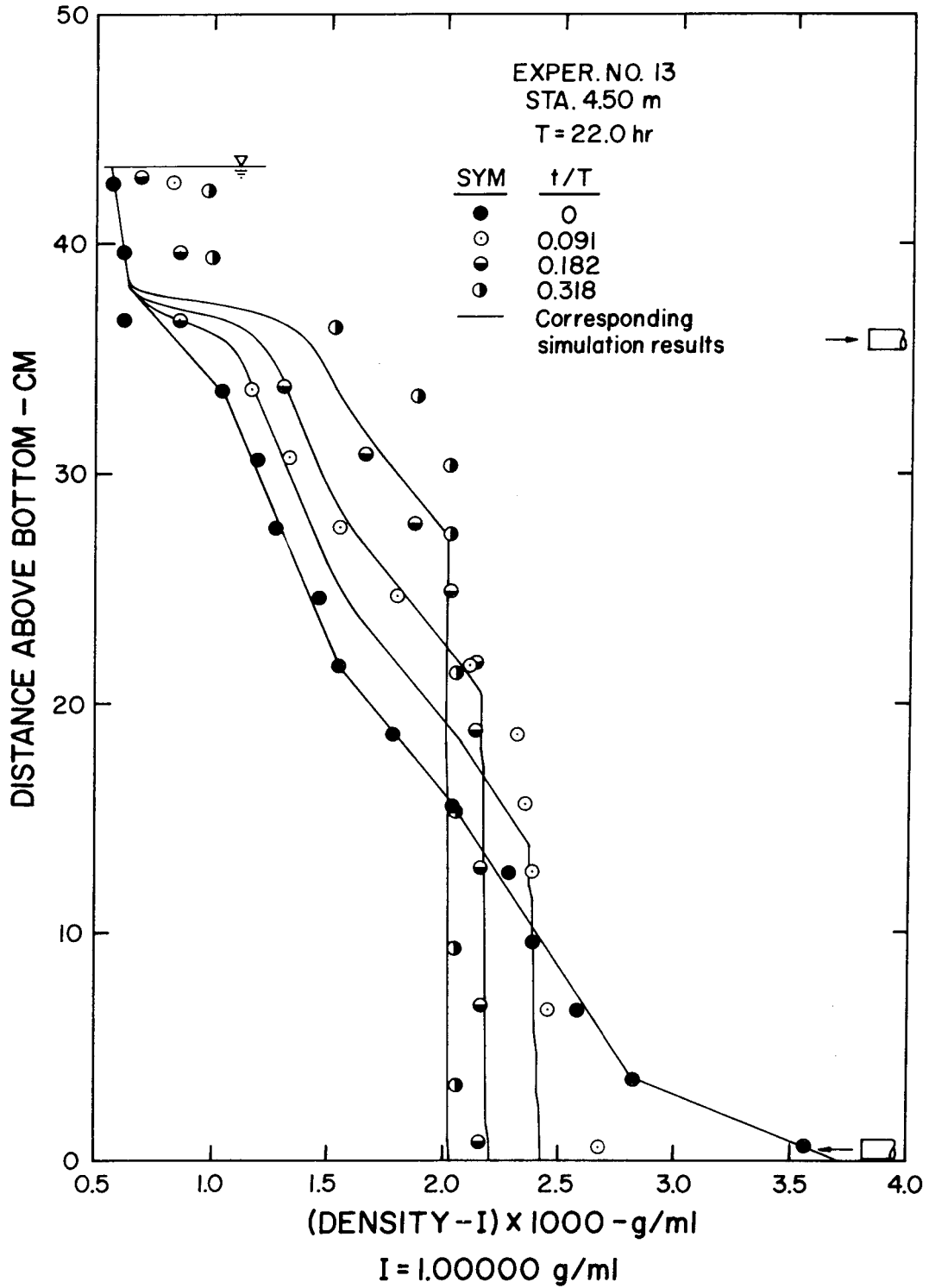


Figure 4.20 Measured and simulated density profiles for Experiment Number 13, at Station 4.50m

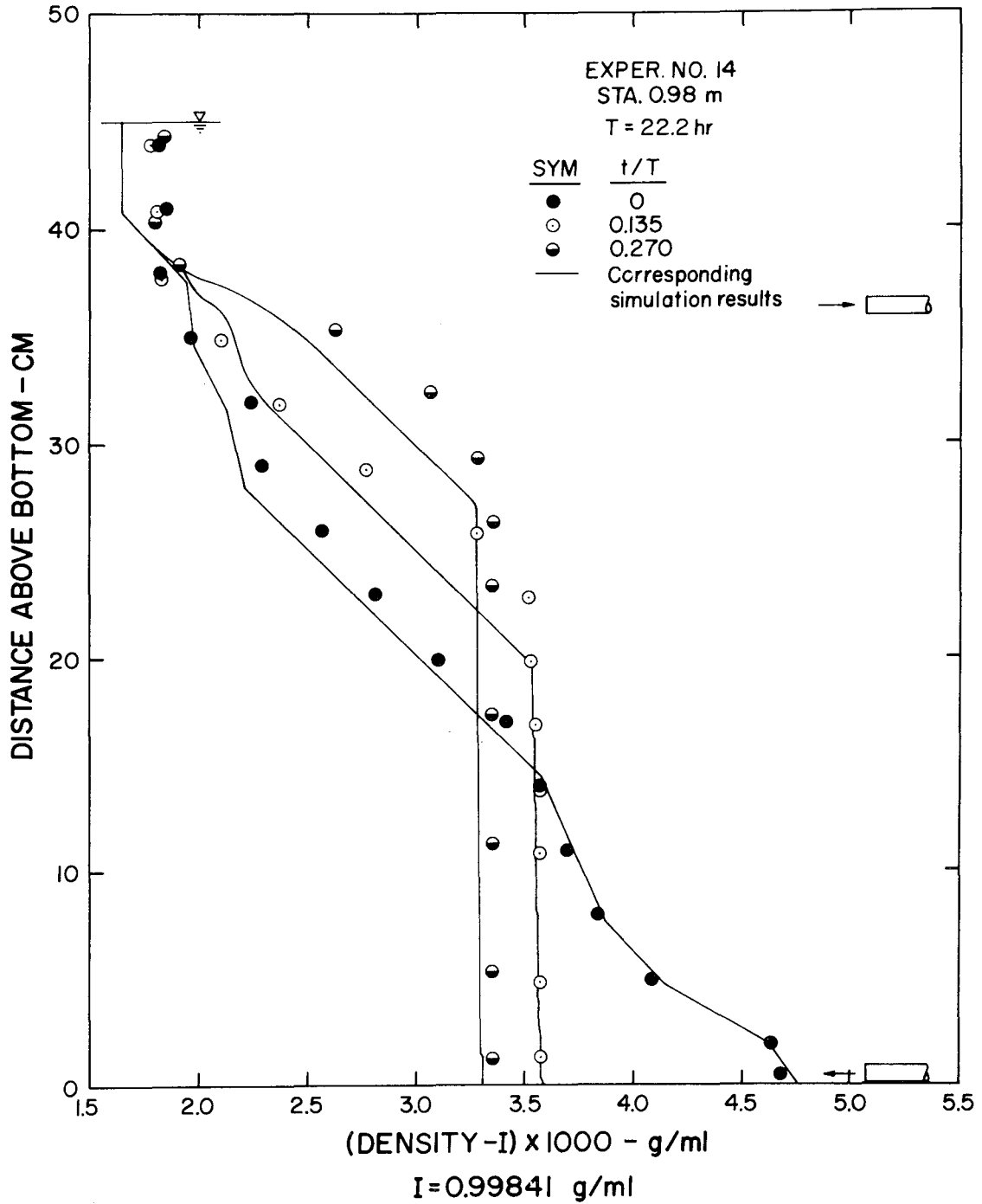


Figure 4.21 Measured and simulated density profiles for Experiment Number 14, at Station 0.98m

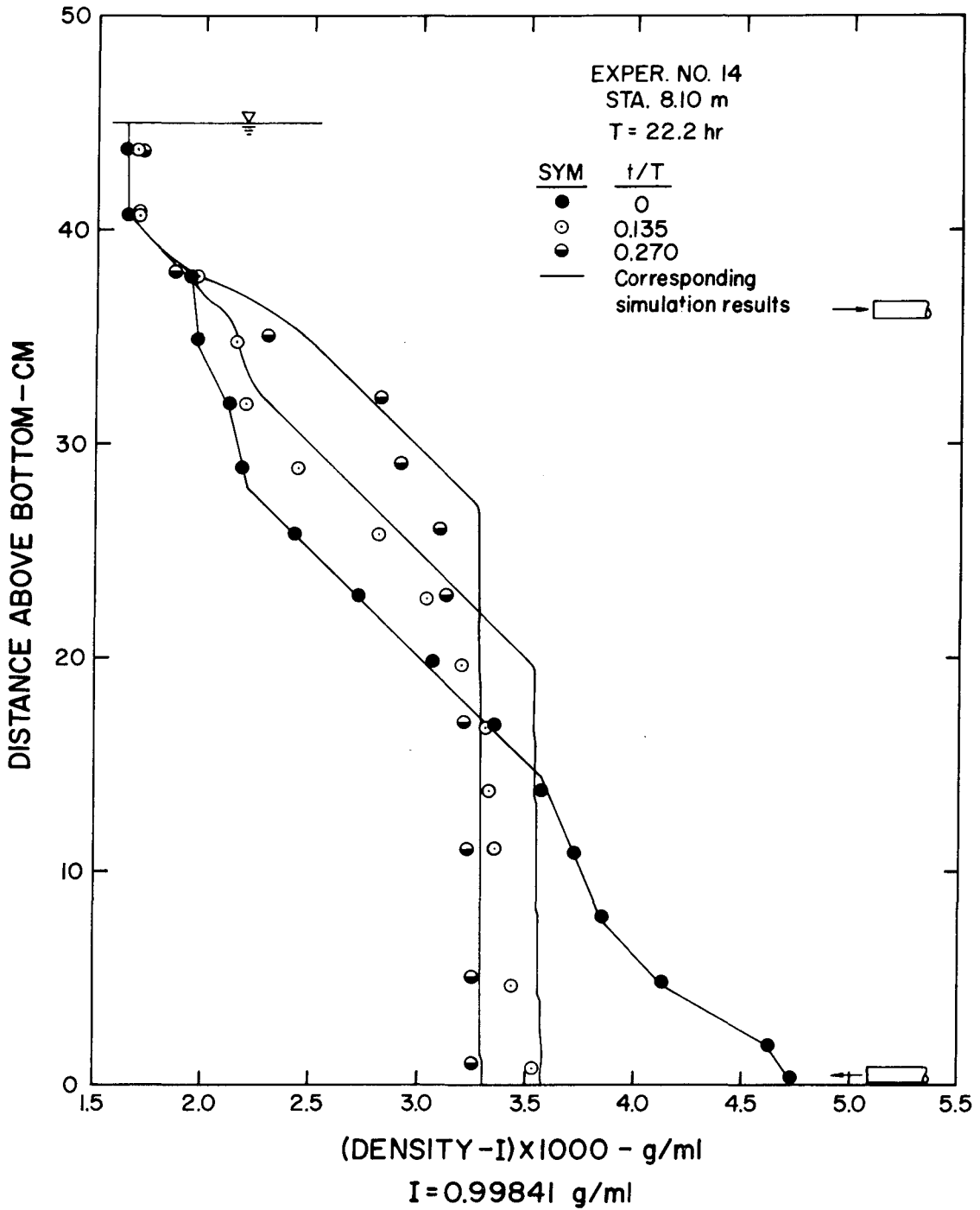


Figure 4.22 Measured and simulated density profiles for Experiment Number 14, at Station 8.10m



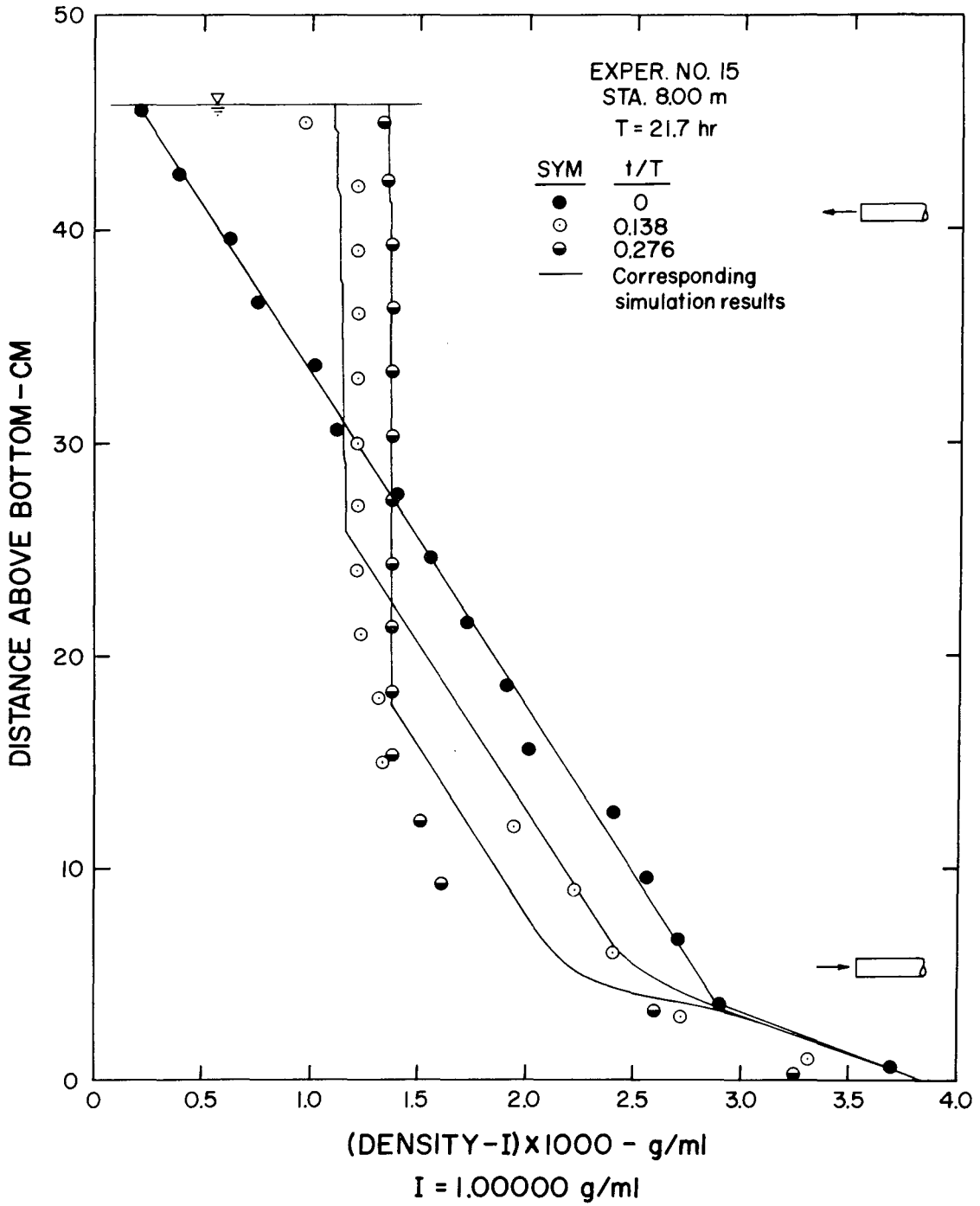


Figure 4.23 Measured and simulated density profiles for Experiment Number 15

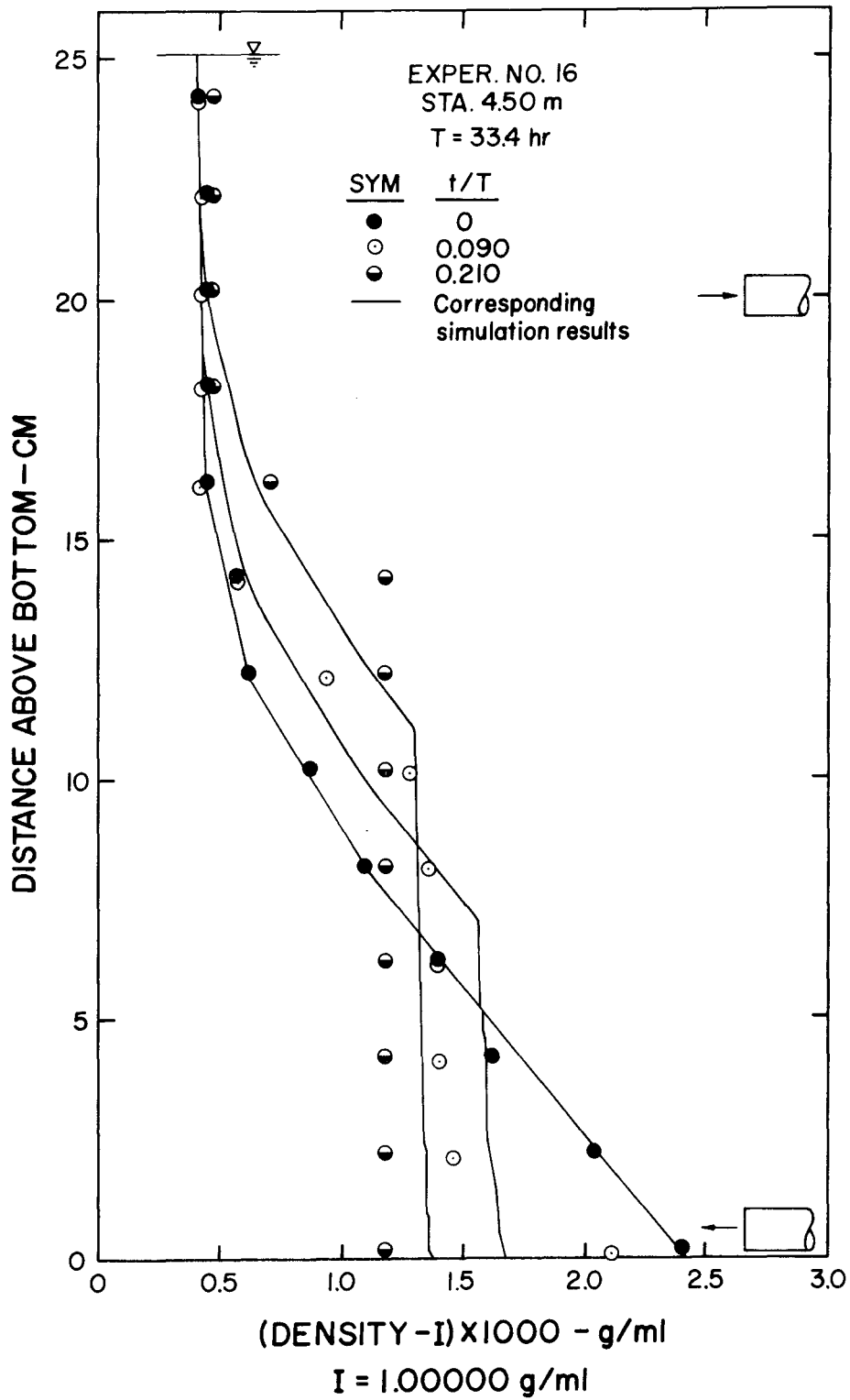


Figure 4.24 Measured and simulated density profiles for Experiment Number 16

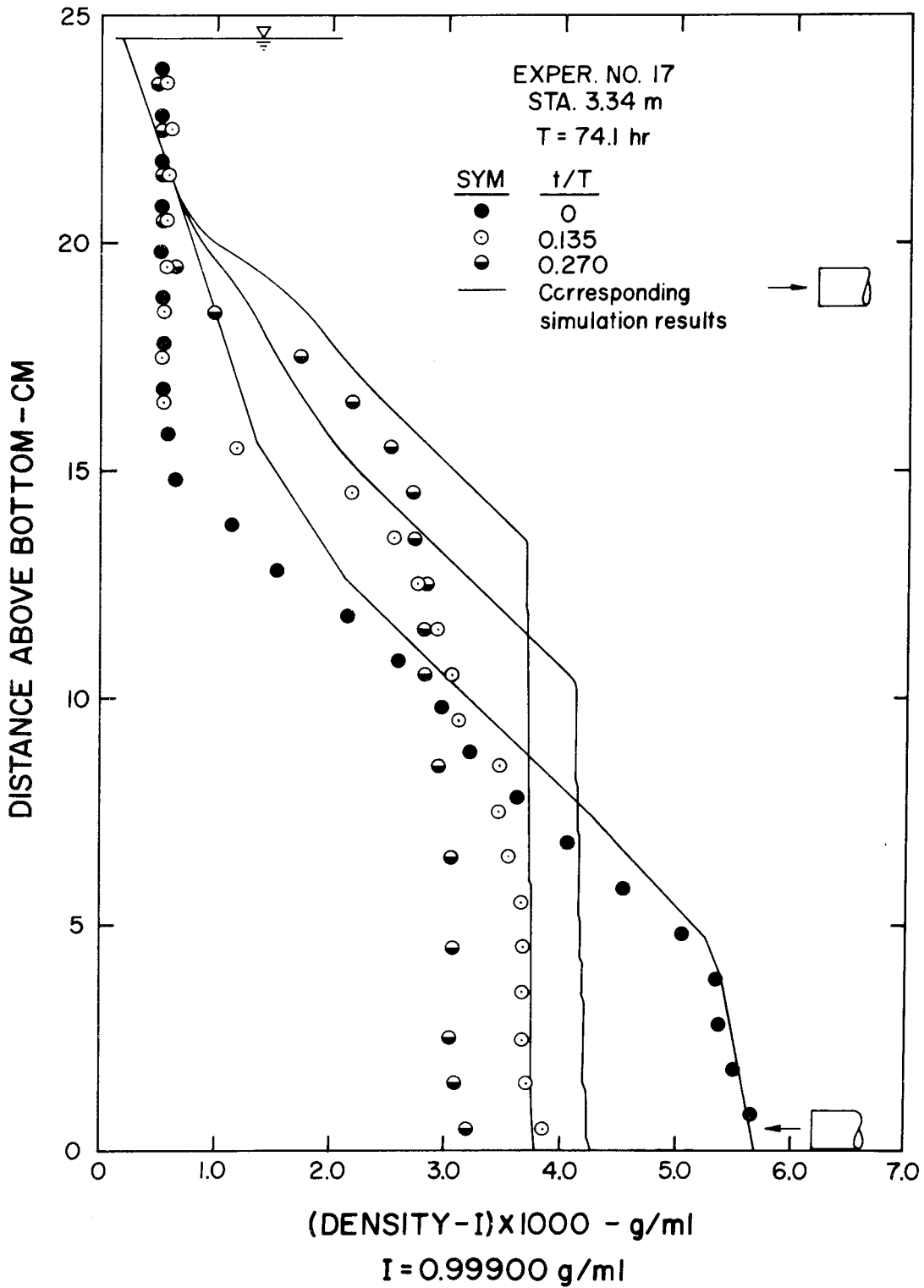


Figure 4.25 Measured and simulated density profiles for Experiment Number 17, at Station 3.34m

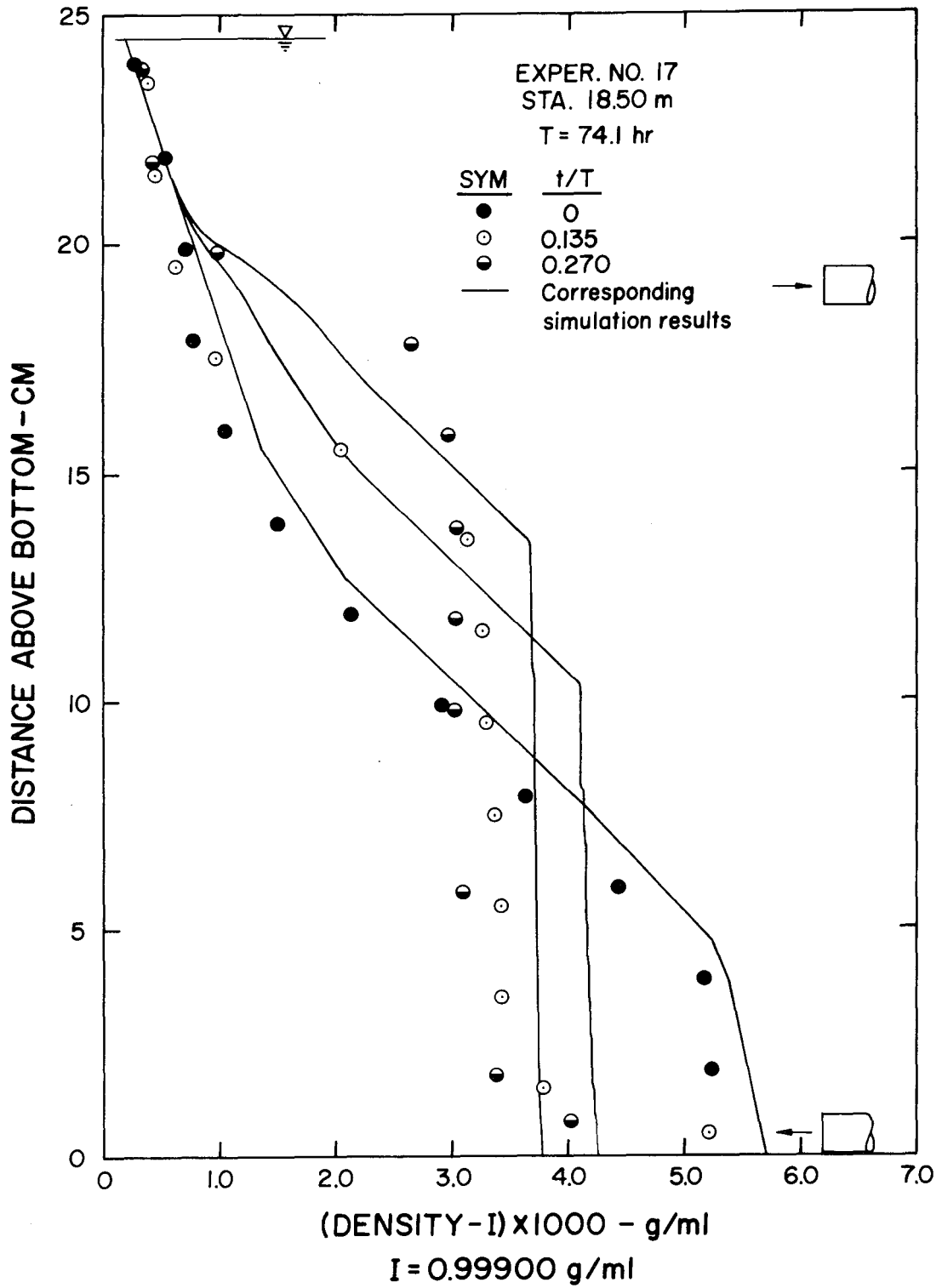


Figure 4.26 Measured and simulated density profiles for Experiment Number 17, at Station 18.50m

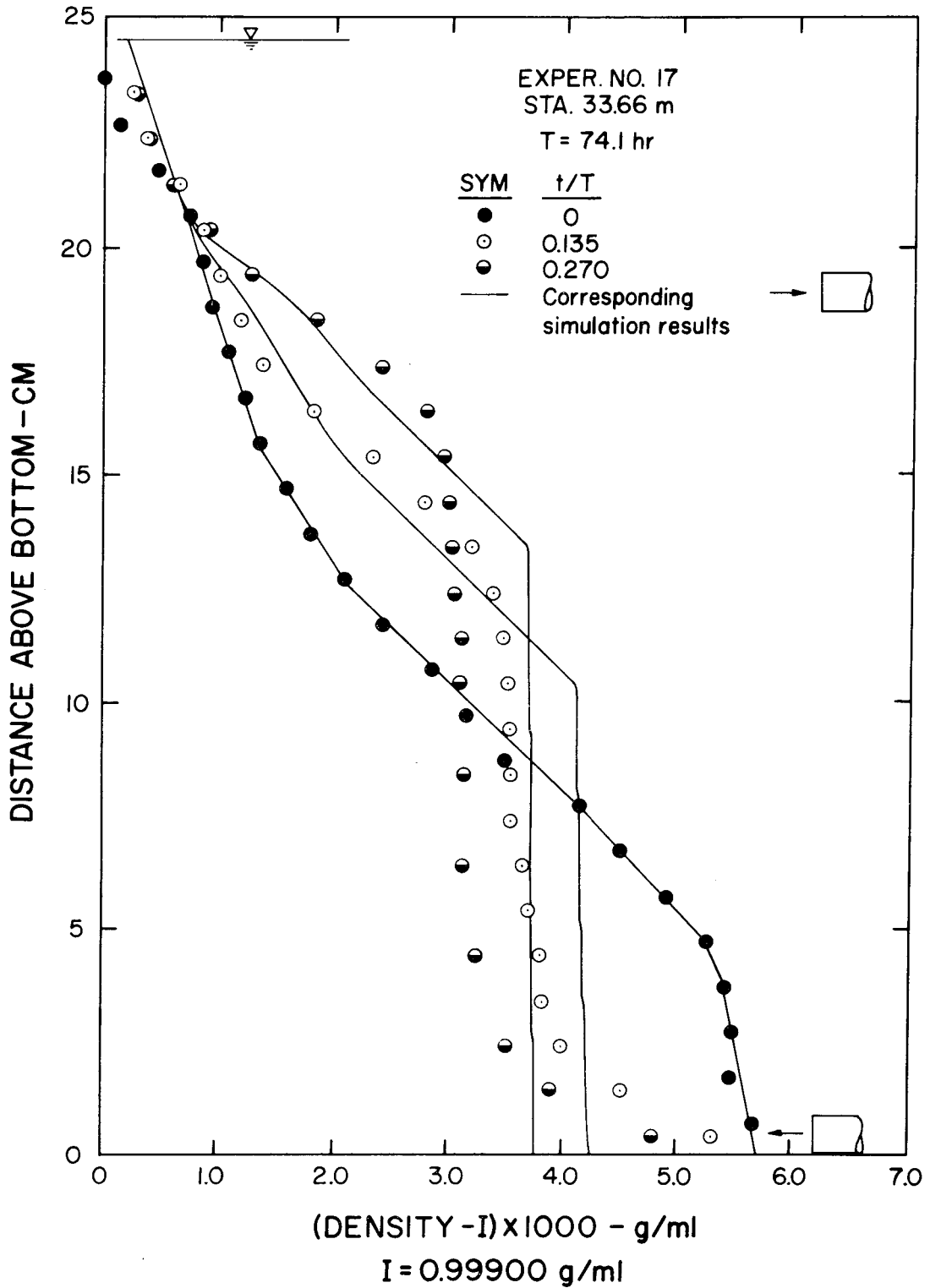


Figure 4.27 Measured and simulated density profiles for Experiment Number 17, at Station 33.66m

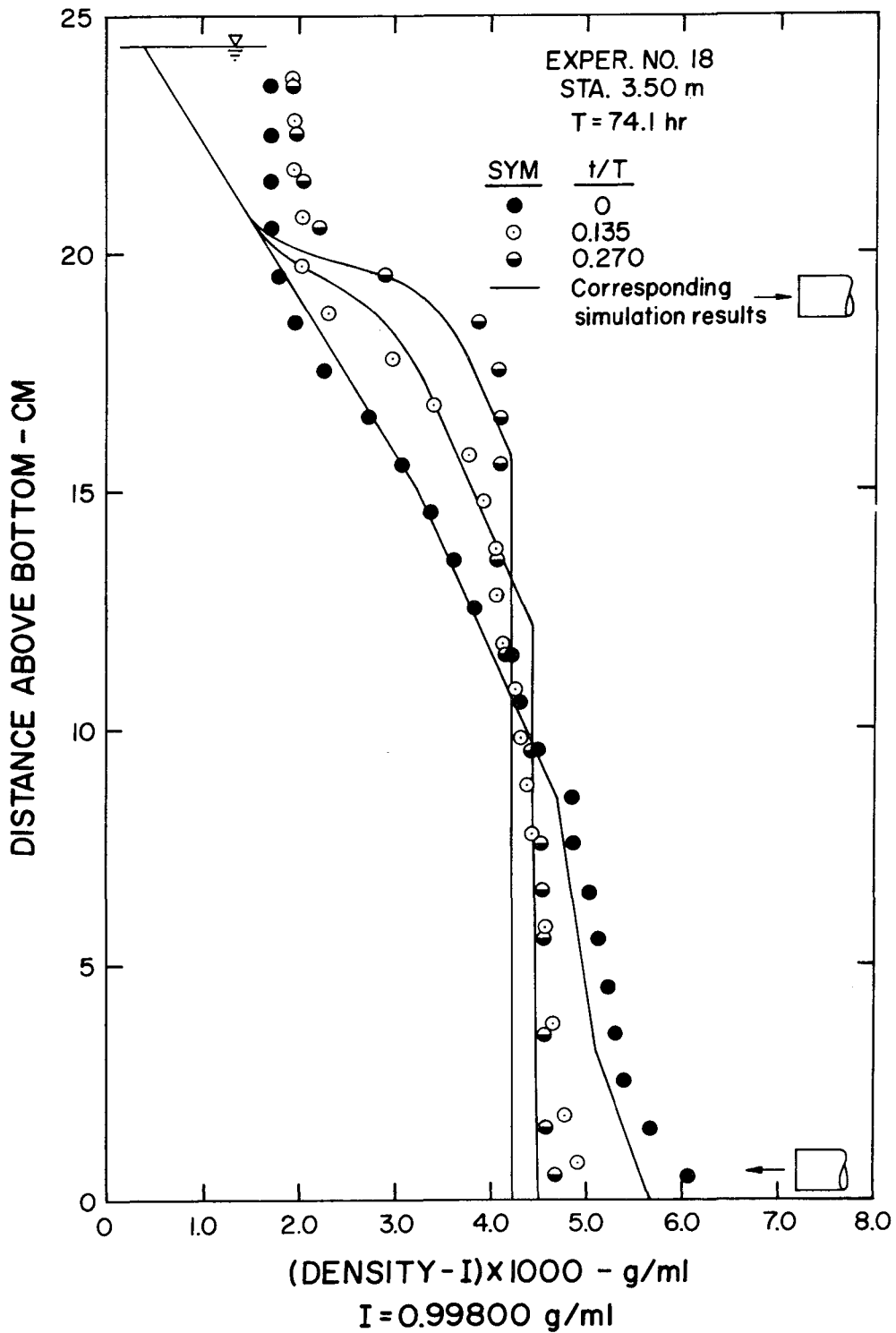


Figure 4.28 Measured and simulated density profiles for Experiment Number 18, at Station 3.50m

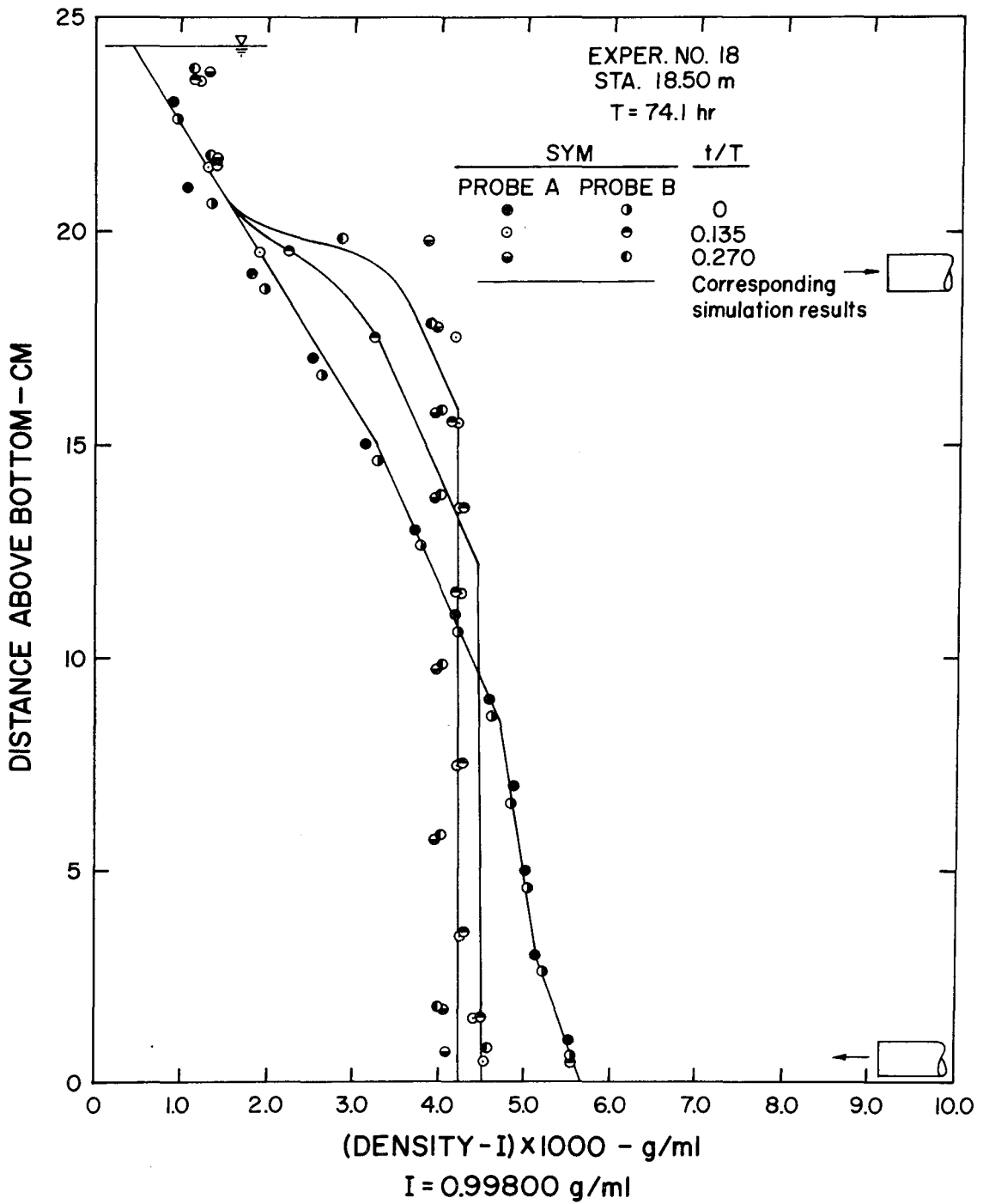


Figure 4.29 Measured and simulated density profiles for Experiment Number 18, at Station 18.50m

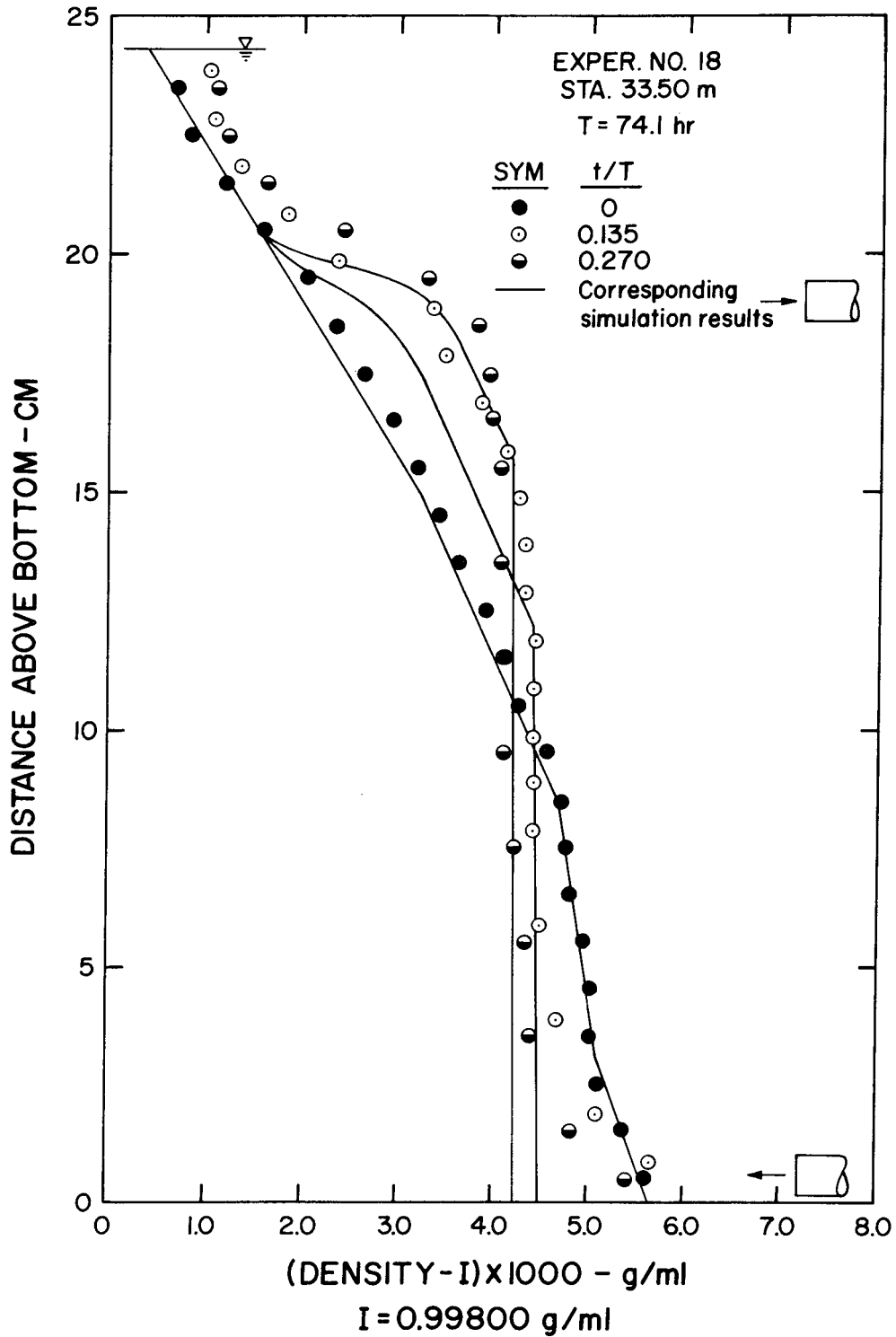


Figure 4.30 Measured and simulated density profiles for Experiment Number 18, at Station 33.50m



#### 4.3.2 General Description of Results

The degree of agreement between the density profiles measured and those predicted by the simulation varies from experiment to experiment. However, a general description of the results will be presented and particular exceptions will be noted.

The initial density profile for each experiment was measured just prior to the beginning of pumping. If the fluid in the tank were in hydrostatic and thermodynamic equilibrium, the initial density profiles would be identical at all locations in the tank. The results for experiments in which simultaneous initial density profiles were measured at two or more locations show that this was not always the case. These differences in the initial density profiles in the same tank were most apparent in the 9-meter and 40-meter flumes. The initial density profiles selected as input for the simulation results presented usually were chosen to approximate one of the initial profiles measured. Therefore, in experiments where density profiles provided are for two or more locations in the tank, the simulation results are the same for both locations as the same initial profile was used. An exception to this practice is Experiment No. 10 for which the simulation at each location is based on the particular initial density profile measured at that location (see Figs. 4.15 and 4.16).

Most of the density profiles were measured at intervals on the order of hours, so that clearly detectable changes in the profile could be discerned. As a result of this, many of the details of the change in the initial profile due to entrainment by the buoyant jet cannot be

detected in the first profile after pumping had begun. Most results show that the density profile near the jet is nearly uniform by this time. Experiment No. 6 (Fig. 4.11) was arranged so that several density profiles in the lower region of the tank were measured shortly after pumping had begun. Although the quantitative agreement between experiment and simulation is not particularly good, the changes of the initial density profile during mixing are in qualitative agreement. Simulation results plotted at more frequent intervals than those presented show these details to a greater degree.

In Fig. 4.11 the profiles produced by the simulation extend only to the center line of the discharge jet tube and do not reach the bottom of the tank. The simulation technique incorporates the assumption that entrainment by the jet from the ambient environment occurs at elevations along the center line trajectory of the jet. This assumption is quite good as the buoyant jet axis becomes vertical, but it is clear that while the axis is nearly horizontal some entrainment will occur below the jet center line. For most of the experiments the jet was sufficiently near the bottom of the tank that, for the purposes of the simulation, it was assumed to be at the bottom. Hence, most simulated density profiles extend from the surface to the bottom.

Fig. 4.23 shows the results of Experiment No. 15 in which the jet was located near the surface and the withdrawal tube was located near the bottom of the tank. Both experimental and simulation results look similar, though inverted, to the results of other experiments.

The general characteristics of the agreement between experimental and simulation results for given location in the tank are summarized here. The agreement in the region of the density profile which has been influenced by the buoyant jet is satisfactory. After the initial stages of mixing, densities are uniform over much of this region. The region of transition between the zone influenced by the buoyant jet and the zone of no entrainment, or purely kinematic motion, shows a marked difference between experimental and simulation results. Simulation results in this region display a discontinuity in the slope of the density profile. This occurs because the simulation is constructed under the assumption that the jet spreads uniformly across the impoundment at the level of neutral buoyancy. Experimental results in this region of the density profile generally do not demonstrate this discontinuity. Moreover, measured density profiles usually extend beyond simulated profiles in this region. In the zone of kinematic motion, where the initial profile is simply shifted upward, experimental results show better agreement with simulation results at elevations near the withdrawal region than near the region influenced by the jet. This is due to the tendency of experimental profiles to have the region of jet influence extended further than the simulation. The changes in the density profile in the withdrawal region are small relative to the effects of the buoyant jet in other parts of the profile. Experimental results agree qualitatively with simulation results, if not quantitatively. Generally, experimental profiles in this region show

agreement with the simulations with regard to the location of the top of the withdrawal layer as the elevation beyond which the profile does not change.

The differences among density profiles taken at several locations in the tanks during mixing experiments are shown for Experiments Nos. 10, 12, 13, 14, 17, and 18 in Figs. 4.15 and 4.16; 4.17 and 4.18; 4.19 and 4.20; 4.21 and 4.22; 4.25, 4.26, and 4.27; and 4.28, 4.29, and 4.30; respectively. The purpose of these measurements was to investigate the validity of the assumption that the isopycnic surfaces are horizontal planes. As pointed out previously, the initial density profiles measured in some experiments indicate that this condition did not exist initially as required by hydrostatic equilibrium probably because of heat exchange with the laboratory environment. As a result of this initial disequilibrium, it is difficult to distinguish deviations from horizontal isopycnic surfaces due to the mixing process from those due to the initial density structure.

Comparisons of density profiles at different locations in the tanks show that at a given time during mixing the isopycnic surfaces are generally not horizontal planes. The longitudinal variations of density along the tank at a given elevation and time are generally not extreme. Longitudinal density gradients based on the data from measured vertical density profiles (corrected for temperature differences) were less than  $10^{-4}$  g/ml/m and, average gradients were  $10^{-5}$  to  $10^{-6}$  g/ml/m.

The effect of the location and orientation of the pumping system is evident in the measured density profiles for some experiments. No density profiles are presented which were measured directly in or in the vicinity of the buoyant jet, as these profiles obviously have local disturbances not representative of locations remote from the jet. However, density profiles equally far removed from the jet also indicate sloping isopycnic surfaces. Consider profiles from Experiment No. 17 at Sta. 3.34m (Fig. 4.25) and Sta. 33.66m (Fig. 4.27). The jet was directed from Sta. 17.40m toward Sta. 3.34m during mixing. It is seen that the lower region of the profile at Sta. 3.34m is more nearly uniform than the same region at Sta. 33.66m. Similar results are noted for Experiment No. 18 (Figs. 4.28 and 4.30) which was also performed in the 40-meter flume. The results from experiments in the smaller tanks do not exhibit the effect of jet location in any clear or consistent manner, though profiles differ longitudinally in the tank.

#### 4.4 DISCUSSION OF RESULTS

The density profiles measured during mixing experiments and the corresponding simulated profiles provide information on the issues posed as the experimental objectives. The experimental results supply a wide range of conditions against which the assumptions and results of the simulation technique are tested.

The establishment of an initial density profile with horizontal isopycnic surfaces throughout the tank was required as the proper initial condition for the simulation. That this condition did not exist

for some experiments makes evaluation of the experimental results relative to the simulated results difficult. For most experiments, however, the essential features of the mixing process were not greatly affected by this slight alteration in initial condition.

A related problem is that of maintaining a closed system during the mixing process. For the experimental technique employed, this meant maintaining the salt solution at a constant temperature throughout the tank during mixing. This was accomplished in the 2-meter tank and 9-meter flume, but it was not accomplished in the 40-meter flume for Experiments Nos. 17 and 18. Table 4.3 shows the history of temperature measurements at various depths and locations during Experiments Nos. 17 and 18. Longitudinal and vertical temperature gradients existed in this tank due to differences in temperature between the water and air and due to variations in air temperature along the flume. Temperature measurements were used in addition to conductivity measurements to calculate the density profiles for these two experiments. However, fluxes of heat into or from the tank set up density gradients which induced motions independent of the mixing process. When viewing the measured profiles, the effect of these motions cannot be uncoupled from the mixing.

The quality of the measured results depends on the reliability and representativeness of the individual density determinations; in addition to violations of the required initial and boundary conditions. Changes in calibration of the conductivity probes during the measurement of a vertical profile due to electronic changes in the recorder

Table 4.3 Detailed Temperature Data For Experiments Number 17 and 18

Experiment No. 17

Time t/T	Station	Temperature -°C			
		Air	Surface	Mid-depth	Bottom
0.	33.66 m	18.9	20.3	20.8	21.3
	18.50 m	19.0	19.3	20.1	20.7
	3.34 m	17.8	18.3	18.5	18.9
0.135	33.66 m	18.9	20.4	20.6	21.1
	18.50 m	19.1	19.9	20.3	20.4
	3.34 m	18.9	18.4	18.9	19.1
0.270	33.66 m	17.9	20.7	20.9	21.1
	18.50 m	19.2	20.2	20.2	20.6
	3.34 m	19.8	18.9	19.8	19.9

Experiment No. 18

Time t/T	Station	Temperature -°C			Bottom
		Surface	1/3 Depth	2/3 Depth	
0.	33.50 m	19.8	20.0	20.1	20.5
	18.50 m	18.8	19.2	19.5	19.9
	3.50 m	17.2	17.7	18.5	19.2
0.135	33.50 m	19.4	19.7	20.0	20.3
	18.50 m	18.8	19.2	19.3	19.3
	3.50 m	17.0	17.8	18.6	18.6
0.270	33.50 m	19.6	19.9	20.0	20.3
	18.50 m	18.7	19.4	19.4	19.5
	3.50 m	17.6	18.6	19.0	18.8

Note: At 20°C for distilled water

$$\frac{1}{\rho} \frac{d\rho}{dT} = -.00020 \text{ (}^{\circ}\text{C)}^{-1}$$

were possible. The effect of these changes was minimized by a check of one point on the calibration curve after each profile. The time required to take the measurements required for a complete profile was kept small relative to mixing time scales ( $\Delta t/T < .02$ ), as mentioned previously. Strictly though, points at top and bottom of a profile were measured at different times, while corresponding simulation results were all for the time midway through the measured profile.

A more important and less well understood aspect of the measurements is their representative nature. The particular shape of the end of the conductivity probes used is such that fluid might be partially trapped between the electrodes as the probe is moved downward. The mixing caused by fluid motions around the probe and between the electrodes added to the integrated nature of the measurements over the electrode area. Though differences between measured and simulated results are in general in the opposite sense, this may be due to other factors and the effect of trapping may be obscured. Moreover, that this integrated measurement "at a point" was representative of the other points in the plane at this elevation is questionable. The previous description of longitudinal density gradients documents this problem. The simulated density profiles have been calculated so that their accuracy in terms of additional or reduction of mass to the system is about 5% or less. Comparisons of mass conservation based on measured profiles with that calculated for simulated profiles often show



that such accuracy is not available for some measured profiles and indicate that longitudinal gradients and/or measurement inaccuracies exist.

To this point the results have been discussed in terms of the experimental approximations to the required initial and boundary conditions and of the validity of the measurements themselves. The experiments point to aspects of the simulation which do not model exactly the physical mixing process. The inability of the simulation to include or model properly these phenomena is cause for some of the disagreement between experimental and simulated results.

The simulation procedure models the withdrawal region in a simple and imperfect manner. The experimental results show scattered agreement with simulated densities in this region, but greater precision in simulating the withdrawal layer would have little or no effect on the simulated profile as a whole.

Proper simulation of the buoyant jet mechanics is important as the jet influences the changes in the density profile more than any other component of the system. The location of the jet origin has an effect on the simulated profiles. As explained previously and illustrated in Fig. 4.11 for Experiment No. 6, the simulation predicts no change in the density profile below the jet origin. Experiments show that jets which are near the tank bottom, though not on it, do mix the region below their origin. Therefore, mass balances made for the tank over the entire depth do not agree with those made for simulated profiles. Most experiments were made with the jet very near the

bottom, and the corresponding simulations were made assuming the origin of the jet to be at the bottom of the tank. This approximation to the experiments assures simulated results in which the lower region of the tank was influenced by the jet. However, it results in a level of neutral buoyancy lower than if the jet were not on the bottom and may account in part for the simulated density profiles being below experimental profiles in the region near the level of neutral buoyancy.

The buoyant jet mechanics used in the simulation are appropriate for a jet in a fluid of infinite extent, and the fact that the jets in the experiments were near a solid boundary was not incorporated in the simulation. It would be difficult to assess the effect of the wall and to modify the simulation to reflect it, but the wall probably reduces jet entrainment initially in the experiments with the result of higher jet penetration. This could also contribute to the disagreement between experimental and simulated profiles in the region of the level of neutral buoyancy.

The location of the level of neutral buoyancy was chosen for the simulation as that elevation at which the center line density of the buoyant jet equals the density of the fluid in the impoundment. Physically, the jet fluid has vertical momentum at this elevation and continues above this elevation before coming back down to rest at a level of neutral buoyancy. The actual level of neutral buoyancy is difficult to predict as the similarity analysis breaks down here and the mixing that occurs is complex. It may be that, for the horizontally discharged buoyant jet used for the pumping system, the elevation

chosen as the neutrally buoyant level is too low. An elevation somewhere between the point chosen and the maximum height of rise of the jet may be a better representation of the level of neutral buoyancy. Such a choice would promote closer agreement between experimental and simulation results in this region of the density profiles.

The simulation technique treats the lateral spreading of the jet at the level of neutral buoyancy in a simple manner. The fluid delivered to this elevation is assumed to be spread uniformly across the impoundment instantaneously. In computational terms, the volume of fluid delivered in time step,  $\Delta t$ , is made to occupy a depth,  $\Delta d$ , in the impoundment. Physically, the problem of a neutrally buoyant fluid intruding into a density stratified environment is complex. Determination of the speed with which a front moves outward from the jet is complicated by the possibility of a change from turbulent to laminar flow. Such spreading also involves mixing caused by the shearing of the intruding layer. Also, the jet fluid which spreads laterally may not be uniform in density throughout the layer as assumed for the simulation. An experimental study of intruding layers by Wu (56) showed that internal waves are generated, further complicating analysis. An analysis of a slow speed, creeping flow intruding layer by List (32) makes it clear that the complexity of even this simplified case precludes the inclusion of a proper description of the spreading in the simulation. The mixing caused by the spreading jet may provide the explanation of the smooth transition between the regions of jet influence and purely kinematic motion in the experimental density profiles, which

was noted to contrast with the discontinuity in slope in the simulation results. The finite time required for the spreading jet to extend across the entire impoundment undoubtedly adds to the production of longitudinal density gradients in the impoundment. The effect of spreading was most evident in the experiments in the large flume at high values of a shape parameter  $S$  (volume divided by the depth cubed).

The experimental results have been described and compared with the density profiles produced by the simulation technique. The discrepancies between the density profiles have been attributed in part to experimental difficulties and in large measure to the simplified nature of the simulation mode. Although the differences are real, the simulation technique does predict reasonably well the changes in the density structure of the impoundment during the mixing process for the experiments performed. The prediction of these changes, in a gross sense, is good and often quite accurate in detail.



## CHAPTER 5

### FIELD AND LABORATORY EXPERIMENTS

#### BY OTHER INVESTIGATORS

There are few reported mixing experiments which employ mechanical pumping systems. Reported field mixing experiments on lakes and reservoirs using this technique are limited to a series of experiments by a group of investigators from the Federal Water Pollution Control Administration (23, 46, 47 and 48) and the mixing of some water supply reservoirs in England (41). A laboratory study of an exploratory nature which employed pumping, among other techniques, was reported by Brush, et al. (9). Comparisons of some of the results of these studies with the results of simulated mixing experiments are presented in this chapter.

#### 5.1 FIELD EXPERIMENTS

The field experiments by the Federal Water Pollution Control Administration (FWPCA) provide the more detailed information of the two reported field experiments, and they will be considered here. A large portion of the data gathered during these studies was related to water quality, though the time-histories of the temperature-depth profiles are available for some experiments.

### 5.1.1 Summary of Mixing Experiments

Six field experiments were conducted by the FWPCA group at five small lakes. Prior to mixing, each lake was observed to be temperature-stratified with density profiles which usually were continuous from surface to bottom. The mixing was accomplished with a barge-mounted pumping system which withdrew water from near the bottom of the lake and discharged it horizontally near the surface. Essentially the same equipment was used for all of the experiments.

Some general features of the lakes and the mixing are summarized in Table 5.1. Steward Hollow Lake was mixed twice. The parameters S, F, and P are the impoundment shape parameter, densimetric Froude number for the jet (based on the initial density profile), and the plume parameter, respectively. These parameters are discussed in detail in Chapter 6 with regard to generalized solutions and are presented here for reference only. The parameter  $t_{\max}^*$  is the normalized mixing time,

$$t_{\max}^* = t_{\max} Q/V \quad . \quad (5.1)$$

In most cases the lakes were of uniform temperature vertically, when mixing was stopped. Initial and final temperature profiles were reported for all mixings, and temperature profiles during mixing were reported for the mixing of Vesuvius Lake and Boltz Lake. At Vesuvius Lake vertical temperature profiles were reported at four different locations in the lake for approximately the same times during the

Table 5.1 Summary of Data From FWPCA Field Experiments

Lake	Surface Area Acres	Max. Depth feet	Average Depth feet	Volume Acre-feet	S Eq. (6.7)	F Eq. (6.4)	P Eq. (6.6)	Mixing Time $t_{\max}$ hrs	$t^*_{\max}$ Eq. (5.1)
Steward Hollow	8	24	15	120	378.	25.	$6.8 \times 10^{-3}$	20.5	.093
Steward Hollow	8	24	15	120	378.	28.	$7.5 \times 10^{-3}$	13.5	.061
Caldwell	10	20	10	100	545.	24.	$1.0 \times 10^{-2}$	8.0	.023
Pine	14	17	7	98	869.	27.	$1.7 \times 10^{-2}$	35.0	.200
Vesuvius	105	30	12	1260	2033.	25.	$3.8 \times 10^{-3}$	208.0	.091
Boltz	96	62	30	2900	530.	28.	$7.1 \times 10^{-4}$	912.0	.171

$t_{\max}$  - time for which lake was mixed

For all mixings

Jet diameter = 1.0 ft  
Jet discharge = 6.4 cfs

Data from References 23, 46 and 47



experiment. The mixing experiment at Boltz Lake was accompanied by observations of the natural changes in stratification of a lake of similar size in the vicinity. This was the only experiment for which a control lake was studied.

#### 5.1.2 Comparison of Field Data and Simulation Results

Although the field experiments do not provide all of the boundary conditions and the closed system posed by the assumptions underlying the simulation technique, the simulation was applied to the mixing of Vesuvius Lake and Boltz Lake.

The temperature profiles measured during the field experiment at Vesuvius Lake and the profiles predicted by the simulation technique are shown in Fig. 5.1. The simulation technique was modified to conserve heat and to account for the nonlinear temperature-density relationship, as suggested in Sect. 3.3. The temperature profiles were calculated as well as density profiles for comparison with measured data. The initial temperature profile was measured at the pump site just prior to the beginning of pumping. The area-depth relationship for Vesuvius Lake was chosen to be linear in close agreement with measurements (45). The pump discharge was fixed at 6.4 cfs, as reported, though this discharge was determined under different conditions. The experimental temperature profiles shown were taken after 2.5-days and 8.5-days of pumping at a point approximately a quarter of a mile from the pump site and at right angles to the direction of discharge. Temperature profiles at the three other stations in the lake

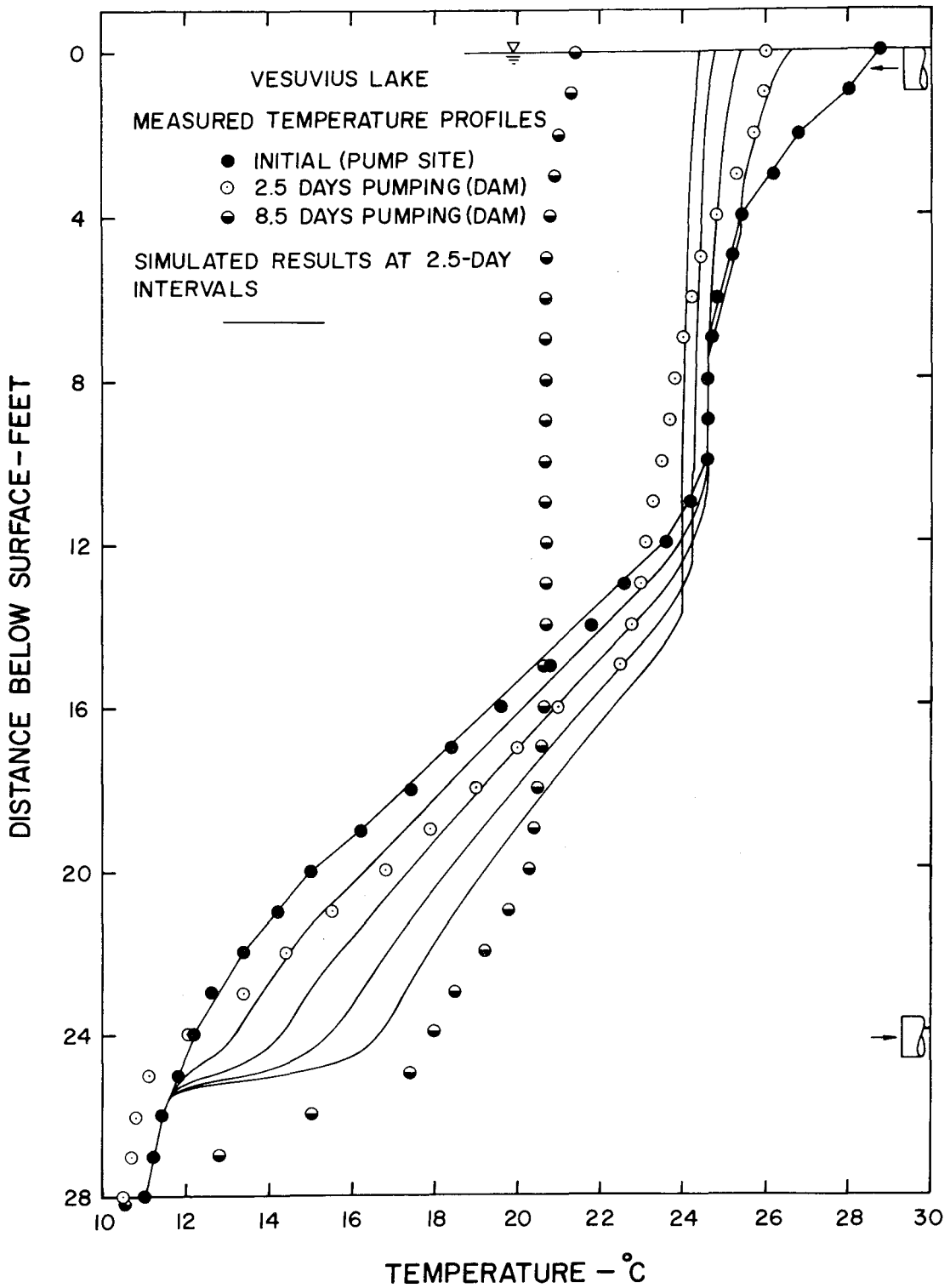


Figure 5.1 Measured and simulated temperature profiles for FWPCA field experiment at Vesuvius Lake

indicate the existence of longitudinal gradients (about  $2^{\circ}\text{C}/\text{mile}$ ), though the profiles are quite similar. Temperature profiles generated by the simulation are shown for 2.5-day intervals from the beginning of pumping.

The agreement between experimental and simulation results is better for the 2.5-day profile than the 8.5-day profile. In particular, the agreement between the 2.5-day profiles is good in the lower part of the lake. The fact that the field experiment is not closed to external influences probably accounts for the lack of agreement between field and simulation profiles near the surface and after 8.5-days pumping. The experiment was conducted in late September, when cool evenings might have as much, or more, effect on lowering surface temperatures than the pumping system. In terms of a heat balance, experimental temperature profiles for 2.5 and 8.5-days reflect decreases in heat relative to the initial profile of temperature. The simulation technique was, however, designed for a closed (adiabatic) system.

Temperature measurements at Boltz Lake are shown with simulation results in Fig. 5.2. Again, simulation results were obtained using the simulation technique modified to include the nonlinear temperature-density relationship. The pumping system for this experiment was the same as that used at Vesuvius Lake, although the withdrawal tube was lengthened. Temperature measurements were reported (47) for five elevations in the lake for each of five weeks of pumping. These measurements were made at the pump site. Similar measurements were reported for the control lake. A linear area-depth relationship was assumed for the simulation (45).

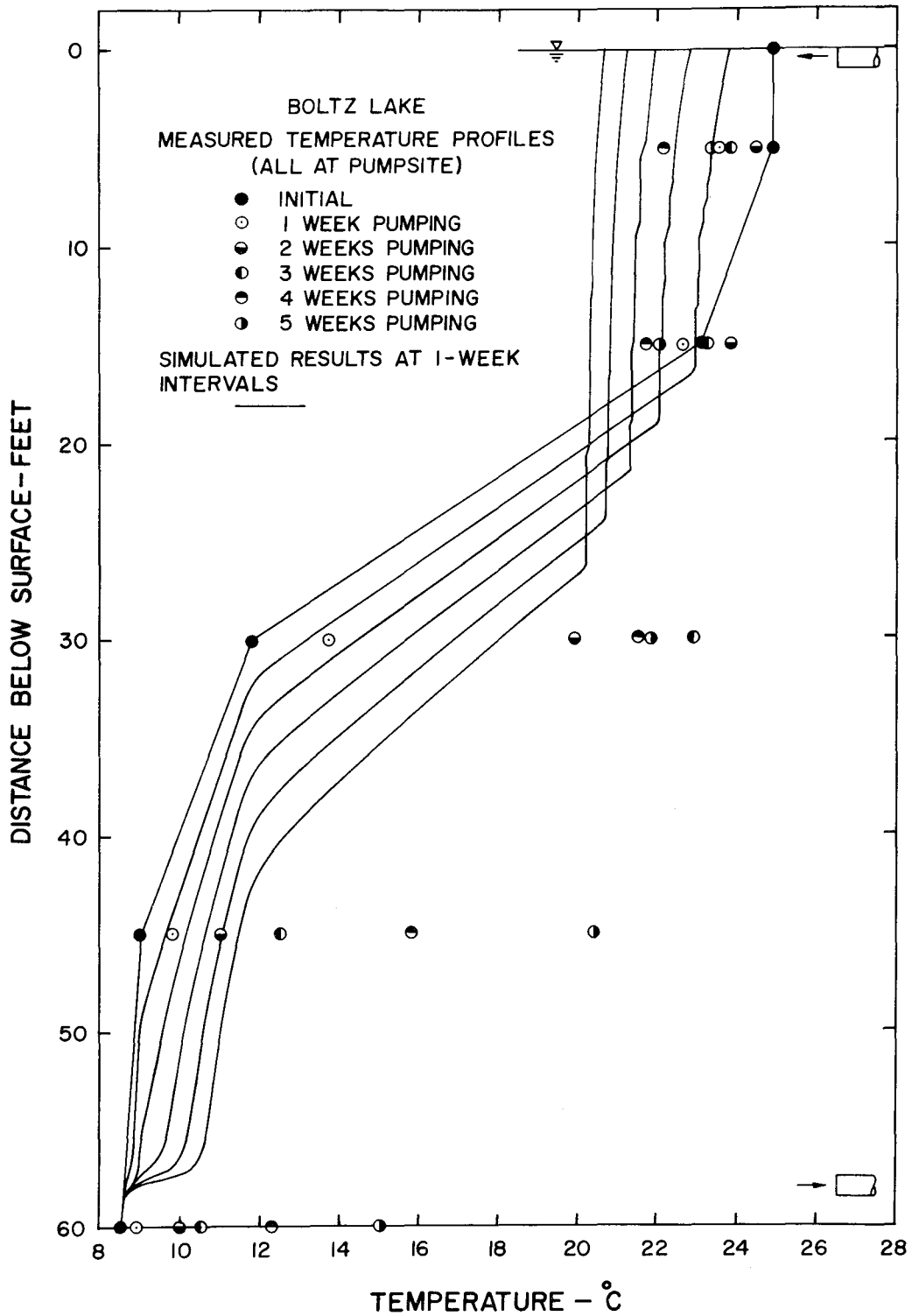


Figure 5.2 Measured and simulated temperature profile for FWPCA field experiment at Boltz Lake

The agreement between experimental and simulation results is not good. The measured data are not always consistent in that some measurements at a given elevation indicate increases in temperature followed by decreases in temperature a week later. The measurements show that the bottom region becomes warmer than the simulation predicts. Heat balances relative to the initial temperature profile reflect increases in heat for profiles during pumping. The measurements at the control lake do not indicate enough increase in temperatures in the bottom region due to natural processes to account for these results. A probable explanation is that the measurements taken at the pump site indicate a greater degree of mixing than exists elsewhere in the lake. The experiment at Vesuvius Lake indicates that the measurements taken at locations other than the pump site show a lesser degree of mixing. Similar results were noted for some laboratory experiments discussed in Chapter 4.

The validity of the simulation technique cannot be adequately verified from these two experiments, though the effects of the closed system boundary condition and one dimensional aspects of the simulation model can be observed.

## 5.2 LABORATORY EXPERIMENTS

The pumping experiments reported by Brush, et al. (9) were of an exploratory nature. A circular tank 12 feet in diameter and 3 feet deep was filled with a layer of salt solution upon which a layer of fresh water was spread. It was estimated that a pycnocline was formed over

one-eighth of the total depth. No measurements of density profiles were reported, but one layer was dyed and samples of water were withdrawn at various elevations to estimate the progress of mixing. Mixing experiments were performed using withdrawal tubes and jets at various elevations in the tank. The total pumping times required for complete mixing were reported based on the dye samples.

The pumped discharge and tank volume were held constant for all experiments; and the characteristic time ( $V/Q$ ) to pump this volume was 265 minutes. The mixing times varied from 31 minutes to 75 minutes depending on the location of jet and intake, and dimensionless mixing times,  $t^*_{\max}$ , were 0.12 to 0.28. The densimetric Froude number for the jet based on the initial profile was  $F = 80$  for all experiments.

The simulation technique was employed to model experiment "Run No. f". For this experiment the jet was located near the bottom of the tank and an intake was floated near the surface. Simulated density profiles from the elevation of the jet to the surface are shown in Fig. 5.3. Density profiles are shown for 6-minute intervals up to 42 minutes, the reported time for complete mixing. The simulation results do not show complete mixing. The high Froude number ( $F = 80$ ) and small tank probably result in circulations and turbulent mixing which are not included in the simulation model. The rates of mixing induced by these motions may be large enough to account for the more rapid mixing observed.

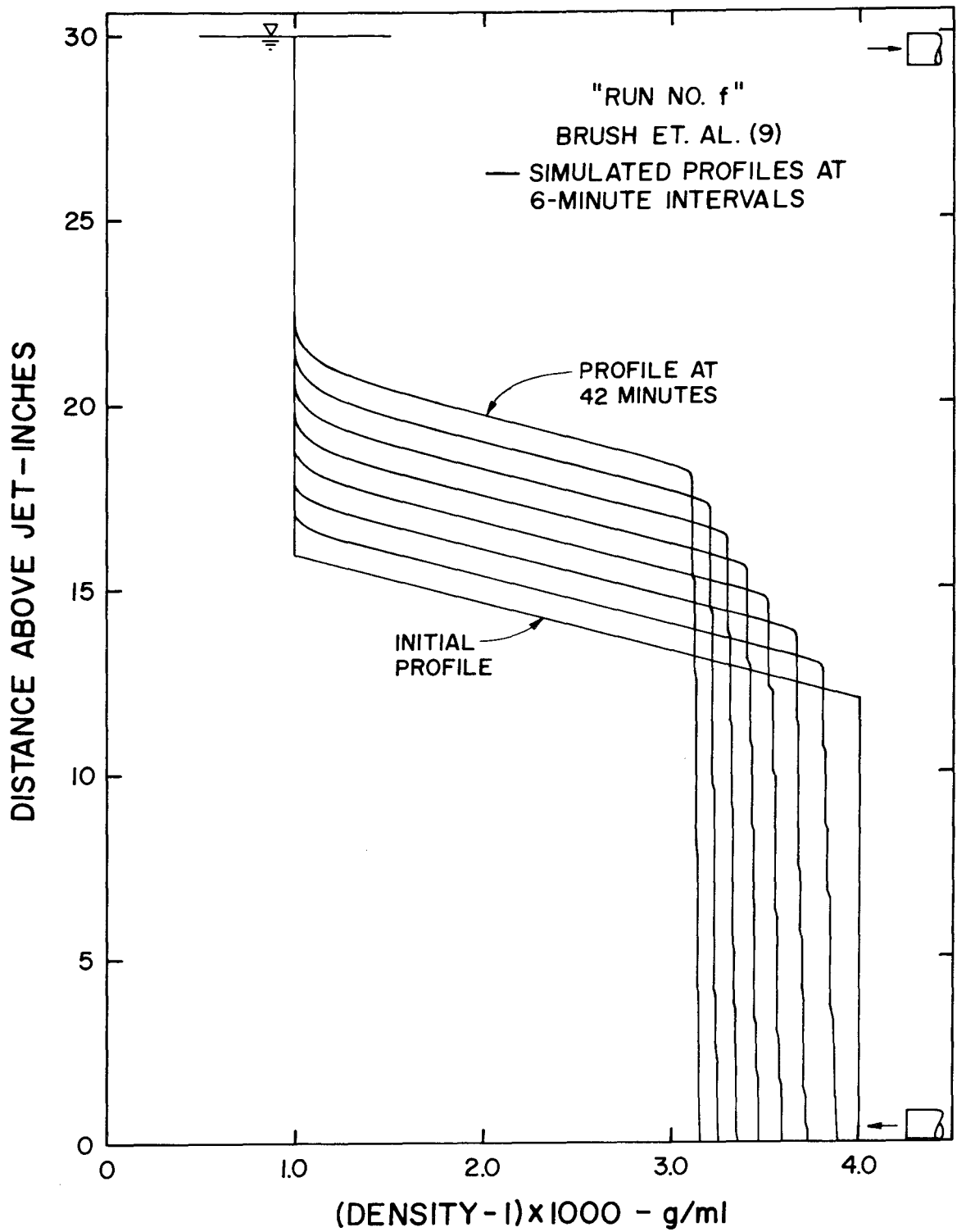


Figure 5.3 Simulated density profiles for "Run No. f" of Brush, et al. (9)

The comparisons of simulated mixing experiments with a few field and laboratory experiments by other investigators do not show good agreement. In the case of the field experiments, the effects of the environment external to the impoundment may account for the lack of agreement. Coupling the simulation technique to a simulation of the reservoir heat budget may provide closer agreement with the field measurements. Better agreement with the laboratory experiment used for comparison may require modification of the simulation technique to account for induced circulations not modeled by the simulation. In summary, although the few mixing experiments presented in this chapter do not add to the verification of the simulation technique, they do not confute it as the boundary conditions often were not comparable and the data may not have been representative of the impoundment response to mixing.





## CHAPTER 6

## IMPLICATIONS OF SIMULATION TECHNIQUE

## 6.1 PURPOSE

The purpose of this chapter is to demonstrate the use of the simulation technique to generate numerical mixing experiments and to analyze the results of these experiments to provide some general conclusions about the mixing process.

The ability of the simulation technique to predict the time-history of the density-depth profiles of a laboratory impoundment during mixing has been established in Chapter 4. The boundary conditions and other assumptions required for the simulation are somewhat ideal relative to those which might exist during the mixing of an impoundment in the natural environment. However, the fact that the simulation is uncoupled from external influences and produces the response of the impoundment to the pumping system only makes the simulation a useful tool. The simulation technique provides a means of systematically investigating the effects on the mixing process of variations in the components of the pumping system.

## 6.2 GENERALIZED SOLUTIONS

The simulation procedure accepts any gravitational stable initial density profile as input. The area-depth relationship may be any arbitrary continuous function. The simulation of the mixing process is

an initial value problem. That is, for a given impoundment geometry (area-depth relationship) and pumping system (jet and intake elevations, jet diameter, and jet discharge), the response is uniquely determined by the initial density profile. An initial density-depth profile which is linear allows a generalization of the pumping system parameters and the response of the impoundment. While the case of an initially linear density profile may not be the rule in natural impoundments, approximations to it frequently exist. Moreover, the results of these generalized problems yield information concerning the importance of the various components of the pumping system and the strategy for efficient mixing which may be independent of this particular choice of initial density profile.

#### 6.2.1 Dimensional Analysis for Initially Linear Profiles

A schematic diagram of the pumping system for an impoundment which initially has a linear density profile is shown in Fig. 6.1. The pumping system is shown with the withdrawal tube near the surface and the jet tube at the bottom, although the analysis is valid for the reverse setup. The jet tube need not be positioned at the bottom, though, as described previously, the simulation assumes that the jet does not influence the region below the jet center line.

The initial density profile is characterized by the density difference,  $\Delta\rho$ , between the elevations of the withdrawal tube and the jet and by the reference density,  $\rho_0$  (density of fluid discharged initially). The following physical variables describing the initial profile and fixed components of a particular pumping system were used for the dimensional analysis:

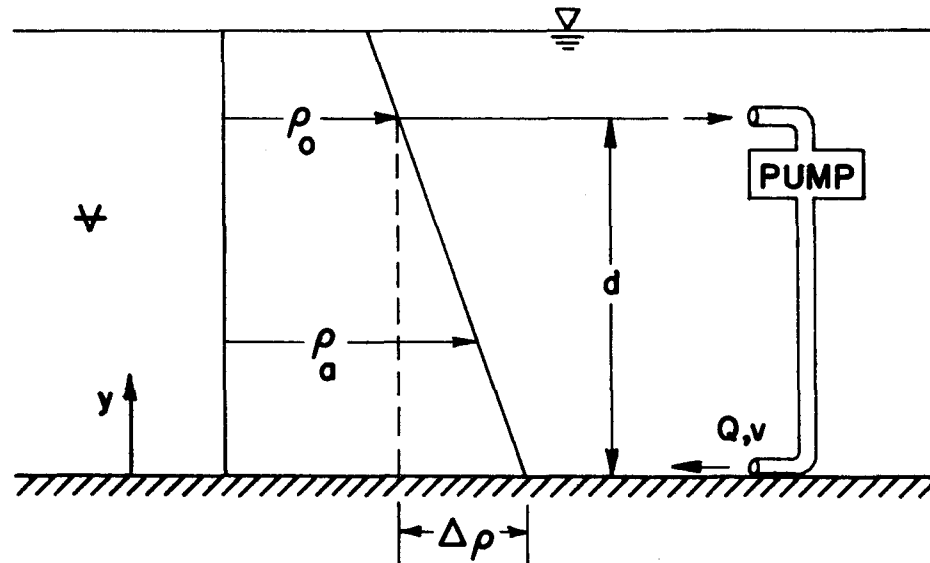


Figure 6.1 Schematic diagram of a pumping system in an impoundment with an initially linear density profile

$\frac{-g}{\rho_o} \frac{d\rho_a}{dy}$	initial gradient of unit weight (normalized)
$d$	distance between jet and withdrawal tubes
$\nabla$	volume of impoundment over the depth, $d$
$Q$	pumped discharge at jet
$v$	initial velocity of jet

The following physical variables describing the density profiles during the mixing process were used for the dimensional analysis:

$y$	elevation above the jet center line
$t$	time since the beginning of pumping
$g \left( \frac{\rho - \rho_o}{\rho_o} \right)$	normalized density at any $y$ and $t$

A dimensional analysis using these physical variables yields the following six dimensionless parameters:

$$y^* = y/d \quad \text{normalized elevation} \quad (6.1)$$

$$t^* = t/T = Qt/\nabla \quad \text{normalized time} \quad (6.2)$$

$$\rho^* = \frac{\rho - \rho_o}{\Delta\rho} = \frac{g \left( \frac{\rho - \rho_o}{\rho_o} \right)}{\frac{-g}{\rho_o} \frac{d\rho_a}{dy} d} \quad \text{normalized density} \quad (6.3)$$

$$F = \frac{v}{\left( \frac{g}{\rho_o} \Delta\rho D \right)^{\frac{1}{2}}} = \frac{v}{\left( \frac{-g}{\rho_o} \frac{d\rho_a}{dy} d D \right)^{\frac{1}{2}}} \quad \begin{array}{c} \text{jet densimetric Froude} \\ \text{number} \end{array} \quad (6.4)$$

$$\text{where } D = \left( \frac{4Q}{\pi v} \right)^{\frac{1}{2}} \quad \text{nominal jet diameter} \quad (6.5)$$

$$P = \frac{Q}{\left( \frac{g}{\rho_o} \Delta \rho \right)^{\frac{1}{2}} d^{5/2}} = \frac{Q}{\left( \frac{-g}{\rho_o} \frac{d\rho_a}{dy} d \right)^{\frac{1}{2}} d^{5/2}} \quad \text{plume parameter} \quad (6.6)$$

$$S = \frac{V}{d^3} \quad \text{shape parameter} \quad (6.7)$$

Note that  $F$  and  $P$  are used throughout as initial values based on the initial density profile.

The dimensionless parameters  $\rho^*$  and  $y^*$  define a normalized density-depth profile at any dimensionless time,  $t^*$ . The characteristic time for the problem,  $T$ , is defined as the time required to pump the volume of the impoundment,  $V$ , which is included between the planes of the jet and withdrawal tubes. Therefore,

$$\rho^* = f(y^*, t^*, F, P, S) . \quad (6.8)$$

The parameters  $F$  and  $P$  characterize the buoyant jet in the initially linear density profile. Since the simulation is an initial value problem,  $F$  and  $P$  characterize the mixing process also. Fan (18) has shown that the buoyant jet in a linearly stratified environment is characterized by two parameters, a jet Froude Number,

$$F_f = \frac{v}{\left( g \frac{(\rho_2 - \rho_1)}{\rho_2} D \right)^{\frac{1}{2}}} \quad (6.9)$$

where  $(\rho_2 - \rho_1)$  is the initial density difference between the fluid discharged from the jet and the ambient environment, and a stratification parameter,

$$T_f = \frac{\rho_2 - \rho_1}{\left(\frac{-d\rho_a}{dy}\right) D} \quad (6.10)$$

where  $\frac{d\rho_a}{dy}$  is the density gradient in the ambient fluid. For the pumping system shown in Fig. 6.1 and considered in the dimensional analysis,

$$\frac{\rho_2 - \rho_1}{\rho_2} = \frac{\Delta\rho}{\rho_0}$$

and

$$\frac{-d\rho_a}{dy} = \frac{\Delta\rho}{d}.$$

Thus, for the mixing system  $F_f$  and  $T_f$  become

$$F_f = \frac{v}{\left(\frac{g}{\rho_0} \Delta\rho D\right)^{\frac{1}{2}}} \quad (6.11)$$

and

$$T_f = \frac{d}{D} \quad (6.12)$$

The parameters  $F$  and  $P$  can be expressed as

$$F = F_f \quad (6.13)$$

and

$$P = \left(\frac{\pi}{4}\right) F_f T_f^{-5/2} \quad (6.14)$$

demonstrating that  $F$  and  $P$  characterize the buoyant jet for the pumping system. The composition of these parameters is now such that the discharge velocity (or diameter  $D$ ) appears only in  $F$ , and the depth  $d$  only in  $P$ .

The dimensionless parameter  $P$  is the only parameter required to characterize a simple plume in a linearly stratified environment. This has been shown by Morton, Taylor, and Turner (34) in the dimensionless solution to the problem. A simple plume has no initial momentum flux and is the limiting case of the buoyant jet as the densimetric Froude number,  $F$ , goes to zero. Therefore, as the initial buoyant jet for the pumping system becomes more plume-like (i. e.  $F \rightarrow 0$ ), the parameters required to characterize the results of mixing are reduced by one. For this case,  $F$  and  $P$  can be replaced by the plume parameter,  $P$ , alone. That is,

$$\rho^* = f(y^*, t^*, P, S) . \quad (6.15)$$

The dimensionless parameter  $S$  reflects the shape or aspect ratio of the impoundment. Large values of  $S$  indicate shallow impoundments of large area, and small values indicate relatively deep impoundments of small area. The parameter  $S$  is of interest because the response of the impoundment to the pumping system may depend on the distance of its boundaries from the jet and intake tubes. As pointed out in Chapter 4, the experiments in the longest flume (40 meter) with the highest experiment  $S$  values demonstrated isopycnic surfaces which



were not horizontal. While experimental results were in general agreement with the simulation results, the effects of the finite time required for changes to propagate across the impoundment were observed.

That the simulation technique does not account for the finite time required for horizontal spreading was discussed in Chapters 2 and 4. The one-dimensional nature of the simulation model prohibits the inclusion of this effect. Therefore, the shape parameter,  $S$ , is not a governing parameter for the simulation model of an impoundment which has an initially linear density profile other than as it affects the withdrawal layer thickness. This can be demonstrated more rigorously by examining the governing equations of the simulation model,

$$\frac{\partial(vA)}{\partial y} = q_e \quad (2.1)$$

$$\frac{\partial c}{\partial t} + v \frac{\partial c}{\partial y} = 0 \quad (2.3)$$

These equations can be normalized using the physical variables of the dimensional analysis to yield the following equations:

$$\frac{\partial(v^*A^*)}{\partial y^*} = q_e^* \quad (6.16)$$

$$\frac{\partial c^*}{\partial t^*} + v^* \frac{\partial c^*}{\partial y^*} = 0 \quad (6.17)$$

where:  $y^* = y/d$  ,

$t^* = t/T$  ,

$c^* = c/c_o$  ,

$A^* = \frac{Ad}{V}$  ,

$q_e^* = \frac{q_e d}{Q}$  and,

$v^* = \frac{vV}{Qd}$  .

The shape factor,  $S$ , does not appear as a parameter in these equations or their initial and boundary conditions.

The entrainment from the impoundment,  $q_e$ , is calculated using the mechanics of buoyant jets and selective withdrawal. The buoyant jet in a linearly stratified environment is not characterized by  $S$  but only by  $F$  and  $P$  as shown previously.

The only influence  $S$  has on the simulation results occurs indirectly in the determination of the thickness of the withdrawal region. As discussed in Sect. 2.2.5, the thickness of the withdrawal region is determined in the simulation by the average of the thicknesses calculated for a two-dimensional flow using an inviscid theory near the withdrawal tube and using a turbulent flow theory near the boundary of the impoundment. The two-dimensional discharge is determined by dividing the pumped discharge by the average width of the impoundment at the elevation of the intake. The width of the impoundment and the distance from the intake to the impoundment boundary are related to  $S$  indirectly.

However, the influence of the parameter  $S$  upon simulation results for cases with initially linear density profiles was found to be small because withdrawal region size is affected only indirectly by  $S$  and because the withdrawal region itself exerts only a small effect on the density profile as a whole.

The dimensional analysis indicates that for cases with initially linear density profiles the results of the simulation technique can be presented uniquely in a generalized way. Density-depth profiles are plots of  $\rho^*$  and  $y^*$  at various times,  $t^*$ . Each such time-history of mixing is a function of the initial densimetric Froude number,  $F$ , and the plume parameter,  $P$ . The shape factor,  $S$ , is neglected for the reasons discussed above, although it may influence actual mixing results. An example of the results of a simulated mixing experiment in generalized form is shown in Fig. 6.2.

### 6.2.2 Potential Energy Increase

The mixing process increases the potential energy of the impoundment. As mixing proceeds and the density profile changes, the center of mass of the impoundment moves upward while the total weight remains constant for a closed system. The increase in potential energy of the impoundment is the product of the weight of the fluid in the impoundment and the increase in elevation of the center of mass.

Consider the volume of fluid  $V$  to be affected by the mixing process to be that region over the distance  $d$  included between planes at the elevations of the withdrawal and jet tubes. The area-depth

relationship is given as  $A(y)$ , and the mean density in this region is  $\rho_m$ . The center of mass for this region given any density profile  $\rho_a(y)$  is

$$y_{c.m.} = \frac{1}{\rho_m V} \int_0^d \rho_a(y) A(y) y dy , \quad (6.18)$$

where

$$\rho_m = \frac{1}{V} \int_0^d \rho_a(y) A(y) dy . \quad (6.19)$$

For the particular case of an initially linear density profile and a prismatic impoundment (constant area), Eqs. 6.18 and 6.19 are easily evaluated. While impoundments of constant area over the depth are not usually the case, the analysis of this situation is uncomplicated and the results are informative. For this particular case, referring to Fig. 6.1, the center of mass is

$$y_{c.m.} = \frac{\rho_o d}{2\rho_m} + \frac{\Delta\rho d}{6\rho_m} , \quad (6.20)$$

where

$$\rho_m = \rho_o + \frac{\Delta\rho}{2} . \quad (6.21)$$

When mixing is complete and the density is uniformly  $\rho_m$  over the depth,  $d$ , the center of mass is

$$y_{c.m.} = \frac{d}{2} . \quad (6.22)$$

Therefore, the change in elevation of the center of mass of the impoundment from the initial linear density stratification to the completely uniform condition is

$$\Delta y_{c.m.} = \frac{\Delta \rho}{\rho_m} \frac{d}{12} , \quad (6.23)$$

and in the increase in potential energy acquired is

$$\Delta P.E. = \frac{\Delta \rho g d V}{12} . \quad (6.24)$$

The increase in the potential energy of the impoundment is calculated at regular time intervals during the simulation of the mixing process. The ratio of the increase in potential energy at any particular time to the increase in potential energy required for complete mixing, as given in Eq. (6.24), is a measure of the degree to which mixing has proceeded. This ratio, the fraction of required potential energy increase for complete mixing, takes the range of values from 0.0 to slightly greater than 1.0. The upper limit is not exactly equal to 1.0 as the withdrawal region affects the density of a small part of the impoundment above the center line of the withdrawal tube.

This ratio is a gross measure of the mixing process as the dimensionless density-depth profiles are not uniquely reflected by this number. It is possible to have several profile time-histories of the mixing process which differ in shape and detail, yet which have reached identical fractions of the required potential energy increase. A plot of this quantity as a function of dimensionless time,  $t^*$ , for a particular

mixing simulation of a prismatic impoundment is shown in Fig. 6.4. Such curves always indicate a decreasing rate of potential energy increase as the mixing process continues to completion.

Since this analysis has been carried out for prismatic impoundments with initially linear profiles, the results apply exactly to the inverse type of pumping system, that is, a reversed pumping direction so that the jet is discharged near the surface. The governing equations for the buoyant jet in a linear density profile are the same for this case, and simulated density profiles are the same though inverted.

### 6.2.3 Effect of the Densimetric Froude Number

The densimetric Froude number based on the initial linear density profile,  $F$ , and the plume parameter,  $P$ , characterize the initial buoyant jet, the stratification, and the simulation results. In particular, the Froude number indicates the nature of the buoyant jet relative to its limiting cases:  $F = \infty$ , a simple momentum jet and  $F = 0$ , a simple plume.

The effects on simulation results of changes in only the Froude number,  $F$ , are illustrated by the following simulation experiments. The impoundments were assumed prismatic and linearly stratified initially. The plume and shape parameter were fixed at  $P = 1.092 \times 10^{-3}$   $S = 2929.7$ , respectively, for four mixing simulations. The Froude numbers were  $F = 1.0, 3.0, 12.0$ , and  $24.0$ , a range from weak to strong jets. In terms of the physical variables of the pumping system, this range of Froude numbers was achieved by holding all independent variables the same, except for the diameter and initial velocity of the jet.

The results of three of these simulation experiments are shown in dimensionless form in Figs. 6.2 and 6.3. The density-depth profiles are shown at the same dimensionless times for all simulations. The density profiles indicate that the pumping systems with large Froude numbers,  $F = 12.0$  and  $24.0$ , mix the lower regions of the impoundment rapidly. The density profiles are nearly vertical in this region for  $F = 24.0$ , while they have considerable gradients at the same time,  $t^*$ , for  $F = 1.0$ . The simulation results for  $F = 1.0$  show that the effects of mixing reach slightly higher elevations in the impoundment than do the simulations for larger Froude numbers. These results are consistent with the behavior of buoyant jets in a linearly stratified environment. Jets with large  $F$  entrain fluid rapidly at the beginning of their trajectories and reach a maximum height of rise at elevations which are lower than those attained by jets with small  $F$  which entrain fluid less rapidly. Figs. 6.2 and 6.3 show, however, that by the time  $t^* = 0.225$  (last profile calculated), the density profiles do not differ substantially among these three simulations.

The effects of the Froude number on the mixing process can be viewed in terms of the increases in potential energy of the impoundment, as suggested in Sect. 6.2.2. Fig. 6.4 is a plot of the fraction of the potential energy increase required for complete mixing versus the dimensionless time of mixing,  $t^*$ , for four simulations for  $F = 1.0$ ,  $3.0$ ,  $12.0$ , and  $24.0$ . This time-history of the increase in potential energy shows that the larger Froude number systems result in larger increases in potential energy throughout the mixing process. However,

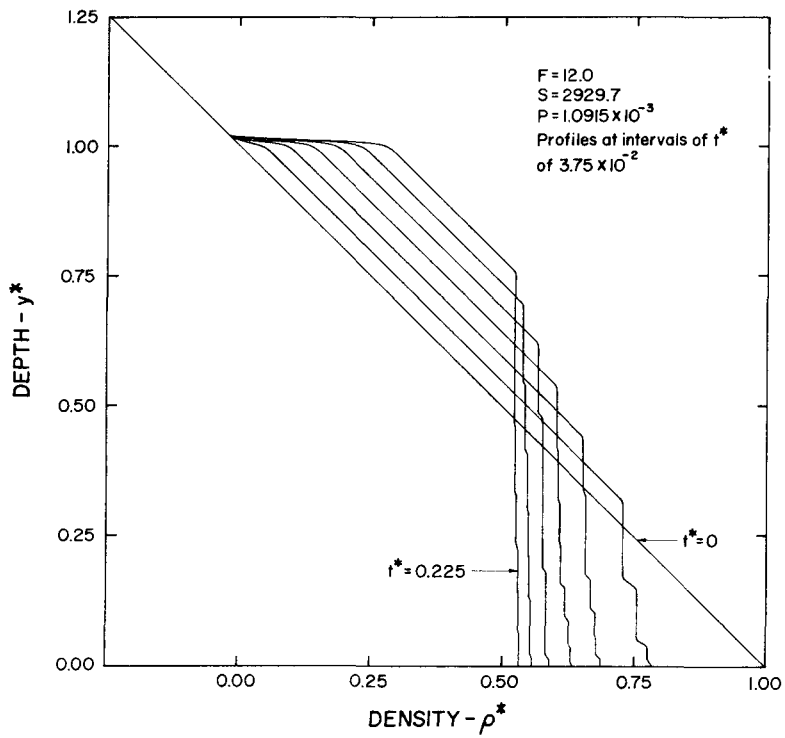
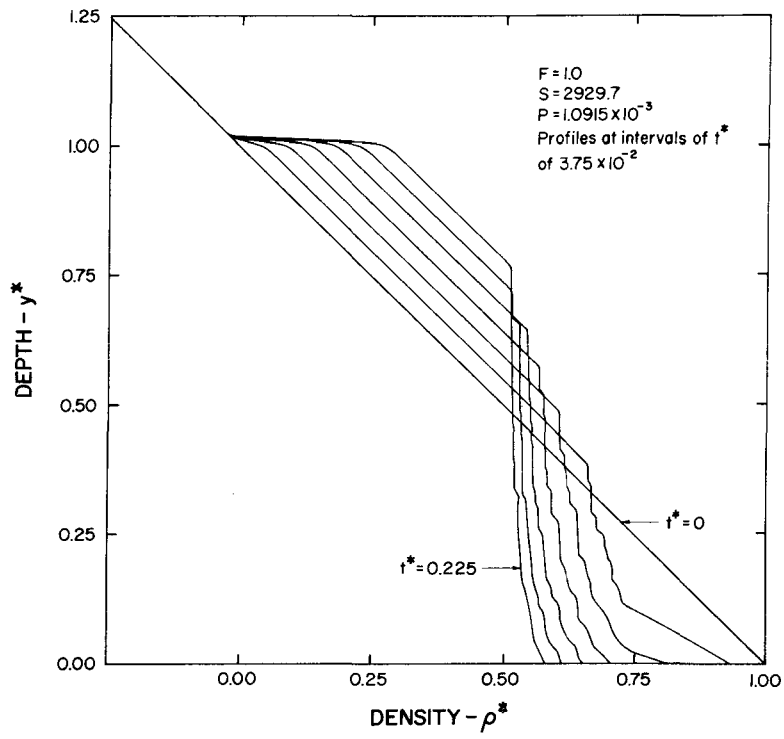


Figure 6.2 Generalized simulation results for  $F = 1.0$  and  $F = 12.0$



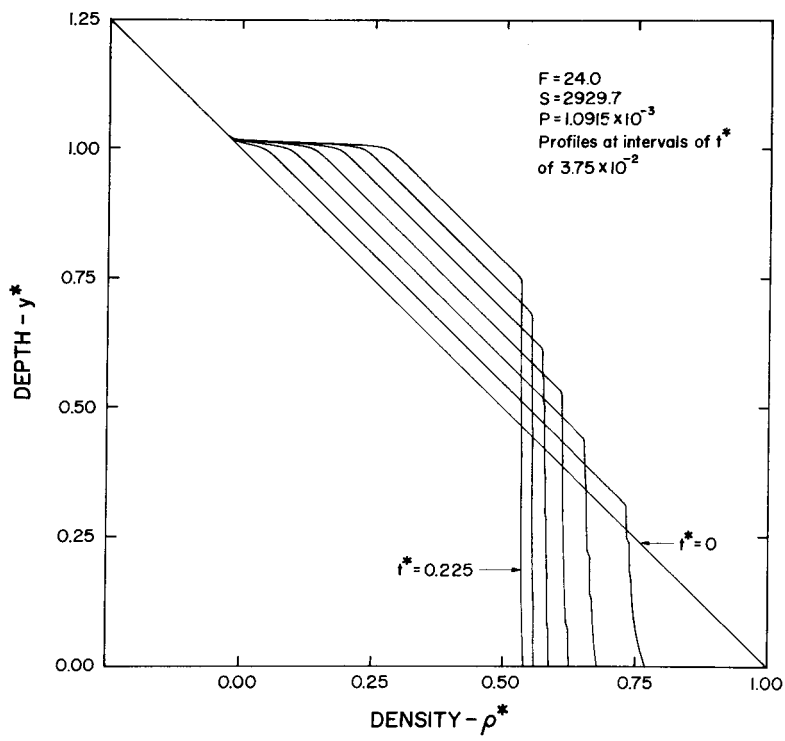


Figure 6.3 Generalized simulation results for  $F = 24.0$

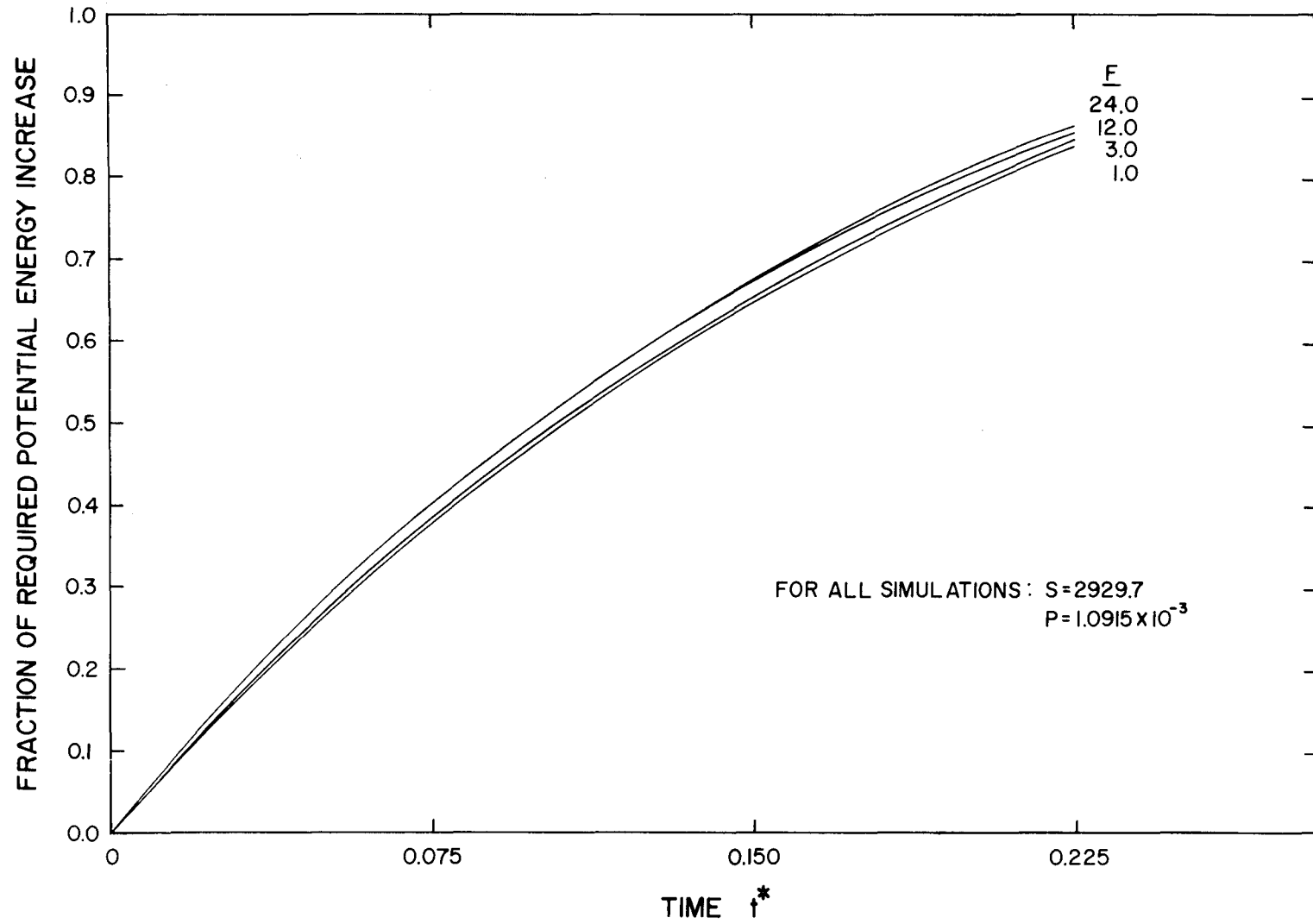


Figure 6.4 Effect of densimetric Froude number on the increase in potential energy with time

the differences in the fraction of required potential energy increase among the four simulations are small. By the time that the mixing is 80% completed, the differences in completion among these simulations are less than 3%.

The fact that essentially little difference exists among the simulation results for this range of Froude numbers raises the question as to which pumping system is the most efficient. The response of the impoundment to systems of various Froude numbers has been shown in terms of the increases in potential energy, but the inputs of energy have yet to be discussed. It is difficult to determine in generalized terms the input energy required to drive a particular pumping system. A major portion of the losses in a system are unique to the particular pumping system and its detailed design. While consideration of these details is important to the design of a particular pumping system, the purpose of this analysis is to find results which will guide the general, rather than detailed, design of the system. For this reason, the following treatment of the energy inputs to the pumping system will be somewhat idealized so that general criteria concerning the efficiency of the system can be formulated.

Considering the initial density profile shown in Fig. 6.1, the pumping head due solely to the pressure difference caused by the density stratification between the intake and jet is

$$H_p = \frac{d \Delta \rho}{2 \rho_o} \quad , \quad (6.25)$$

and the required power is

$$G_p = Q \gamma H_p = \frac{Q d g \Delta \rho}{2} . \quad (6.26)$$

The power requirement is quite small because  $\Delta \rho$  is small. This term is based on the initial density profile and decreases as the mixing proceeds because the density profile becomes more uniform and  $\Delta \rho$  decreases.

Energy losses due to the exit loss, friction, bends in the pipe, and other fittings contribute to the pumping head, but they are difficult to treat in a general way. For this simple model such losses are considered to be proportional to the velocity head at the jet so that

$$H_L = \beta \frac{v^2}{2g} , \quad (6.27)$$

and the power requirement is

$$G_L = \beta Q \gamma H_L = \frac{\beta Q \rho_o v^2}{2} , \quad (6.28)$$

where  $\beta =$  a coefficient  $> 1.0$ .

For the purpose of comparing the efficiencies of these three pumping systems of varying Froude number, the input energy for the systems is chosen as

$$\text{Input Energy} = (G_p + G_L) t \quad (6.29)$$

where:

$\Delta \rho$  is fixed at the initial value

$t$  - time from the beginning of pumping.

The efficiency of the system is defined as follows:

$$\text{Efficiency} = \frac{M \Delta P. E.}{(G_p + G_L) t} \quad , \quad (6.30)$$

where  $\Delta P. E.$  = potential energy increase required for complete mixing (Eq. 6.24)

$M$  = fraction of  $\Delta P. E.$  reached in time,  $t$ .

The efficiency (Eq. 6.30) can be normalized and written in terms of the dimensionless parameters:

$$\text{Efficiency} = \frac{M}{6t^*} \frac{1}{\left(1 + \beta \left(\frac{4}{\pi}\right)^{2/5} F^{8/5} P^{2/5}\right)} \quad . \quad (6.31)$$

Using this definition with  $\beta = 1.0$  for the sake of comparison only, efficiencies of the three pumping systems with  $F = 24.0$ ,  $F = 12.0$ , and  $F = 1.0$  were 0.041, 0.105, and 0.465, respectively. The system with  $F = 1.0$  was approximately ten times as efficient as the system with  $F = 24.0$ . These efficiencies have no meaning in an absolute sense because of the artificial nature of the definition of efficiency (Eq. 6.30 with  $\beta = 1.0$ ). They are meant to be viewed only in a relative sense.

It is clear from the normalized form of the efficiency (Eq. 6.31) that the efficiency increases as the Froude number decreases. For fixed plume parameter,  $P$ , the fraction of the required potential energy increase,  $M$ , varies only slightly with  $F$  at a given  $t^*$  (see Fig. 6.4); thus decreased  $F$  must result in increased efficiency.

The interpretation of these efficiency calculations in a relative sense leads to the conclusion that the lower the Froude number, all other parameters fixed, the greater the efficiency of the system. In terms of the physical variables for the three pumping systems examined, the large Froude numbers represented large velocity heads and a large input of kinetic energy. However, the simulation demonstrates that the response of the impoundment to the increased input of kinetic energy is such that the efficiency is less than that for lower values of  $F$ . As the Froude number is decreased and approaches zero, the buoyant jet becomes more like a simple plume. A simple plume has no initial momentum flux, and the input energy to drive a simple plume pumping system is entirely potential. For this case ( $F \rightarrow 0$ ),

$$\rho^* = f(y^*, t^*, P) . \quad (6.32)$$

Although low Froude number jets provide for more efficient pumping systems than high Froude number jets, there may be cases for which high Froude number systems are preferable, though less efficient. A situation in which it is necessary to mix the region near the jet outlet as rapidly as possible is an example of such a case (contrast cases for  $F = 1.0$  and  $F = 24.0$  in Figs. 6.2 and 6.3).

#### 6.2.4 Results of Generalized Simulations

Since pumping systems with low Froude number, plume-like buoyant jets have been shown to be the most efficient ones, a series of simulation experiments with low Froude number were performed.

The impoundments for these experiments are assumed to be prismatic, and the initial profiles were linear. The Froude number was held fixed at  $F = 3.0$ . This value of the Froude number is larger than the smallest value,  $F = 1.0$ , used in Sect. 6.2.4. The fraction of required potential energy increase versus time for  $F = 3.0$  and  $F = 1.0$  is shown in Fig. 6.4. The efficiencies for these two cases at  $t^* = 0.225$  were 0.359 for  $F = 3.0$  and 0.465 for  $F = 1.0$ . The value  $F = 3.0$ , though resulting in a slightly less efficient system, was chosen because it represents a plume-like case which still allows for the small amount of initial momentum flux that exists for any real pumping system. A true plume pumping system would require an extremely large jet diameter to discharge the required flow at sufficiently low velocities.

For Froude numbers,  $F = 3.0$  and lower, the buoyant jets are very much plume-like and are characterized only by the plume parameter,  $P$  (see Eq. 6.32). The dimensionless density profiles generated by the simulation experiments are characterized by the plume parameter alone, since  $F$  is small and  $S$  is not a significant governing parameter in the simulations. Simulation experiments were performed over a range of the parameter  $P$ , from  $10^{-6}$  to  $10^{-1}$ . To demonstrate that the shape factor,  $S$  is not a governing parameter for the simulated mixings, experiments with  $S$  values of 500 and 50,000 were simulated.

The dimensionless density profiles for simulation experiments for which  $S = 500$  and  $P$  ranges from  $2.5 \times 10^{-6}$  to  $2.5 \times 10^{-2}$  are shown in Figs. 6.5, 6.6, and 6.7. The density profiles are plotted at

intervals of time,  $t^*$ , of  $3.75 \times 10^{-2}$ . This series of mixing simulations indicates that the impoundment is not as uniformly mixed near the bottom for the high values of the plume parameter,  $P$ , as it is for the low values of  $P$ . High values of the plume parameter also result in larger withdrawal regions about  $y^* = 1.0$  than do low values. After the mixing process has progressed beyond  $t^* = 0.15$ , the resulting profiles do not differ greatly from one another in a general sense for the range of  $P$  values. Fig. 6.8 shows the time-history of the increases in potential energy,  $M$ , for each simulation relative to that required for complete mixing. The larger the plume parameter,  $P$ , the greater the increase in potential energy for any given time,  $t^*$ . However, the difference in potential energy increases,  $M$ , among the mixings for this range of  $P$  values is less than 10%.

The series of dimensionless profiles for simulation experiments for which  $S = 50,000$  and  $P$  ranges from  $1.16 \times 10^{-4}$  to  $1.16 \times 10^{-1}$  are shown in Figs. 6.9 and 6.10. A plot of potential energy increases versus time is shown in Fig. 6.11 for  $S = 50,000$ . As predicted the simulation results show negligible effects due to the change in the shape parameter,  $S$ . The variations in the density profiles and potential energy increases due to changes in the plume parameter,  $P$ , follow the patterns outlined above for the series for which  $S = 500$ .

The results of several simulated mixings are summarized in Fig. 6.12. The dimensionless time,  $t^*$ , for given fraction of the required potential energy increase is plotted against the plume parameter,  $P$ . This plot shows that the shape parameter,  $S$ , is not a



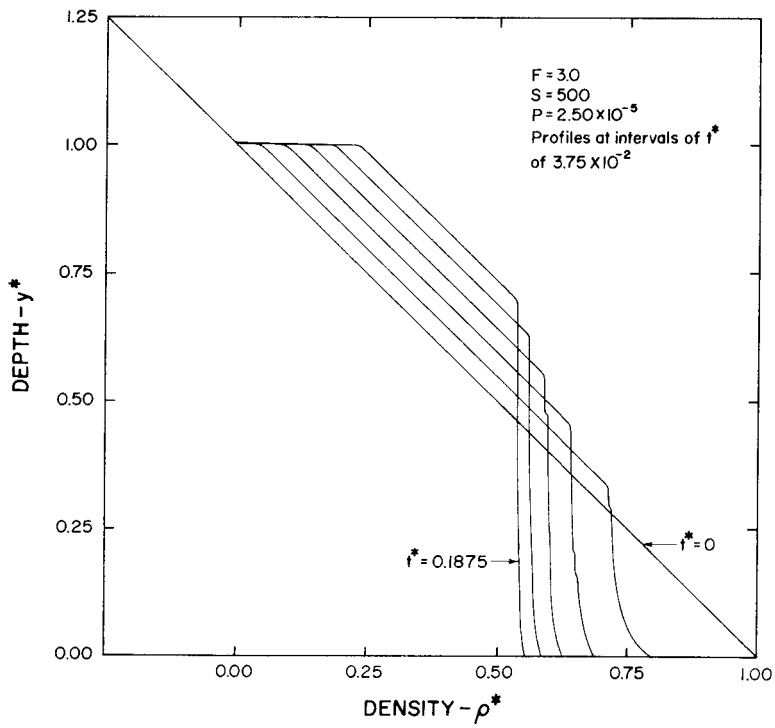
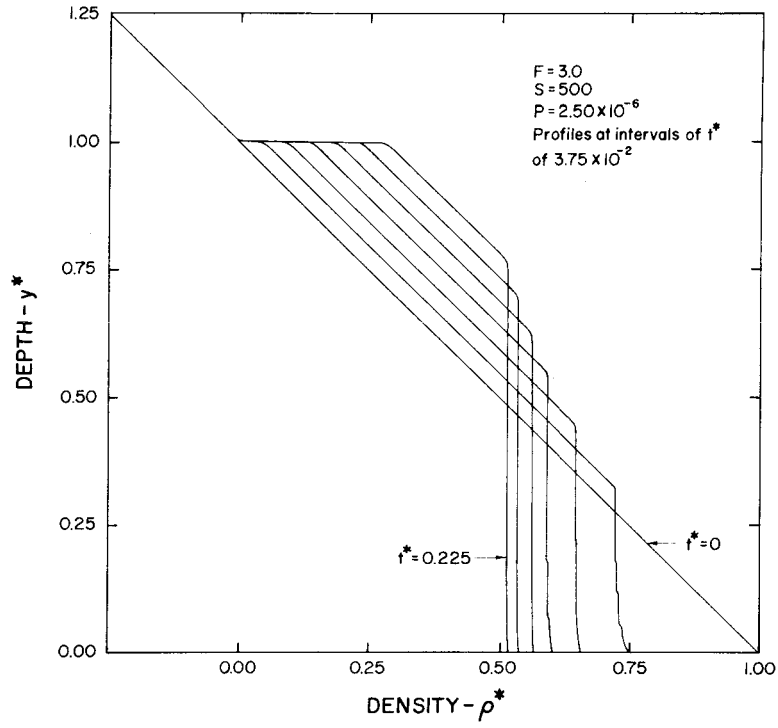


Figure 6.5 Generalized simulation results for  $P = 2.50 \times 10^{-6}$  and  $P = 2.50 \times 10^{-5}$ ;  $S = 500$  and  $F = 3.0$

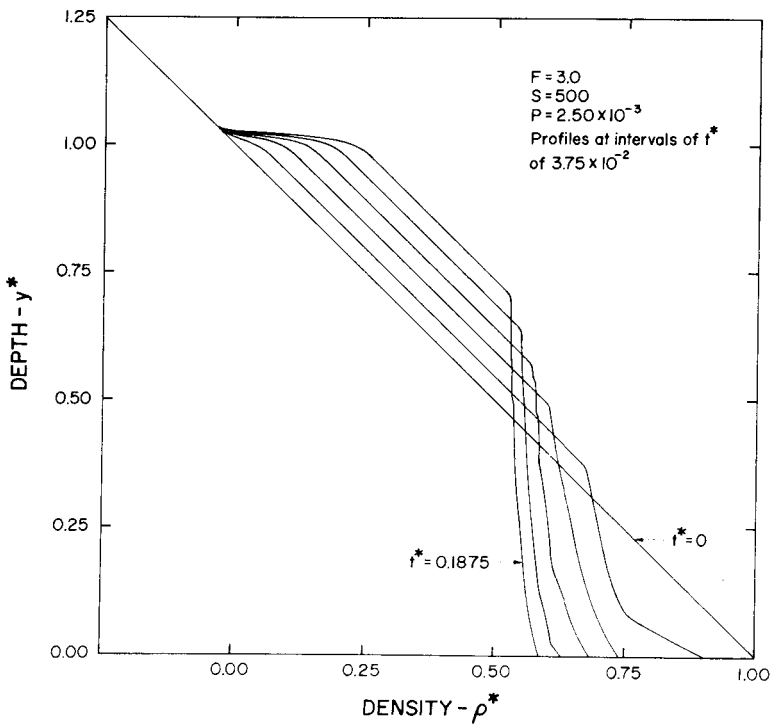
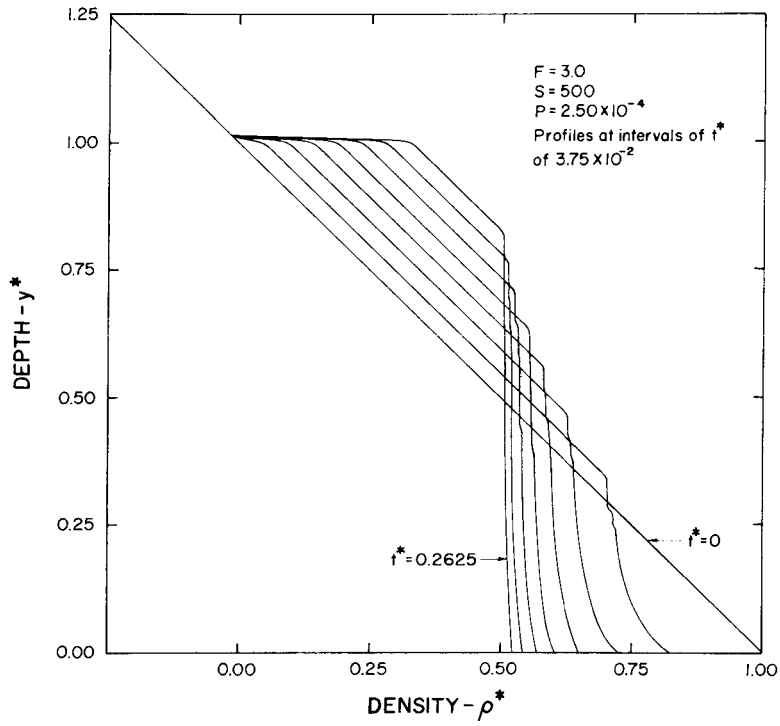


Figure 6.6 Generalized simulation results for  $P = 2.50 \times 10^{-4}$  and  $P = 2.50 \times 10^{-3}$ ;  $S = 500$  and  $F = 3.0$

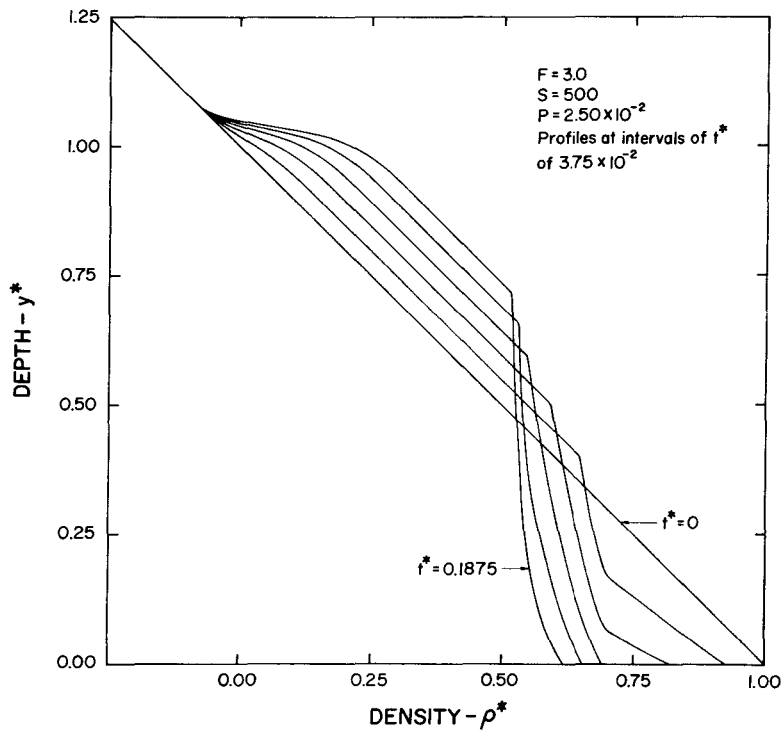


Figure 6.7 Generalized simulation results for  $P = 2.50 \times 10^{-2}$ :  
 $S = 500$  and  $F = 3.0$

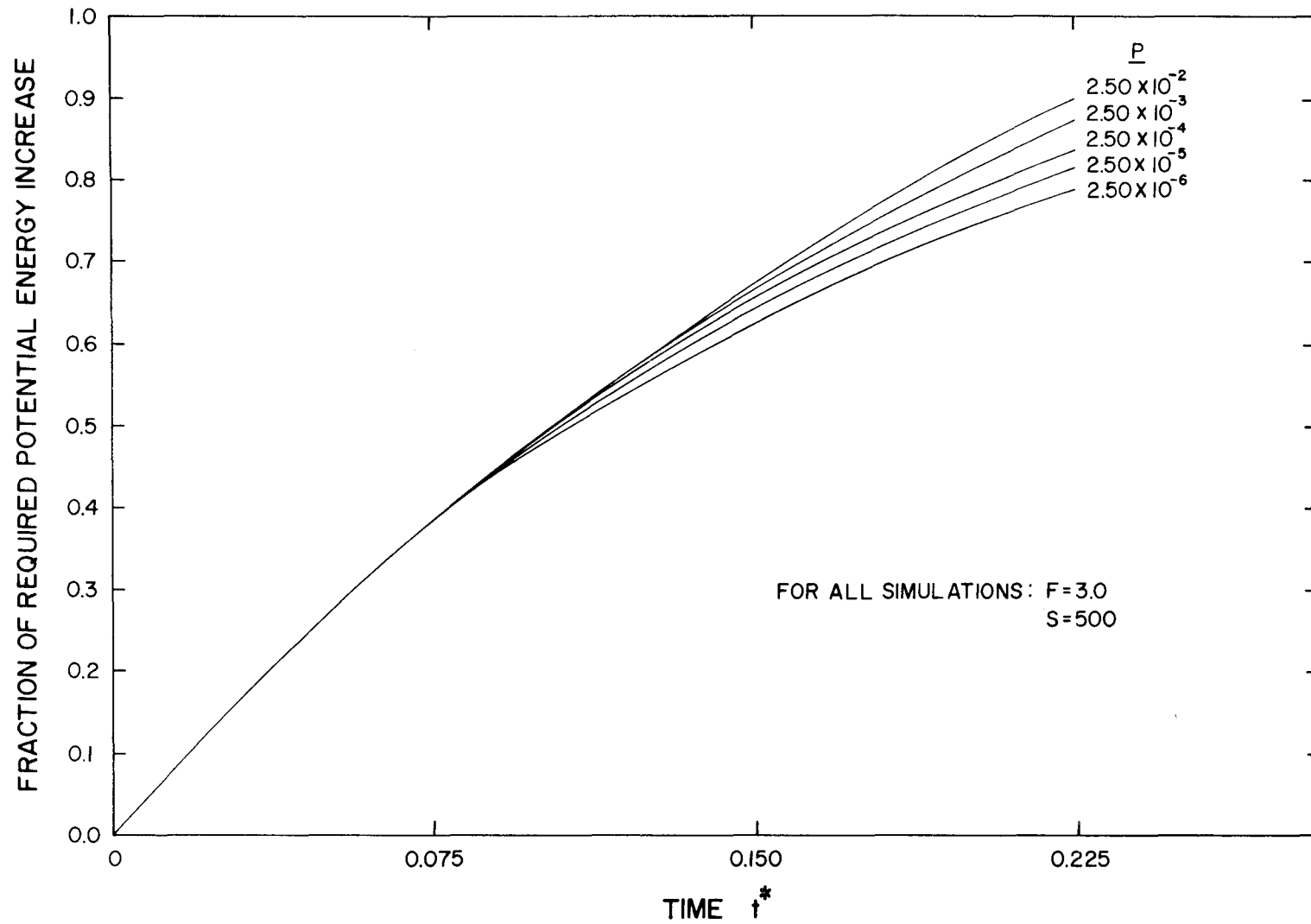


Figure 6.8 Effect of plume parameter,  $P$ , on the increase in potential energy with time ( $S = 500$  and  $F = 3.0$ )

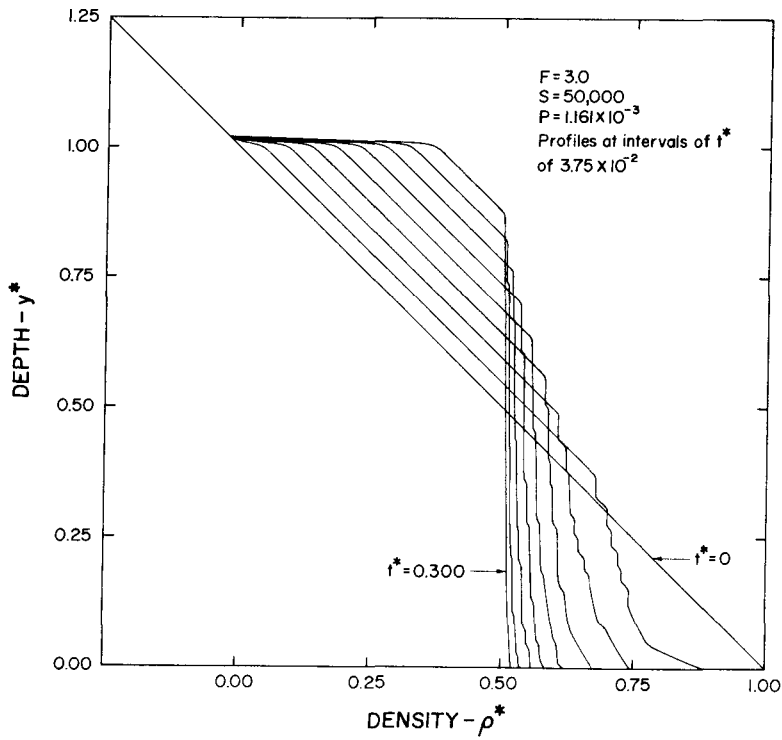
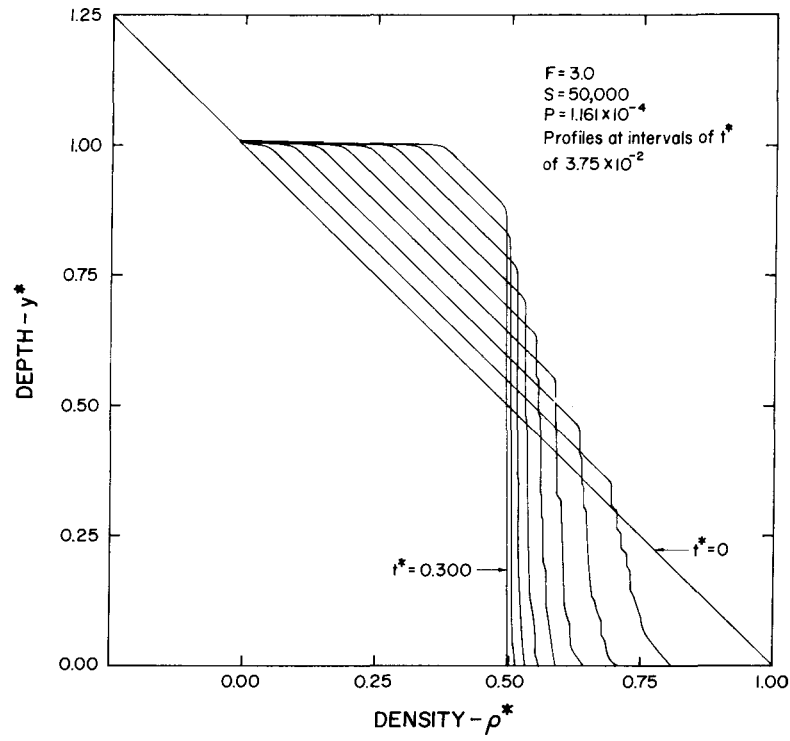


Figure 6.9 Generalized simulation results for  $P = 1.16 \times 10^{-4}$  and  $P = 1.16 \times 10^{-3}$ ;  $S = 50,000$  and  $F = 3.0$

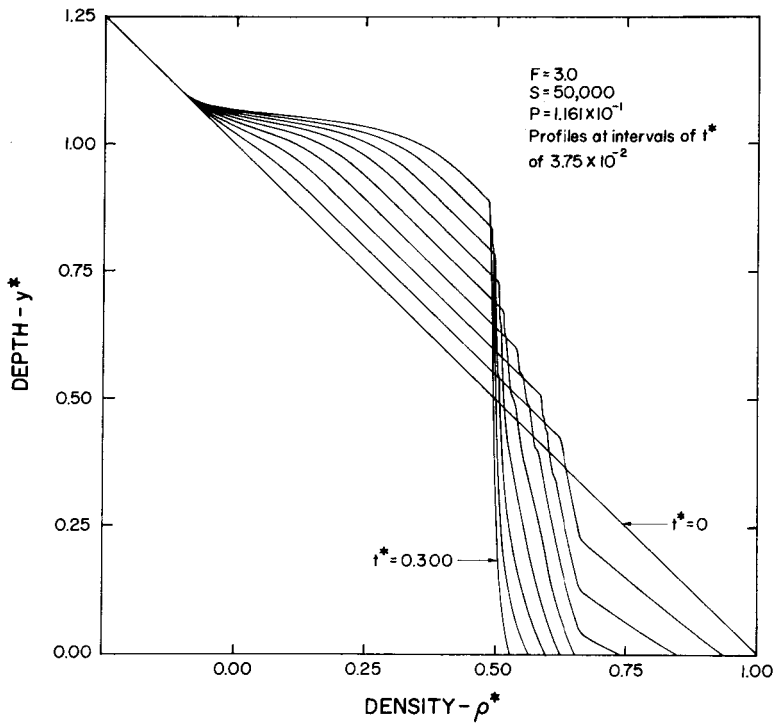
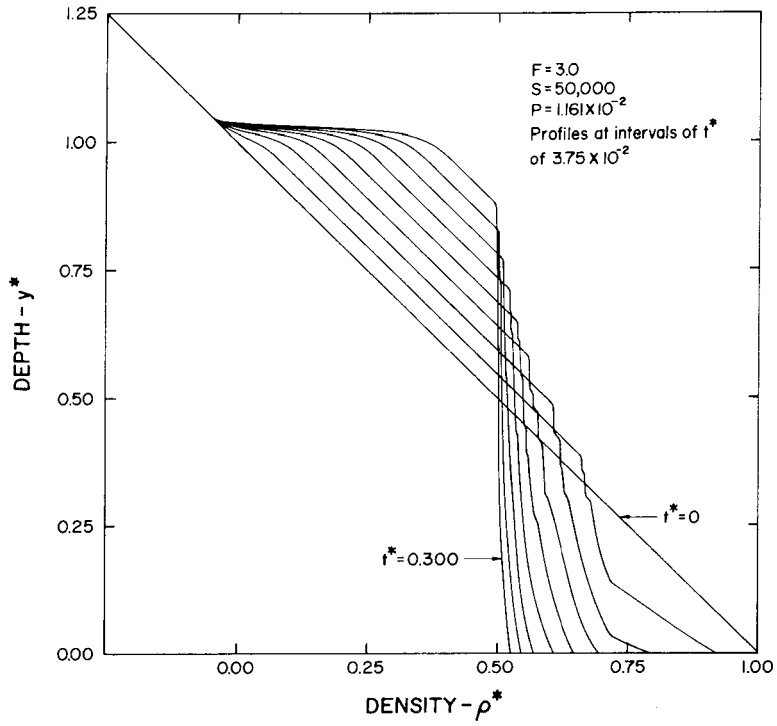


Figure 6.10 Generalized simulation results for  $P = 1.16 \times 10^{-2}$  and  $P = 1.16 \times 10^{-1}$ ;  $S = 50,000$  and  $F = 3.0$

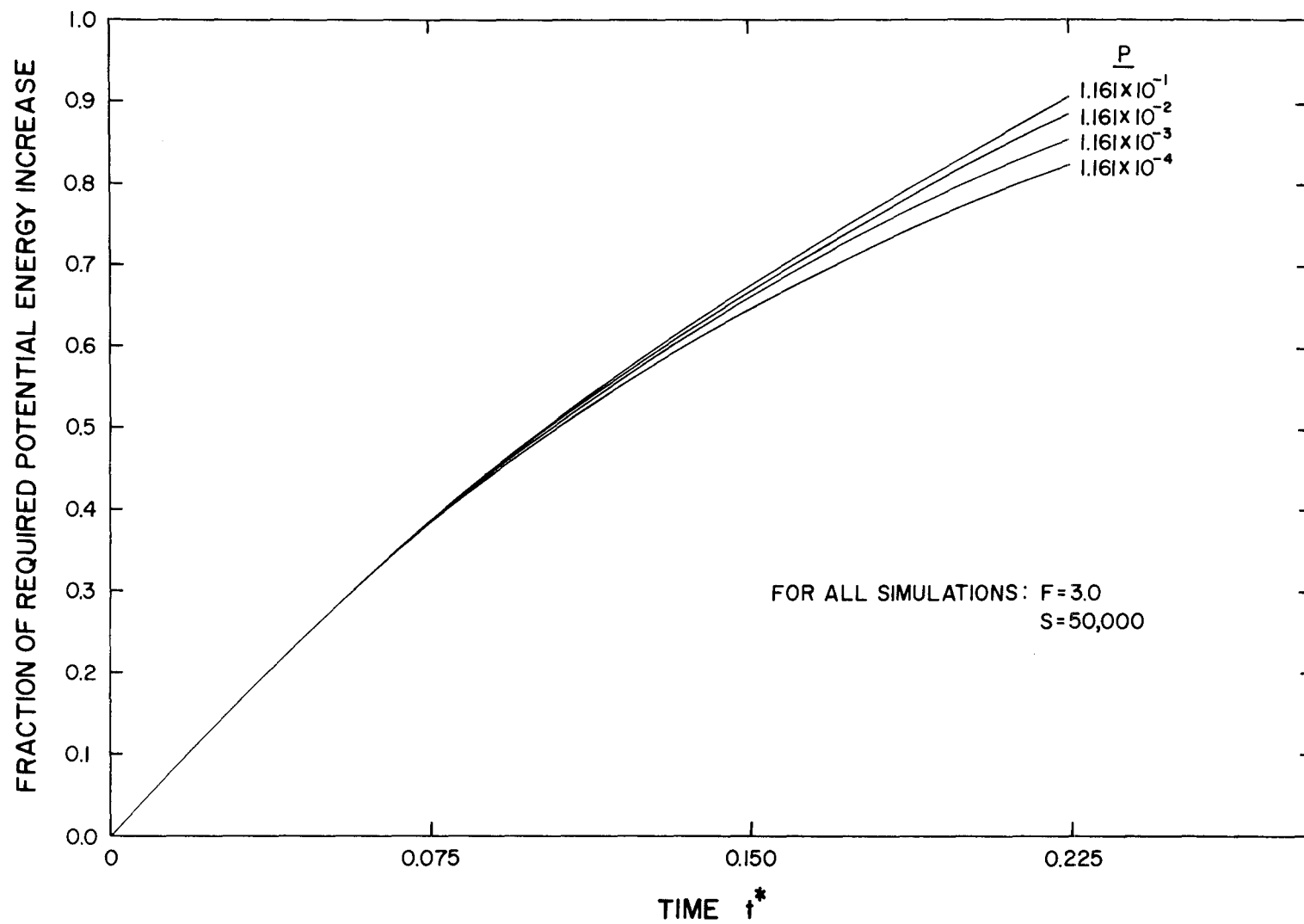


Figure 6.11 Effect of plume parameter,  $P$ , on the increase in potential energy with time ( $S = 50,000$  and  $F = 3.0$ )

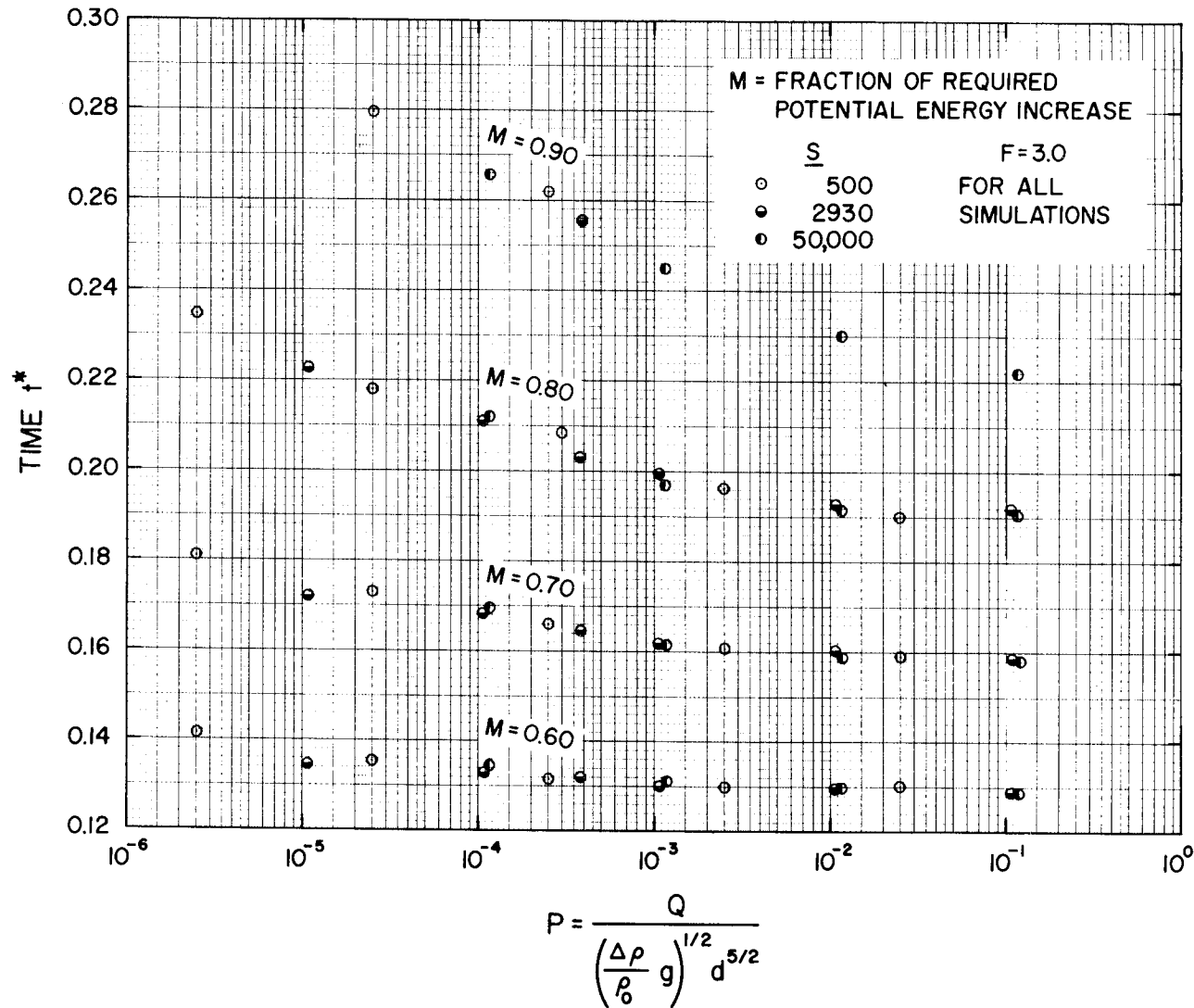


Figure 6.12 Summary of generalized simulation results: fraction of required potential energy increase as a function of P and t\*



governing parameter for the simulated mixings as results for all  $S$  values lie on the same curves. The high values of  $P$ , in the range examined, indicate smaller dimensionless times,  $t^*$ , for a given fraction of potential energy increase than do the low values. However, over the range of  $P$  values presented, the dimensionless times for a given amount of mixing vary less than 10%. This indicates that the time, in dimensionless terms, required for mixing is nearly independent of the plume parameter.

### 6.3 IMPLICATIONS OF SIMULATION FOR THE DESIGN OF PUMPING SYSTEMS

The results of the simulated mixing experiments in generalized form provide some guidelines for the design of efficient pumping systems. However, these results must be applied with caution because of the simplified form of the simulation technique. The generalized solutions were calculated for prismatic shaped impoundments with initially linear density profiles. In particular, most solutions represent cases where the densimetric Froude number is  $F = 3.0$ . The simulation results do not account for the effect of the shape parameter,  $S$ , on the mixing process. Despite these limitations, some general conclusions can be drawn from the simulation results which suggest strategies for the design of mixing systems.

The experiments summarized in Fig. 6.12 indicate that, for low Froude numbers and over a wide range of plume parameters, the dimensionless time in which 80% of the potential energy increase

required for complete mixing is attained is  $t^* = 0.210 \pm 0.020$ . In physical variables,

$$t^* = \frac{Qt}{V} = \frac{t}{T} \quad . \quad (6.2)$$

For  $t^* = 0.210$ , the time, in real units, for mixing to be approximately 80% accomplished is

$$t = 0.210T = 0.210 \frac{V}{Q} \quad . \quad (6.33)$$

If one uses this measure of 80% completion of mixing, the choice of the mixing period ( $t$ ) and the volume ( $V$ ) dictate the required discharge ( $Q$ ) for the pumping system. Eq. (6.33) is so simple an expression that the options for adjusting  $t$  and/or  $V$  are a matter of proportionality. For instance, for a fixed volume,  $t$  is inversely proportional to  $Q$  and can be increased or decreased accordingly. Another option is to divide the impoundment into  $n$  regions, each with volume  $V/n$  and each provided with a pumping system. Such an arrangement could reduce the time of mixing,  $t$ , for the whole impoundment or reduce the required discharge for each of the individual pumping systems. This type of design might be prudent for impoundments for which the shape factor,  $S = V/d^3$ , is large. The value of  $S$  would then be reduced by a factor of  $n$ . The reduced lateral dimension of each region would yield closer agreement between simulation results, which take inadequate account of lateral spreading, and physical results, in which lateral spreading may be important. This partitioning would lead to more uniform mixing of the impoundment.

Given the discharge,  $Q$ , for a particular pumping system, the choice of the discharge jet diameter fixes the densimetric Froude number for the system. The effects of various Froude numbers for a particular system have been discussed in detail in Sect. 6.2.3. In terms of the response of the impoundment, it was shown that the larger the Froude number, the greater the increase in potential energy of the impoundment after a fixed time of pumping. However, calculations of efficiencies showed that high Froude number systems were less efficient than low Froude number ( $F < 3.0$ ) systems. It is possible that an efficient pumping system in terms of energy may not be the criterion by which to design. If the impoundment were to be mixed very rapidly, an increased Froude number for a system of fixed discharge could decrease the mixing time at the expense of efficiency. The range of  $t^*$  for 80% completion of mixing for Froude numbers  $F = 1.0$  and  $F = 24.0$  is shown in Fig. 6.4 for a particular plume parameter,  $P$ . These two points give an indication of the shift of the 80% curve in Fig. 6.12 with Froude number. Should a design objective be to mix the fluid at a particular elevation with the fluid at other elevations, this could be accomplished most readily by placing a high Froude number jet at that elevation.

Since the simulated mixings were performed for prismatic impoundments with initially linear stratification, the results apply to systems in which pumping is from top to bottom and in which pumping is from bottom to top. These results do not apply to impoundments for the area is a function of depth, though simulated mixing can be per-

formed for this case. Typically, the area of the impoundment increases from the bottom upward. In situations in which this departure from a prismatic impoundment is marked, pumping from top to bottom may prove the better strategy. A system with the jet at the bottom would be advantageous in this case because the lower region of the impoundment would respond to the mixing more rapidly than the upper region as the volume of this region is smaller. In a given time a zone of greater vertical extent would be affected by mixing with the jet at the bottom than with the jet near the surface. From a water quality perspective, the elimination of stratification throughout the bottom zone of the impoundment would permit increased diffusion of oxygen into the zone where it would be most beneficial.

The simulated mixing results, though calculated for prismatic impoundments with linear profiles initially, may serve as guides for a prismatic impoundment with an initial profile which can be approximated by a linear profile. For two-layer stratification or other highly discontinuous stratifications, the results have little meaning. These special cases can be the objects of other series of generalized or individual simulations.



## CHAPTER 7

## SUMMARY AND CONCLUSIONS

Prior to this study most of the information concerning the use of pumping systems to mix density-stratified impoundments was limited to the results of a few field experiments. These experiments (reviewed in Chapter 1) demonstrated that pumping systems were successfully used to alter or eliminate density stratification and that significant beneficial water quality changes often accompanied the mixing. However, these experiments provided few observations about the physical processes governing the mixing and, as a result, furnish sparse information useful for predicting the results of mixing.

## 7.1 CONTRIBUTIONS OF THE PRESENT STUDY

The two main contributions of this study are:

- 1) the development of a simulation technique for the prediction of changes in the density structure of an impoundment due to mixing by a pumping system, and
- 2) the presentation of generalized results (in terms of dimensionless parameters) for special conditions to a series of mixing experiment simulations.

### 7.1.1 The Simulation Technique

The simulation technique developed in Chapter 2 predicts the time-history of the density profiles in an impoundment which is mixed by a pumping system. The simulation model is a closed-system; that is, it includes only the effects of the pumping system on the impoundment and excludes the effects of natural influences on the density structure. The impoundment is divided conceptually into two regions: Region 1 is the stratified impoundment exclusive of the buoyant jet and withdrawal layer, and Region 2 includes the buoyant jet and withdrawal layer, the principal features of the pumping system. The impoundment (Region 1) is treated in a one-dimensional sense, and the buoyant jet and withdrawal layer (Region 2) are modeled in a three-dimensional sense. The response of the impoundment to the pumping system is determined by the transport of fluid between these two regions.

The simulation model requires as input a description of the initial conditions and of the pumping system. Any initial density profile in the impoundment can be provided. The area-depth relationship for the impoundment, the elevations of the jet and intake tubes, and the jet discharge and diameter are required. Given this information, the simulation predicts the density profiles at successive time steps during the mixing process.

The redistribution of a conservative tracer substance due to mixing can be predicted (Chapter 3). Temperature can be used as the tracer, and the nonlinear temperature-density relationship can be accounted for in the simulation as described in Chapter 3.

Laboratory studies (Chapter 4) of the mixing of density-stratified impoundments by pumping indicate that the simulation technique predicts the gross features of mixing reasonably well. The comparisons of experimentally determined density profiles with simulation predictions show some disagreement in the details of the profiles. The nature of these disagreements between experimental and simulation results and the explanation of why they occur is given in Section 4.4.

Comparisons of the results of two field mixing studies with simulation predictions (Chapter 5) were inconclusive. The impoundments studied were subjected to natural changes in the heat budget in addition to mixing by the pumping system. The simulation model did not account for this effect, and the agreement between field and simulation results was not good.

The simulation technique consistently predicted the gross response of stratified impoundments to mixing by pumping systems for laboratory experiments at three different scales (Chapter 4). For the case of closed-systems, the simulation technique provides a good approximation to the response of the impoundment to mixing and a basis for comparison of the effects of different types of pumping systems. The applicability of the simulation technique to cases of mixing lakes and reservoirs which are clearly not closed-systems is discussed in Sect. 7.2.



### 7.1.2 The Generalized Solutions

A series of simulated mixing experiments were computed for prismatic shaped impoundments which had linear density profiles initially (Chapter 6). The results of these experiments were presented in generalized form and reveal characteristics of the pumping systems which may guide the development of design criteria for efficient mixing systems.

A dimensional analysis for this particular type of impoundment and initial density profile showed that the density profiles during mixing could be given in the general form,

$$\rho^* = f(y^*, t^*, F, P, S) \quad , \quad (6.8)$$

where:

$\rho^*$  = normalized density, Eq. (6.3)

$y^*$  = normalized elevation, Eq. (6.1)

$t^*$  = normalized time, Eq. (6.2)

$F$  = jet densimetric Froude number, Eq. (6.4)

$P$  = plume parameter, Eq. (6.6)

$S$  = shape parameter, Eq. (6.7).

A measure of the degree of the completeness of mixing is the increase in potential energy of the impoundment at any time relative to the total increase required for complete mixing. The efficiencies of several pumping systems were analyzed based on this measure of response of the impoundment relative to a theoretical input energy.

Efficiency, as defined here, decreased with increased densimetric Froude number,  $F$ . It was concluded that systems with weak buoyant jets (low  $F$ ) were most efficient, and generalized results were calculated for cases with  $F = 3.0$ . Also, the shape parameter,  $S$ , was not found to be a primary parameter for the simulation model, though it probably has an effect in the actual mixing process.

The results of low  $F$  mixing experiments are shown in Fig. 6.12 and

$$\rho^* = f(y^*, t^*, P) \quad (6.32)$$

for these cases. The plume parameter,  $P$ , also has only a small effect on the results; for instance, the dimensionless time,  $t^*$ , required for 90% completion of mixing (in terms of potential energy increases) varies less than 20% over the range of  $P$  from  $10^{-6}$  to  $10^{-1}$ . This means that the changes of the dimensionless density profiles with dimensionless time are practically the same for all  $P$  when  $F$  is small, i. e.,

$$\rho^* = f(y^*, t^*) \quad (F < 3)$$

and that at approximately  $t^* = 0.25$  the impoundment is nearly mixed. The value of  $t^*$  is much less than 1 due to the large lower layer entrainment of the buoyant jet.

The solutions for this particular case of initially linear density profiles in prismatic impoundments point to two broad design criteria:

- 1) All other parameters remaining fixed, the efficiency of the pumping system increases as the densimetric Froude number,  $F$ , decreases.
- 2) The time for complete mixing depends strongly on  $t^*$ , or in physical units on  $T = V/Q$ , the characteristic time for the system. Although the values of  $t^*$  calculated for this special case do not apply to all initial profiles, an estimate of the time required for mixing probably can be based on a fraction of  $T$ .

## 7.2 APPLICATION OF SIMULATION TECHNIQUE TO LAKES AND RESERVOIRS

The application of the simulation technique and the generalized results obtained in this study to the mixing of lakes and reservoirs by pumping systems is possible with certain restrictions. The assumptions underlying the simulation model must be recognized for useful application of the simulation technique.

The simulation model is a closed-system and accounts only for changes in the density profile due to the pumping system. Often natural changes in the impoundment heat budget occur during mixing and can alter the effect of the mixing due to pumping. This was evident in the limited comparisons of field and simulation results discussed in Chapter 5. Unless the simulation of the mixing system is coupled with a simulation of the effects of a changing heat budget, conclusions based on the pumping simulation alone must be tempered with judgments about the influence of these effects.

The approximate time required to mix the impoundment completely is necessary if one is going to estimate the effect of natural changes on the simulation predictions. This time,  $t_{\max}$ , can be found from the generalized results (Fig. 6.12), if the impoundment is nearly prismatic in shape and the initial density profile can be approximated by a linear profile. If the generalized results cannot be used, the characteristic time,  $T = V/Q$ , provides an order of magnitude approximation to  $t_{\max}$ . The field experiments with pumping systems show (Table 5.1) that

$$t_{\max}^* = t_{\max}/T < 0.3 \quad ,$$

and simulation computations show  $t_{\max}^*$  of this order. An approximation of  $t_{\max}$  based on a fraction of  $T$  should indicate whether the time required for mixing is large or small relative to the time scale of natural changes in the density profile. Should the time required for mixing by the pumping system be small relative to that required for natural changes, the simulation model can be applied directly. However, should the mixing time be large relative to that required for natural changes, the results provided by the simulation technique must be viewed accordingly. For instance, the simulation results for a lake which is losing heat due to natural processes will provide a conservative estimate of the required mixing time. The reverse would be true for a lake subjected to large net inputs of heat.

The application of the generalized results (Fig. 6.12) requires that the jet densimetric Froude number  $F$  be  $\leq 3$ . If the shape of the impoundment or initial density profile are such that the generalized results are not applicable and the full simulation technique must be used, low values of  $F$  are recommended for efficient pumping systems.

Laboratory experiments showed (Chapter 4) that for large values of the shape parameter,  $S$ , lateral density gradients existed in the impoundment contrary to the one-dimensional assumption underlying the simulation model. In the interest of better mixing and more appropriate application of the simulation technique, impoundments with large  $S$  values (large area, but relatively shallow) might be divided into two or more regions each with its own pumping system as suggested in Sect. 6.3.

The choice of the pumped discharge,  $Q$ , may be determined by the estimate of the time,  $t_{\max}$ , in which the mixing must be accomplished. The effects of changes in the elevations of the jet and intake tubes, discharge jet diameter, and changes in the initial density profile can be found in a broad sense from the generalized results (Chapter 6) or for a particular case from the simulation technique (Chapters 2 and 3).

### 7.3 RECOMMENDATIONS FOR FUTURE RESEARCH

The simulation model proposed in this study establishes the framework to which additions or modifications can provide models for the simulation of related problems.

The value of coupling a simulation of an impoundment heat balance to the pumping system simulation has been mentioned previously. Because the solution to the pumping system model is a stepwise solution in time, the possibility of alternating changes in the density profile due to external effects with changes due to the mixing by pumping exists. Similarly, the redistribution of a reacting tracer substance (as discussed in Chapter 3) can be handled by alternating changes due to the effects of chemical and biological reactions with those due to mixing.

The mixing of a reservoir due to the discharge of inflow by a jet (38) can be studied by adjusting the simulation model to allow for variable storage and by removing the withdrawal zone if necessary.

The mixing of a density-stratified impoundment by releasing compressed-air bubbles near the bottom might be modeled by removing the withdrawal zone and replacing the buoyant jet mechanics of entrainment with those of an air-bubble plume in a stratified environment. The simulation of the air-bubble mixing system would permit comparison of the relative efficiency of this type of system with that of the pumping system.

Field experiments with mixing systems on lakes and reservoirs are difficult to conduct. However, an effort should be made to gather data important to understanding the physical processes of mixing as well as the results of such mixing on the chemical and biological constituents of the impoundment. Density or temperature profiles measured

simultaneously at several locations in the impoundment during mixing provide information necessary to improve the simulation model and other predictive techniques. Heat budget data would be useful for testing the validity of a coupled heat budget and pumping system simulations.

## NOTATION

$A$	horizontal cross-sectional area of impoundment
$A_m$	coefficient defined by Eq. (2.53)
$A^*$	normalized area, $Ad/\Psi$
$a$	characteristic length for withdrawal layer, defined by Eq. (2.32)
$b$	nominal half-width of jet ( $\sqrt{2}b = 2\sigma$ )
$b_o$	half-width of jet at the end of the zone of flow establishment
$c$	density-stratifying agent, concentration of mass or temperature
$c_l$	center line concentration of tracer in jet only
$c_l^*$	local concentration of tracer in jet only
$c_s$	tracer concentration in the impoundment
$c_s^*$	tracer concentration in return flow from jet into the impoundment
$D, D_j$	initial jet diameter
$d$	vertical distance between intake and jet tubes
$d_j$	elevation of jet tube
$d_t$	total depth of impoundment
$d_w$	elevation of intake or withdrawal tube
$E_m$	eddy diffusivity for turbulent withdrawal layer



## NOTATION (Continued)

$F$	jet densimetric Froude number, defined by Eq. (6.4)
$F_f$	Froude number used by Fan (18), defined by Eq. (6.9)
$G_L$	power requirement due to pumping head, defined by Eq. (6.28)
$G_p$	power requirement due to losses, defined by Eq. (6.26)
$g$	acceleration due to gravity
$H_L$	losses proportional to velocity head
$H_p$	pumping head due to pressure difference, defined by Eq. (6.25)
$h$	local space step, $\Delta_y$
$I$	arbitrary constant of order 1 g/ml
$i, j$	indicies for space and time coordinates
$k$	local time step, $\Delta t$
$k_1, k_2$	constants of proportionality, defined by Eq. (2.36)
$t$	time coordinate
$M$	fraction of $\Delta P.E.$ reached in time $t$
$m$	integer, order of harmonic
$(n)$	order of derivative
$P$	plume parameter, defined by Eq. (6.6)
$Q, Q_j$	discharge from jet
$q$	two-dimensional flow in withdrawal layer
$q_e$	volume rate of flow per unit depth to impoundment (Region 1)
$q_e^*$	normalized $q_e$ , $q_e d/Q$

## NOTATION (Continued)

$r$	distance measured from jet axis
$S$	shape parameter, defined by Eq. (6.7)
$s$	parametric distance along the jet axis
$T$	characteristic time, $\Psi/Q$
$T_f$	stratification parameter used by Fan (18), defined by Eq. (6.10)
$T^0$	center line temperature of jet
$T^{0*}$	local temperature in jet
$T_a^0$	temperature of ambient fluid
$T_a^{0*}$	local ambient fluid temperature
$t$	time, usually from the beginning of pumping
$t^*$	normalized time, $t/T$
$t_{\max}$	maximum pumping time
$t_{\max}^*$	normalized maximum pumping time, $t_{\max}/T$
$u$	jet velocity along center line; velocity in withdrawal layer
$u^*$	local jet velocity
$u_*$	normalized velocity in withdrawal layer
$u_o$	center line velocity of jet at the end of the zone of flow establishment; center line velocity in withdrawal layer
$\Psi$	volume of impoundment included between intake and jet tubes
$v$	vertical transport velocity; in Chapter 6, initial jet velocity
$v^*$	normalized transport velocity $v\Psi/Qd$

## NOTATION (Continued)

$x$	coordinate axis for the jet in the horizontal plane from the jet origin; horizontal distance from intake for withdrawal layer
$y$	elevation above bottom of impoundment
$y^*$	normalized elevation, $y/d$
$y_*$	normalized elevation in withdrawal layer, $2y/\delta$
$y_{c.m.}$	elevation of the center of mass of impoundment
$y_{\ell nb}$	elevation of the level of neutral buoyancy
$\alpha$	coefficient of entrainment
$\beta$	a coefficient $\beta > 1$
$\gamma$	specific weight
$\Delta t$	local time step
$\Delta y$	local space step
$\Delta P.E.$	change in potential energy, defined by Eq. (6.24)
$\Delta \rho$	initial ambient density difference between the inlet and jet tube elevations
$\delta$	thickness of withdrawal layer
$\epsilon$	density gradient parameter, defined by Eq. (2.33)
$\theta$	angle of inclination of jet axis relative to horizontal
$\theta_o$	initial angle of inclination of jet axis relative to horizontal
$\lambda$	jet spreading ratio between buoyancy (or temperature) and velocity profiles ( $1/\lambda^2 =$ turbulent Schmidt number)
$\pi$	3.1416. . . .

## NOTATION (Continued)

$\rho, \rho_j$	center line jet density
$\rho_a$	density of ambient (impoundment) fluid
$\rho_a^*$	local ambient density
$\rho^*$	local density within the jet; in Chapter 6, the normalized density
$\rho_m$	mean density, defined by Eq. (6.19)
$\rho_o$	reference density
$\phi$	functional relationship of temperature to density



## LIST OF REFERENCES

1. Abraham, G., "Jet Diffusion in Stagnant Ambient Fluid", Delft Hyd. Lab. Pub. No. 29, 1963.
2. Albertson, M. L., Dai, Y. B., Jensen, R. A., and Rouse, H., "Diffusion of Submerged Jets", Trans. ASCE, Vol. 115, 1950, pp. 639-697.
3. Bella, D. A. and Dobbins, W. E., "Difference Modeling of Stream Pollution", J. San. Eng. Div., ASCE, Vol. 94, No. SA5, Oct., 1968, pp. 995-1016.
4. Bernhardt, H., "Aeration of Wahnbach Reservoir", J. Amer. Water Works Assoc., Vol. 59, No. 8, Aug., 1967, pp. 943-964.
5. Bohan, J. P. and Grace, J. L., Jr., "Mechanics of Flow From Stratified Reservoirs in the Interest of Water Quality", Hyd. Div. U. S. Army Engineer Waterways Experiment Station, Tech. Report H-69-10, Vicksburg, Mississippi, 1969.
6. Brainard, J. P., "Induced Mixing in a Thermally Stratified Fluid", M.S. Thesis, Massachusetts Institute of Technology, 1967.
7. Brezonik, P. L., Delfino, J. J., and Lee, G. F., "Chemistry of N and M<sub>n</sub> In Cox Hollow Lake", J. San. Eng. Div., ASCE, Vol. 95, No. SA5, Oct., 1969, pp. 929-940.
8. Brooks, N. H. and Koh, R. C. Y., "Selective Withdrawal From Density-Stratified Reservoirs", J. Hyd. Div., ASCE, Vol. 95, No. HY4, July, 1969, pp. 1369-1400.

## LIST OF REFERENCES (Continued)

9. Brush, L. M., Jr., McMichael, F. C., and Kuo, C. Y.,  
"Artificial Mixing of Density-Stratified Fluids: A Laboratory Investigation", L. F. Moody Hydrodynamics Lab., Report No. MH-R-2, Princeton University, Dec., 1968.
10. Bryan, J. G., "Improvement in the Quality of Reservoir Discharges Through Reservoir Mixing and Aeration", Symposium on Streamflow Regulation for Quality Control, U. S. Public Health Service Publ. No. 999-WP-30, June, 1965, pp. 317-333.
11. Churchill, M. A. and Nicholas, W. R., "Effects of Impoundments on Water Quality", J. San. Eng. Div., ASCE, Vol. 93, No. SA6, Dec., 1967, pp. 73-90.
12. Clark, C. D., Stockhausen, P. J., and Kennedy, J. F., "A Method for Generating Linear Density Profiles in Laboratory Tanks", Jour. of Geophy. Res., Vol. 72, No. 4, Feb. 15, 1967, pp. 1393-1395.
13. Cooley, P. and Harris, S. L., "The Prevention of Stratification in Reservoirs", J. Inst. of Water Engineers, Vol. 8, July, 1954, pp. 517-537.
14. Dake, J. M. K. and Harleman, D. R. F., "An Analytical and Experimental Investigation of Thermal Stratification in Lakes and Ponds", Hydrodynamics Lab., Report No. 99, Massachusetts Institute of Technology, Sept., 1966.

## LIST OF REFERENCES (Continued)

15. Dake, J. M. K. and Harleman, D. R. F., "Thermal Stratification in Lakes: Analytical and Laboratory Studies", Water Resources Research, Vol. 5, No. 2, Apr., 1969, pp. 484-495.
16. Debler, W. R., "Stratified Flow Into a Line Sink", J. Eng. Mech. Div., ASCE, Vol. 85, No. EM3, July, 1959, pp. 51-65.
17. Ditmars, J. D., "Computer Program for Round Buoyant Jets Into Stratified Ambient Environments", W. M. Keck Lab. of Hydraulics and Water Resources, Tech. Memo. 69-1, California Institute of Technology, 1969.
18. Fan, L. -N., "Turbulent Buoyant Jets Into Stratified or Flowing Ambient Fluids", W. M. Keck Lab. of Hydraulics and Water Resources, Report No. KH-R-15, California Institute of Technology, 1967.
19. Fan, L. -N. and Brooks, N. H., "Numerical Solutions of Turbulent Buoyant Jet Problems", W. M. Keck Lab. of Hydraulics and Water Resources, Report No. KH-R-18, California Institute of Technology, 1969.
20. Hart, W. E., "Jet Discharge Into a Fluid With a Density Gradient", J. Hyd. Div., ASCE, Vol. 87, No. HY6, Nov., 1961, pp. 171-200.
21. Hedman, E. R. and Tyley, S. J., "Elimination of Stratification at Lake Cachuma, California", U. S. Geological Survey, Water Resources Div., Open-File Report, Menlo Park, Calif., May, 1969.



## LIST OF REFERENCES (Continued)

22. Huber, W. C. and Harleman, D. R. F., "Laboratory and Analytical Studies of Thermal Stratification of Reservoirs", Hydrodynamics Lab., Report No. 112, Massachusetts Institute of Technology, Oct., 1968.
23. Irwin, W. H., Symons, J. M., and Robeck, G. G., "Impoundment Destratification by Mechanical Pumping", J. San Eng. Div., ASCE, Vol. 92, No. SA6, Dec., 1966, pp. 21-40.
24. King, D. L., "Hydraulics of Stratified Flow, Second Progress Report, Selective Withdrawal from Reservoirs", Hydraulics Branch, Div. Research, Bur. of Reclamation, Report No. Hyd-595, Denver, Colo., 1969.
25. Koberg, G. E. and Ford, M. E., Jr., "Elimination of Thermal Stratification in Reservoirs and the Resulting Benefits", U. S. Geological Survey, Water Supply Paper 1809-M, 1965.
26. Koh, R. C. Y., "Viscous Stratified Flow Towards a Line Sink", W. M. Keck Lab. of Hydraulics and Water Resources, Report No. KH-R-6, California Institute of Technology, 1964.
27. Koh, R. C. Y., "Viscous Stratified Flow Towards a Sink", J. Fluid Mechanics, Vol. 24, Part 3, Mar., 1966, pp. 555-575.
28. "Lake Erie: Dying But Not Dead", Environmental Science and Technology, Vol. 1, No. 3, Mar., 1967, pp. 212-218.
29. Lake Erie Report - A Plan for Water Pollution Control, U. S. Dept. of Interior, Fed. Water Pollution Control Admin., Great Lakes Div., Aug., 1968.

## LIST OF REFERENCES (Continued)

30. Leach, L. E., Duffer, W. R., and Harlin, C. C., Jr., "Pilot Study of Dynamics of Reservoir Destratification", U. S. Dept. of Interior, Fed. Water Pollution Control Admin., Robert S. Kerr Water Research Center, Ada, Okla., 1968.
31. Liggett, J. A. and Woolhiser, D. A., "Difference Solutions of the Shallow-Water Equation", J. Eng. Mech. Div., ASCE, Vol. 93, No. EM2, Apr., 1967, pp. 39-71.
32. List, E. J., "Lateral Momentum Jet in a Stratified Fluid", (submitted to J. Fluid Mechanics).
33. Morton, B. R., "Forced Plumes", J. of Fluid Mech., Vol. 5, Part 1, Jan., 1959, pp. 151-163.
34. Morton, B. R., Taylor, G. I., and Turner, J. S., "Turbulent Gravitational Convection from Maintained and Instantaneous Sources", Proc. Roy. Soc. London, Vol. A234, 1956, pp. 1-23.
35. Orlob, G. T. and Selna, L. G., "Temperature Variations in Deep Reservoirs", J. Hyd. Div., ASCE, Vol. 96, No. HY2, Feb., 1970, pp. 391-410.
36. Owens, W. W., "Density of Aqueous Sodium Chloride Solutions-Tables and Graphs", W. M. Keck Lab. of Hydraulics and Water Resources, Tech. Memo 65-11, California Institute of Technology, 1965.

## LIST OF REFERENCES (Continued)

37. Posey, F. H., Jr. and DeWitt, J. W., "Effect of Reservoir Impoundment on Water Quality", J. Power Div., ASCE, Vol. 96, No. PO1, Jan., 1970, pp. 173-185.
38. Reynolds, J. Z., "Water Quality in Pumped Storage Reservoirs", J. Power Div., ASCE, Vol. 93, No. PO2, Oct., 1967, pp. 15-35.
39. Richtmyer, R. D. and Morton, K. W., Difference Methods For Initial-Value Problems, Interscience Publ., New York, Second Edition, 1967.
40. Riddick, T. M., "Forced Circulation of Large Bodies of Water", J. San. Eng. Div., ASCE, Vol. 84, No. SA4, July, 1958, pp. 1703-1 to 1703-21.
41. Ridley, J. E., Cooley, P., and Steel, J. A. P., "Control of Thermal Stratification in Thames Valley Reservoirs", Proc. Soc. of Water Treatment and Examination, Vol. 15, Part 4, 1966, pp. 225-244.
42. Schmidt, W., "Turbulente Ausbreitung eines Stromes Erhitzter Luft", ZAMM, Vol. 21, 1941, pp. 265-278 and 351-363.
43. Speece, R. E. and Orosco, R., "Design of U-Tube Aeration Systems", J. San Eng. Div., ASCE, Vol. 96, No. SA3, June, 1970, pp. 715-725.
44. Standard Methods for the Examination of Water and Waste Water, American Public Health Association, New York, Twelfth Edition, 1965.

## LIST OF REFERENCES (Continued)

45. Symons, J. M., Personal Communication
46. Symons, J. M., Water Quality Behavior in Reservoirs, U. S. Dept. of Health, Education, and Welfare, Public Health Service Publ. No. 1930, Cincinnati, Ohio, 1969.
47. Symons, J. M., Irwin, W. H., and Robeck, G. G., "Impoundment Water Quality Changes Caused by Mixing", J. San. Eng. Div., ASCE, Vol. 93, No. SA2, Apr., 1967, pp. 1-20.
48. Symons, J. M., Irwin, W. H., Robinson, E. L., and Robeck, G. G., "Impoundment Destratification for Raw Water Quality Control Using Either Mechanical or Diffused-Air Pumping", J. Amer. Water Works Assoc., Vol. 59, No. 10, Oct., 1967, pp. 1268-1291.
49. Symons, J. M., Carswell, J. K., and Robeck, G. G., "Mixing of Water Supply Reservoirs for Quality Control", J. Amer. Water Works Assoc., Vol. 62, No. 5, May, 1970, pp. 322-334.
50. Teerink, J. R. and Martin, C. V., "Consideration of Artificial Destratification in Reservoirs of the California State Water Project", J. Amer. Water Works Assoc., Vol. 61, No. 9, Sept., 1969, pp. 436-440.
51. Tennessee Valley Authority, Div. of Water Control Planning, Engineering Laboratory, "Cherokee Reservoir Selective Withdrawal", Water Resources Research, Lab. Report No. 13, Norris, Tennessee, 1969.

## LIST OF REFERENCES (Continued)

52. Walesh, S. G., "Natural Processes and Their Influence on Reservoir Water Quality", J. Amer. Water Works Assoc., Vol. 59, No. 1, Jan., 1967, pp. 63-79.
53. Walesh, S. G. and Monkmeyer, P. L., "Withdrawal of a Viscous Density-Stratified Fluid From the Bottom of a Reservoir", ASCE, Nat. Water Resources Eng'g. Meeting, Memphis, Tenn., Jan. 28, 1970.
54. Weibe, A. H., "Limnological Observations on Norris Reservoir With Special Reference to Dissolved Oxygen and Temperature", Trans. of the Third North American Wildlife Conference, Amer. Wildlife Inst., 1938, pp. 440-457.
55. Wood, I. R., "Selective Withdrawal From a Stably Stratified Fluid", J. Fluid Mechanics, Vol. 32, Part 2, May, 1968, pp. 209-223.
56. Wu, Jiin, "Mixed Region Collapse With Internal Wave Generation In a Density-Stratified Medium", J. Fluid Mechanics, Vol. 35, Part 3, Feb., 1969, pp. 531-544.
57. Wunderlich, W. O. and Elder, R. A., "Effect of Intake Elevation and Operations on Water Temperature", J. Hyd. Div., ASCE, Vol. No. 95, No. HY6, Nov., 1969, pp. 2081-2091.
58. Wunderlich, W. O. and Elder, R. A., "Discussion of Reference 8", J. Hyd. Div., ASCE, Vol. 96, No. HY5, May, 1970, pp. 1207-1211.
59. Yih, S. -S., "On the Flow of a Stratified Fluid", Proceedings Third National Congress of Applied Mechanics, 1958, pp. 857-861.

## APPENDIX

Listing of Computer Program Outlined in Section 2.3.3

(The impoundment and pumping system data  
are for Experiment Number 13)

```

//SM4E JOB (51402,JDD,C=),D11MARS,MSGLEVEL=1
// SET TIME=(10,0),REGION=125K
//STEP1 EXEC FORFCGLG
//FORT,SYSIN DD *
C THIS PROGRAM IS FOR EXPER. NO.13 WITH JET AT THE BOTTOM
C THIS PROGRAM FINDS THE NEW DENSITY PROFILE AFTER TIME DELTA T
C INCLINED BUOYANT JET IN AN ARBITRARY PROFILE
C Y(1) = CENTERLINE VELOCITY
C Y(2) = JET NOMINAL HALF WIDTH
C Y(4) = THETA, THE ANGLE OF CENTERLINE FROM HORIZONTAL
C Y(5) = X COORD
C Y(6) = Y COORD
C ALPHA = ENTRAINMENT COEFF.
C SCHMD = TURBULENT SCHMID NUMBER
C TENTR(M) = ENTR AT NONUNIFORM Y
C CTENT(M) = INTERPOLATED ENTR AT UNIFORM Y
C WRGY(M) = NONUNIFORM Y
C CRRTY(M) = UNIFORM Y
C GRAV = ACCEL DUE TO GRAVITY
C RHOO = REFERENCE DENSITY
C DENGROD = LOCAL DENSITY GRADIENT
C X = DISTANCE TO BOUNDARY FROM INTAKE
C INTAKE = POINT OF INTAKE ELEVATION
C YSTEP = VERTICAL SPACING INTERVAL
C WIDTH = WIDTH OF RESERVOIR AT INTAKE ELEVATION
C AVETHK = AVER ROUNDED OFF WITH LAYER THICKNESS
C CRRTY(M) = VERTICAL COORD ZERO AT BOTTOM
C ENTRJ = INTEGRATED JET ENTRAINMENT (-)
C ENTRW = INTEGRATED WITHDRAWAL (-)
C ENTRO = INTEGRATED ZERO ENTRAINMENT REGION (+)
C ENTR = SUM OF ALL INTEGRATED ENTRAINMENT
      DIMENSION Y(6),YDOT(6),YNEW1(251),DENGROD(250),ENTR(251),ENTRJ(251)
      1,ENTRW(251),ENTRO(251),CRRTY(251),WRGY(251),AREA(251),TENTR(251),V
      2FL(251),YNEW(3000),V(251),AMDEN(251),DEN(251),DENNEW(3000),DD(3)
      DIMENSION VOLFL(250)
      DIMENSION DEN1(251)
      DIMENSION BSTOP(2),BENTR(2),HY3(2)
      READ(5,101) DISJET,DIAM,THETA0,RHOO,DENDIF
      READ(5,200) GRAV,ALPHA,SCHMD
      READ(5,801) YSTEP,WIDTH,X,INTAKE
      READ(5,201) DELTAS,DELTAT,LIMTIM,INTVAL
201 FORMAT(2F10.5,2I4)
      WRITE(6,300)
      WRITE(6,150) DISJET,DIAM,THETA0,RHOO,DENDIF
      WRITE(6,250) GRAV,ALPHA,SCHMD
      WRITE(6,804) YSTEP,WIDTH,X,INTAKE
      WRITE(6,251) DELTAS,DELTAT,LIMTIM,INTVAL
251 FORMAT(1H0,5X,7HDELTAS=,F10.5,5X,7HDELTAT=,F10.5,5X,7HLIMTIM=,I4,5
      1X,7HINTVAL=,I4)
      M = INTAKE
      NOTIME = 0
      NOINT = INTVAL
C GENERATE THE AMDENS FOR THIS CASE OF LINEAR STRAT. - EVERY 0.2CM
C THE DENSITY = 1.0000000 + (AMDEN * 1000.)
      AMDEN(1) = 3.70
      DO 701 L=2,18
701 AMDEN(L) = AMDEN(L-1) - .04888889
      AMDEN(19) = 2.82
      DO 702 L=20,78
702 AMDEN(L) = AMDEN(L-1) - .013
      AMDEN(79) = 2.04
      DO 703 L=80,108
703 AMDEN(L) = AMDEN(L-1) - .01633333
      AMDEN(109) = 1.55
      DO 704 L=110,168
704 AMDEN(L) = AMDEN(L-1) - .0085
      AMDEN(169) = 1.04
      DO 705 L=170,190
705 AMDEN(L) = AMDEN(L-1) - .018181818
      AMDEN(191) = 0.64
      DO 706 L=192,216
706 AMDEN(L) = AMDEN(L-1) - .003076923
      DO 707 L=217,251
707 AMDEN(L) = 0.56
      DO 505 L=1,251
505 DEN1(L) = AMDEN(L)
C GENERATE THE AREAS FOR THIS CASE ALL ARE EQUAL
      DO 14 L=1,251
14 AREA(L)=52852.32
      CRRTY(1)=0.0

```

```

      DO 59 N = 2,251
      YM = N - 1
59  CRRTY(N) = Y4*YSTEP
      DD(1) = 0
      DD(2) = 0
      DD(3) = 0
      CALL LABEL(0.,1.,50.,0.,12.5,5,21H)DISTANCE ABOVE JET CM,+21,0)
      CALL LABEL(12.5,1.,0.5,4.0,8.75,7,16H(DENSITY-1)X1000,-16,1)
      CALL XYPLOT(251,CRRTY,AMDEN,50.,-10.,0.1,4.1,DD,0)
166 DO 11 I=1,251
      ENTRJ(I)=0.0
      ENTRW(I)=0.0
11  ENTR0(I)=0.0
      DENDIF = ((AMDEN(I) - AMDEN(INTAKE))/1000.)*((1.+(SCHMD**2))/(2.*(S
      ICHMD**2)))
      TENTR(1) = DISJET
      WRGY(1) = 0.0
      DO 12 J = 1,250
12  DENGRO(J) = (AMDEN(J+1)-AMDEN(J))/200.0
C INTEGRATION OF JET ENTRAINMENT
      COEFF = GRAV*(SCHMD**2)/RHOO
      Y(1) = DISJET/(3.1415927*(DIAM**2)/4.0)
      Y(2) = DIAM/1.414214
      Y(3) = DENDIF
      Y(4) = THETA0*3.1415927/180.
      Y(5) = 0.0
      Y(6) = 0.0
      T = 0.0
      I=1
      CALL DEQ(K,6,T,Y,YDOT,DELTAS,5.E-6)
100 GO TO (10,20,20,30),K
10  YDOT(1) = (-2.*ALPHA*Y(1)/Y(2))+(2.*COEFF*Y(3)*SIN(Y(4)))/Y(1)
      YDOT(2) = (2.*ALPHA)-(COEFF*Y(2)*Y(3)*SIN(Y(4)))/(Y(1)**2)
      YDOT(3) = ((1.+(SCHMD**2))*DENGRO(1)*SIN(Y(4))/(SCHMD**2))-2.*
      ALPHA*Y(3)/Y(2)
      YDOT(4) = (2.*COEFF)*Y(3)*COS(Y(4))/(Y(1)**2)
      YDOT(5) = COS(Y(4))
      YDOT(6) = SIN(Y(4))
      CALL DEQ2 (6100,6130)
20  IF((0.0E-65) - Y(3)) 21,23,23
21  BENTR(1) = (3.1415927*Y(1)*(Y(2)**2)) - DISJET
      BSTOP(1) = Y(6)
      BY3(1) = Y(3)
      IF(Y(6)-CRRTY(I+1)) 27,26,26
26  TENTR(I+1)=(3.1415927*Y(1)*(Y(2)**2))-DISJET
      WRGY(I+1) = Y(6)
      I=I+1
27  CALL DEQ1(6100)
130 CONTINUE
      GO TO 27
23  IF(Y(6) - CRRTY(I+1)) 521,522,522
522 I = I + 1
      WRGY(I) = Y(6)
      TENTR(I) = (3.1415927*Y(1)*(Y(2)**2)) - DISJET
521 BSTOP(2) = Y(6)
      BENTR(2) = (3.1415927*Y(1)*(Y(2)**2)) - DISJET
      BY3(2) = Y(3)
      KSIZE = I
      ASTOP = YINTERP(BY3,BSTOP,0.0000000,2,1)
      AENTR = YINTERP(BSTOP,BENTR,ASTOP,2,1)
      J = 1
31  ENTRJ(J) = YINTERP(WRGY,TENTR,CRRTY(J),KSIZE,5)
      ENTRJ(J) = -ENTRJ(J)
      IF(J-KSIZE) 32,33,33
32  J = J+1
      GO TO 31
C NOW CALCULATE WITHDRAWAL LAYER AND INTEGRATE
33 DISC = DISJET/WIDTH
C CALC OF INVISCID THICKNESS
      A = ((DISC**2)/(GRAV*(-DENGRO(INTAKE)/RHOO)))**.25
      THKINV = (2.7)*A
C CALC OF TURB THICKNESS K2 = 10E-3
      IF ((X/A)-6000.) 60,60,61
60  THKTUB = A*8.4*((.001*X/A)**.25)
      GO TO 62
61  THKTUB = A*7.14*((.001*X/A)**.33)
62  AVETHK = (THKINV + THKTUB)/2.0
      PTHK = ((AVETHK/2.0)/YSTEP)+0.5
      ATHK = MTHK
      AVETHK = ATHK*2.0*YSTEP

```



```

C LOCATE BOTTOM OF WITHDRAWAL LAYER
YINTAK = CRRTY(M)
YBWL = YINTAK - (AVETHK/2.0)
K=(YBWL/YSTEP)+1.5
KBOT = K
YTAWL = YINTAK + (AVETHK/2.0)
L=(YTAWL/YSTEP)+1.5
LTOP = L
DO 63 J = K,M
  YSTAR = (YINTAK - CRRTY(J))/(AVETHK*0.5)
63 ENTRW(J) = -(0.96*(1.-YSTAR))-(0.03125*(1.-(YSTAR**2)))+(0.94575*(1.-
  1(YSTAR**3)))-(0.4545*(1.-(YSTAR**4)))
DO 64 J = M,L
  I = (2*M) - J
64 ENTRW(J) = -1.0 - ENTRW(I)
DO 65 J=K,L
65 ENTRW(J) = ENTRW(J) * DISJET
C ASSIGN INTEGRATED VALUE TO POSITIVE ENTRAIN. REGION
N=KSIZE+1
DO 66 J=N,L
66 ENTRO(J) = DISJET
DO 67 J=1,251
  ENTR(J) = ENTR(J)+ENTRW(J)+ENTRO(J)
67 V(J) = ENTR(J)/AREA(J)
  NBEGIN = KSIZE + 1
  KSIZE1 = KSIZE - 1
  VOL = (DELTAT)*(-ENTRJ(KSIZE))
  KSIZE1 = KSIZE - 1
DO 400 L=1,KSIZE1
400 VOLEL(L) = DELTAS*AREA(KSIZE-L)
  L = 1
403 IF(VOL-VOLEL(L)) 401,401,402
402 VOL = VOL-VOLEL(L)
  L = L + 1
  IF(L.GT. KSIZE1) GO TO 711
GO TO 403
711 WRITE(6,712)
712 FORMAT(1H0,40HMOVE GREATER THAN KSIZE DELTAT TOO LARGE)
STOP
401 CONTINUE
DO 70 L=1,KSIZE
70 VFL(L) = -V(L)
  I = 1
71 YNEW(I) = CRRTY(KSIZE+1-I) - (VFL(KSIZE+1-I)*DELTAT)
  IF(YNEW(I) - 0.0) 72,73,74
74 I = I + 1
GO TO 71
72 CORDIS = CRRTY(KSIZE+1-I) - (YNEW(I)/(1.-((VFL(KSIZE+2-I)-VFL(KSIZ
  1E+1-I))*DELTAT/DELTAS)))
  YNEW(I) = 0.0
GO TO 120
73 YNEW(I) = 0.0
120 NMBER = I
DO 124 L=1,NMBER
124 YNEW1(L) = YNEW(L)
DO 121 L=1,NMBER
121 YNEW(L) = YNEW1(NMBER + 1 - L)
  NMBER1 = NMBER + 1
  NMBER2 = NMBER + 2
  YNEW(NMBER1) = ASTOP - ((AENTR/AREA(KSIZE))*DELTAT)
  YNEW(NMBER2) = ASTOP + ((DISJET/AREA(KSIZE))*DELTAT)
  KTOP = LTOP - KSIZE
DO 301 L=1,KTOP
  SPACE = V(KSIZE+L)*DELTAT
301 YNEW(NMBER2 + L) = CRRTY(KSIZE + L) + SPACE
  LIMIT = NMBER2 + KTOP
DO 123 L=1,251
123 DEN(L) = AMDEN(L)
  DENEW(1) = YINTERP(CRRTY,DEN,CORDIS,251,1)
DO 122 L=2,NMBER
122 DENEW(L) = DEN(KSIZE - NMBER + L)
  DENEW(NMBER1) = YINTERP(CRRTY,DEN,ASTOP,251,1)
  DENEW(NMBER2) = DENEW(NMBER1)
DO 125 L=1,KTOP
125 DENEW(NMBER2 + L) = DEN(KSIZE + L)
DO 126 L=1,LTOP
126 DEN(L) = YINTERP(YNEW,DENEW,CRRTY(L),LIMIT,1)
  I = 1
  SUM = 0.0

```

```

561 SUM1 = DEN(I) - DEN1(I)
    SUM = SUM + SUM1
    IF(SUM1 - 0.0) 508,560,560
508 I = I + 1
    GO TO 561
560 SUMA = SUM - SUM1
    I1 = I + 1
    DO 506 I=I1,251
506 SUM = SUM + (DEN(I) - DEN1(I))
    ERROR = (-100./SUMA)*(SUM-(.5*(DEN(1)-DEN1(1)+DEN(251)-DEN1(251))))
1)
    KEPTRK = NOTIME + 1
    WRITE(6,570) ERROR,KEPTRK
570 FORMAT(1H0,27HPERCENT ERROR MASS BALANCE=,F10.5,7X,21HNUMBER OF TI
    ME STEPS=,I4)
    NOTIME = NOTIME + 1
    IF(NOTIME-NOINT) 163,164,164
163 DO 165 L=1,251
165 AMDEN(L) = DEN(L)
    GO TO 166
164 CONTINUE
    IF(NOTIME-LIMTIM) 167,168,168
167 CALL XYPLT(251,CRRTY,DEN,50.,-10.,0.1,4.1,00,0)
    OU 169 L=1,251
169 AMDEN(L) = DEN(L)
    NOINT = NOINT + INTVAL
    GO TO 166
168 CALL XYPLT(251,CRRTY,DEN,50.,-10.,0.1,4.1,00,1)
    STOP
30 WRITE(6,600)
    STOP
101 FORMAT(3F10.5,2F10.7)
200 FORMAT(3F10.4)
801 FORMAT(3F9.4,I3)
300 FORMAT(1H1,42HTHIS PROGRAM FINDS THE NEW DENSITY PROFILE)
150 FORMAT(1H0,5X,7H0ISJET=,F10.5,5X,5HDIAM=,F10.5,5X,7HTHETA0=,F10.5,
    15X,5HRRD0=,F10.7,5X,7HDENDIF=,F10.7)
250 FORMAT(1H0,5X,5HGRAV=,F10.4,5X,6HALPHA=,F10.4,5X,6HSCMD=,F10.4)
804 FORMAT(1H0,5X,6HYSTEP=,F9.4,5X,6HWIDTH=,F9.4,5X,2HX=,F9.4,5X,7HINT
    IAKE=,I3)
806 FORMAT(1H0,11X,1HM,7X,7HCOORD Y,12X,4HV(Y))
808 FORMAT(10X,I4,5X,F9.5,5X,F15.8)
600 FORMAT(22H ERROR RETURN FROM DEQ)
    END
/*
//GD.SYSPLTDN DD SYSOUT=N
//GD.SYSIN DD *
23.94      0.849      0.0      1.00370      0.04
980.      0.082      1.16
0.2      60.96      827.      180
.2      120.      210      30
//

```